Synthesis of the Metallocenes for the Production of Exotic High Energy Ion Beams

Ntombizonke Yvonne Kheswa

UNIVERSITY *of the*
WESTERN CAPE

A thesis is submitted in fulfilment of the requirements for the degree of Doctor of Philosophy in the Department of Physics & Astronomy, University of the Western Cape, South Africa.

Supervised by:

Prof. J. N. Orce,
Department of Physics & Astronomy
University of the Western Cape

Prof. S. Titinchi,
Department of Chemistry,
University of the Western Cape

Dr. R. Thomae
Accelerator and Engineering Department
iThemba LABS

March 2019

DECLARATION

I declare that *Synthesis of the Metallocenes for the Production of Exotic High Energy Ion Beams* is my own work, that it has not been submitted for any degree or examination in any other university, and that all the sources I have used or quoted have been indicated and acknowledged by complete references.

Signed: Ntombizonke Kheswa Date: 1 March 2019

Synthesis of the Metallocenes for the Production of Exotic High Energy Ion Beams

Department of Physics and Astronomy, University of the Western Cape, Private Bag X17, 7535 Bellville, South Africa.

ABSTRACT

The Subatomic Physics Department of iThemba Laboratory for Accelerated Based Sciences (iThemba LABS) conducts experiments that require a variety of particle beams in order to study nuclear properties (reaction, structure, etc.) of various nuclides. These particle beams are accelerated using the K-200 Separated Sector Cyclotron (SSC) and delivered to different physics experimental vaults. Prior to acceleration, the particle beam is first ionised using an Electron Resonance Ion Source (ECRIS). The main goal of this study is the production of exotic metallic beams of $^{60}Ni^{8+}$ and $^{62}Ni^{8+}$ using ECRIS4, which are required for the Coulomb excitation experiments approved by the Programme Advisory Committee (PAC) at iThemba LABS.

In order to provide the metallic beams of nickel, a development study of organometallic materials containing ^{60}Ni and ^{62}Ni isotopes in a form of metallocene complexes was undertaken. The nickelocene ($NiCp_2$) complex, a member of the organometallic family, was synthesised at the Physics Target Laboratory of iThemba LABS for the first time. Method development involved the use of natural nickel during the multi-step synthesis before the use of enriched nickel-60 (^{60}Ni) and nickel-62 (^{62}Ni).

Nine samples of $NiCp_2$ were synthesised; two were isotopically enriched nickelocene ($^{60}NiCp_2$ and $^{62}NiCp_2$). The percentage yields of the synthesised nickelocene samples ranged between 16 to 50 %, and samples were characterised by investigating their crystal structure and bonding arrangements in the complexes by X-ray diffraction (XRD) , Fourier Transform Infrared (FT-IR) spectroscopy, and Proton Nuclear Magnetic Resonance (^1H NMR).

The synthesised nickelocene were further used with ECRIS4 for the production of Ni beams on the Q-line of the cyclotron. The Metal Ions from Volatile Compounds (MIVOC) technique was used for the conversion of ^{60}Ni and ^{62}Ni to ion species. The method used the organometallic compounds which are volatile at specific pressures at ambient temperatures.

Metallic ion beams of nickel were successfully produced after a carefully pre-sample conditioning in the MIVOC container before connecting the MIVOC set-up to the new injection system of the ECRIS4. Measured beam intensities during the experiment for both $^{60}Ni^{+}$ and $^{62}Ni^{+}$ were approximately 30 µA, optimum for physics measurements.

The development of the MIVOC technique opens up new beam-target combinations with the use of new exotic stable beams for new science cases at iThemba LABS. Reactions in inverse kinematics, multi-step Coulomb-excitation and other types of reactions will immensely benefit from these developments.

KEYWORDS

- Organometallic compounds
- Metallocenes
- Nickelocene, $NiCp_2$
- Nickelocene complexes
- Enriched ^{60}Ni and ^{62}Ni
- Metallic Ion Beams
- Electron Cyclotron Resonance Ion Source (ECRIS4)
- Metal Ions from Volatile Compounds (MIVOC)
- Synthesis
- X-ray Diffraction (XRD)
- Fourier Transform Infrared (FT-IR)
- Proton Nuclear Magnetic Resonance (^1H NMR)

AKNOWLEDGEMENTS

I would like to give thanks to the following:

- NRF/iThemba LABS for affording me time and funding to complete my research studies.
- To my supervisors who have been working with me throughout this research:
- Prof. Nico Orce, for acknowledging the potential and capability in me that I am equally ready to take up such an important research study as a PhD. You provided me with academic guidance to ensure that this research go as planned and achieve its goal. I do appreciate also the background lessons in nuclear physics research and what it entails to perform some of those interesting experiments.
- Prof. Salam Titinchi, thank you for your guidance and with the planning of the project with more emphasis on the chemistry part of which you are the expert. The time and advises provided during the sample preparations and their characterisations, provided a valuable component to my research study. Your guidance in interpretations of results and writing is well appreciated by me.
- Dr Rainer Thomae, my colleague and the specialist in ECR-ion sources at NRF/iThemba LABS, my sincere gratitude to you as you had to take me through the ion sources process, from the beginning to the end. Making certain that my interpretation of results is of quality that is appreciated by special community. Thank you for all your patience.
- To my supervisors, all your teachings are highly appreciated and are now part of me. I can assure all that this experience is priceless, my elders always said, never be afraid to learn, knowledge is weightless.
- To Dr Hanno Abbo (UWC) and Mr Raimo Seppälä (JYFL) – thank you both for all the practical guidance you afforded me for the technique in the synthesis of the complexes.
- To my colleagues and considering them as my younger brothers; from the National Metrology Institute of South Africa (NMISA) in Pretoria and Department of Subatomic Physics at iThemba LABS: Dr Tshepo Dinoko for the assistance during sample preparation and proof reading my work. Dr Peane Maleka for assisting with proof reading my work and willingness to read while avoiding any of the laboratory

Dr Obed Shirinda for also making sure that the editing and style of the document are in order and allowed standard. Ngithi kini nobathathu Ubuntu mabande ningapheli amandla nangomuso.

- MRD colleagues, Dr Khumalo and Dr Bucher, thank you for performing XRD characterisation on my samples.
- To my colleagues and younger sisters, Dr Zina Ndlovu and Dr. Thifhe Bucher, thank you both for the moral support you provided, this was much appreciated.
- To my friend at SUN, Dr Setati; Thank you for all the advice you gave me during my study and assistance to make sure that all is in order with my thesis. Kuthiwa indlela ibuzwa kwabaphambili ngoba bayazi kangcono.
- To the University of the Western Cape, Faculty of Natural Science, Department of Physics and Astronomy for allowing me the opportunity to be part of the team.

Kumndeni wami wonke ngithi lencwadi eqoshiwe ingeyenu.

- Abazali bami: abakwaMdluli langizalwa khona kanye nakwaKheswa la engendela khona ngithi ngibonga ukuba nami kuloluhambo. Imikhuleko yenu njalo iye yangimisa idolo.
- Myeni wani, NoZulu bengingeke ngilunge ukulihamba ngedwa loluhambo, ngiyabonga ukusolokho ungikhuthaza njalo.
- Kumagcino wami Nqobile, anginawo amazwi anele okukubonga Ngelosi yami. Ukubakhona kwakho kunginike amandla ngoba ubuhlale ukukhathalele futhi ukuthokozela ukufunda kwami, ngiyethemba ukuthi lokhu kuzokunika ugqozi lokuthi uzithande izincwadi zakho.
- To my big two☺ - Muke noLungi. Benikhathezeka umangabe ningibona sengizibe ilaptop yami, nibuze nithi kathi akusafundwa yini ma, ngoba nikhathazeka ukuthi angizukuqeda. Lemibuzo yenu ibingigqugquzela kakhulu noma sengiphelelwa yithemba.
- Kuzingane zakwethu, uVusi, Thulani no Lindile kanye nezingane zabo ngithi ngibonga amazwi enu enkuthazo.

Lencwadi eqoshiwe ngiyinikela kwintombi KaDonda, umaMbokazi ukhulu wami ongasekhoyo owayeyithanda imfundo ngendleala ebabazekayo. Ngithi gogo, sengiwuye udokotela namhlanje njengesifiso sakho.

TABLE OF CONTENT

LIST OF FIGURES AND TABLES

ABBREVIATIONS

$NiCp_2$ – Nickelocene

MIVOC- Metal Ions from Volatile Compounds

XRD – X-ray Diffraction

^1H NMR – Proton Nuclear Magnetic Resonance

FT-IR – Fourier Transform Infrared

ECRIS – Electron Cyclotron Resonance Ion Source

$CDCl_3$ – Deuterated chloroform

DMSO-d_6 – Deuterated dimethyl sulfoxide

$Ni[(NH_3)_6]Cl_2$- Hexaaminenickel(II)chloride

n.d – No date

Chapter 1 Introduction

This chapter presents the motivation and overview of beam requirements for the nuclear physics experiments at the iThemba Laboratory for Accelerator Based Sciences (iThemba LABS). It highlights how these beams are produced in the electron cyclotron resonance ion sources (ECRIS) before being accelerated by the Separated Sector Cyclotron (SSC). Some scientific motivations to increase the scope of available beams for nuclear physics research are also mentioned in this chapter.

1.1 Motivation

iThemba LABS is a multi-disciplinary laboratory specialising in accelerator-based sciences and applications. The accelerator and ancillary facilities are used for research and training in nuclear and accelerator physics, radiobiology, material sciences, radionuclide production and radiotherapy. The SSC accelerator at iThemba LABS is the heart of this multi-disciplinary facility. The emphasis is on providing scientifically and medically useful radiation through the acceleration of charged particles using the SSC and other appropriate technologies. Amongst the various research departments at iThemba LABS, the Subatomic Physics Department focus primarily on research studies related to nuclear reaction mechanisms and nuclear structures. For these nuclear physics experiments at iThemba LABS, the projectile particles impinge in the stable target nuclei to produce the nucleus of interest, in a nuclear reaction such as,

$$ {}^{A}_{Z}X(a,b){}^{A'}_{Z'}Y \qquad (1.1) $$

where X is the stable target nucleus (e.g. ^{208}Pb, ^{194}Pt, etc.), *a* represent the particle beam of interest (e.g. ^{1}H, ^{4}He, ^{36}Ar, ^{86}Kr), *b* the reaction particle products (e.g. γ-ray, α, *n*,) and Y generally an unstable nucleus product (e.g. ^{9}B, ^{8}He, ^{86}Kr, etc.). In these conditions, both the particle beam and target materials are the crucial components for many (if not all) experiments of interest.

Nuclear physics research uses a large variety of isotopic ion beams (from light elements to heavy elements) to explore the properties of nuclei through accelerator-driven nuclear reactions. These particle beams are accelerated after being produced in a dedicated ion source. To produce ions, atoms or molecules must be injected into a plasma chamber whereby they are ionised by electron impact. The introduction of the material of interest into the ion source can be done in various ways depending on their physical properties. Gas, liquids and materials with high vapour pressure at room temperature can be introduced directly into the ion source via a regulation valve. For materials with low vapour pressure at room temperature as most solids, it is much more complicated to generate ion beams. Due to the strong atomic binding of these elements sufficient vapour pressure is only achieved at very high substrate temperatures. One possible way to avoid this problem is to use of ocene compounds for which the strong inter-atom binding is replaced by cyclopentadienyl rings resulting in much higher vapour pressure compared to solids which allows for the direct injection into the ion source at room temperature. However, ocenes available from natural materials consist commonly of several isotope and some isotopes might have a low abundance. For example, nickel has 5 stable isotopes from 1 % for ^{64}Ni to 68 % for ^{58}Ni. Injecting ocene produced form natural nickel will therefore allow for the extraction of intense ^{58}Ni-ion beam, but not for intense beams for the other 4 isotopes. For the production of ion beams of isotopes with low abundance it is therefore essential to be able to produce ocenes from isotopic enriched materials.

This thesis describes the path towards the production of high intensity nickel-ion beams with high isotopic purity and opens up new beam capabilities for many new science cases at iThemba LABS. This kind of beams were never produced before at iThemba LABS.

Next, two projects requiring this type of beams are presented in the two abstracts.

1) Search for the loss paradigm of surface vibrations (spokesperson: Prof. Nico Orce (UWC))

Abstract: Collective rotations in axially-symmetric well-deformed nuclei are comprehensively described by the collective model of Bohr and Mottelson. The phenomenological description of collective vibrations remains, however, uncertain. Detailed gamma-spectroscopy work by Garrett, Wood and collaborators in the Cd isotopes seems to demand a change to the long-standing picture of low-energy surface vibrations introduced by Bohr and Mottelson. Previously, the sequence of 0+, 2+ and 0+, 2+, 4+ states commonly observed in nearly-spherical nuclei were described as multi-phonon excitations. Some of the Cd isotopes have been the paradigm of quadrupole vibrations for over 50 years. Nevertheless, the E2 strengths determined for the Cd isotopes could better be arranged as part of different quasi-rotational bands. Undeniably, such a multi-phonon sequence is broadly observed along the nuclear chart and the origin for such a pattern might still have a vibrational origin. The breakdown of vibrational motion in the Cd isotopes opens up new fundamental questions:
``Are there any surface vibrations in nuclei?'' and if so, ``where are they?''
Here we propose a search for the loss paradigm in a different region (the nickel isotopes), by determining diagonal and transitional matrix elements and comparing with QPM calculations.
Note: The experiment was approved again with Priority 1 in December 2018 by the PAC at

2) Model-independent measurement of the shape of ^{102}Ru (spokespersons: Dr. Elena Lawrie (iThemba LABS) and Prof. Nico Orce (UWC))

Abstract: Strongly broken chiral symmetry in nuclei can be identified by the observation of a pair of degenerate partner bands. However it seems that in nuclei the chiral symmetry is always weakly broken. This leads to divergence in the properties of the chiral partners, and makes it difficult to unambiguously identify the possible presence of this symmetry. An alternative way to prove that the nucleus possesses chiral symmetry, is to show that apart from the suitable nucleon configuration (with proton and neutron angular momenta predominantly aligned along the short and long nuclear axes), the shape of the nucleus is triaxial. In that case the rotational angular momentum aligns predominantly along the intermediate nuclear axis, and a tri-dimensional chiral geometry is formed.

This new experiments propose a model-independent measurement of the shape of ^{102}Ru, using Coulomb excitation reaction to measure the transition matrix elements, which are in turn used to determine the quadrupole moment and the triaxiality of the nuclear shape. ^{102}Ru is the core of one of the best chiral candidates, ^{104}Rh.

At the time these proposals were originally submitted, the beam production of exotic stable beams at iThemba LABS was limited and, in particular, the acceleration of pure beams of ^{60,62}Ni and ^{102}Ru was not feasible (Thomae *et al*., 2009). However, these two beams were produced in other nuclear research facilities such as JYFL (Finland), RIKEN (Japan) and GANIL (France) via the MIVOC (Metal Ions from Volatile Compounds) method (Leherrisier *et al*., 2007; Kalvas & Koivisto, 2017), which will be explained in detail in chapter 3. Given that the required beams were new at iThemba LABS, it was originally assumed that both of these organometallic compounds could be sourced off the shelf. Investigations using natural abundant organometallic Ni and Ru materials were conducted. Results after investigations by Thomae (2016/7) showed that naturally abundant elements could not provide reasonable beam currents for these nuclear experiments. As a way forward, enriched nickelocene and ruthenocene were henceforth considered the feasible option. A summarised report for the trials of the Ru beam production is attached in the appendix A.1.

In this research study, the motivation will be on nickel beam production which will form part of the development of beams via the MIVOC method. The nickel beams are required for the study of two-phonon excitations in even-even ^{60,62}Ni isotopes through two-step Coulomb excitation (Orce, 2012). This study involves ^{60,62}Ni projectiles bombarded onto heavy targets of ^{208}Pb nuclei. A detailed proposal of these two-step Coulomb-excitation measurements is available in the book of proposals for 2012 and 2017 at the iThemba LABS library. Therefore, this research will involve the synthesis of organometallic materials containing ^{60,62}Ni, which are called nickelocene. These materials will be compounds in a form of a metal sandwiched between two cyclopentadienyl rings which are known as metallocenes. After carefully synthesising the so-called nickelocene complexes (see Figure 1.1), at the iThemba LABS target laboratory, the materials will be further characterised using fundamental methods of chemistry. Finally, test experiments will be conducted at ECRIS4 (Electron Cyclotron Resonance Ion Source 4) to measure ^{60}Ni and ^{62}Ni intensities produced and determine if these intensities will be enough to produce the required beam currents for the above mentioned experiments.

Figure 1.1: *The sandwich molecular structure of the nickelocene molecule (Pugmire, 2001; Crabtree, 2005; Kubiak, 2006).*

1.2 General background of organometallic compounds

Organometallic compounds are known as molecular compounds that form chemical bonds between carbon and the metal. These bonds are formed between the metal from alkaline, alkaline earth metals, and mostly with the transition metals group and with some of the metalloids. Crabtree (2005) further describes organometallic chemistry as the field between organic and inorganic chemistry that produces metal-organic compounds whereby the metal-organic part of the compound is only bound by the metal's heteroatom, for example, $[Ti(OMe)_4]$ (Crabtree, 2005). Numerous methods for the preparation of organometallic compounds are listed in the literature and can mainly be divided into four categories which are paraphrased below (Jones & Gilman, 1954; Liard *et al.*, 2001; Crabtree, 2005). All these methods were abundantly used in organic synthesis and have played a major role both in academic laboratories and industries.

- "The first category is the reaction between an organic halide or pseudo halide and a metal such as the classical oxidative metalation or the halogen–metal exchange".
- "The second category concerns the exchange reactions between acidic hydrogen and basic organometallic derivatives, namely the metalation reactions".
- "The third category concerns all the trans-metalation reactions".

- "The fourth category is related to the hydro- and carbo-metalation reactions across unsaturated systems. This category of synthesis is powerful in a way that the stereo-, diastero- and even enantioselectivity of the reaction have to be controlled".

A new concept is also described for the preparation of organometallic derivatives via a mechanism that differs from those mentioned above. This new formation of organometallic derivatives is based on the complexation (or oxidative coupling) of unsaturated compounds with low-valent transition metals (zirconocene and titanocene type) followed by *ab*-elimination reaction to give an *s*-carbon metal bond (Liard *et. al*., 2001; Mohamed & Ishak, 2011). Early transition metal complexes show both types of reactivity, and thus, in addition to their utility either as a carbanion source or as a synthetic reagent based on transition metal behaviour, it is possible to utilize them for synthetic transformations based on the characteristic features of both types of reactivity (Gmelin, 1997/1998; Barue, 2000; Kubiak, 2006; Liard *et. al*., 2001).

1.3 New Physics with new beams

The main goal of this study is the development of new and exotic stable beams for nuclear physics research at iThemba LABS. To date, nuclear-physics experiments at iThemba LABS have generally been carried out with enriched materials utilised as targets in nuclear reactions of interest. Currently, iThemba LABS has a limited selection of stable beams that can be accelerated to address new and exciting nuclear physics cases. These accelerated beams will open up new areas of research and, for example, permit precise measurements of nuclear lifetimes in inverse kinematics and nuclear shapes through bombarding the nucleus of interest onto a heavy target such as ^{208}Pb. In particular, new beams in conjunction with the GAMKA (GAMma-ray spectrometer for Knowledge in Africa) array of high-resolution HPGe clover + high-efficiency $LaBr_3$ detectors– recently funded by the National Research Foundation (NRF) through the Strategic Equipment Research Programme and state-of-the-art particle detectors will form a phenomenal combination for new physics. As shown in Figure 1.2, the extended angular coverage of the new GAMKA array, together with its high resolution and high efficiency makes it an ideal spectroscopic tool to investigate projectiles either in direct or inverse kinematics.

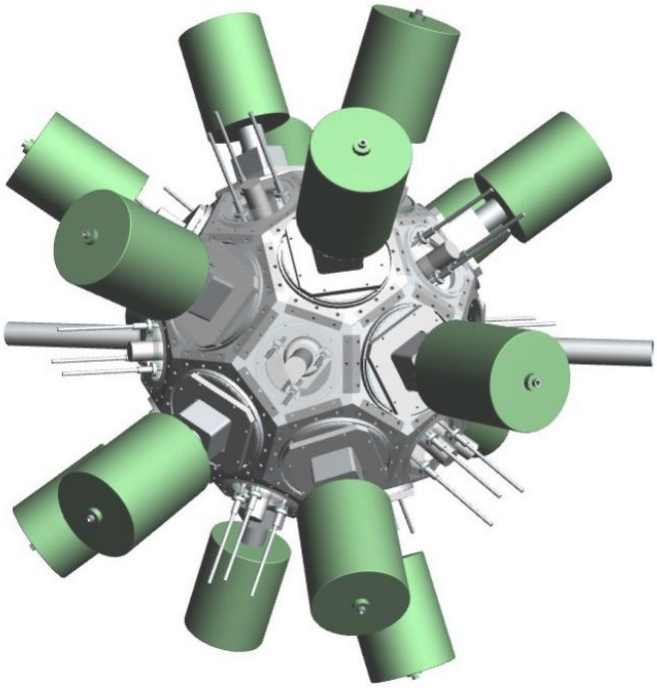

Figure 1.2: *A possible configuration of the GAMKA array recently funded by the NRF comprising 17 clovers and 13 $LaBr_3$ detectors for high-resolution and high efficiency gamma detection, respectively.*

1.3.1 Nuclear Lifetimes

Nuclear lifetimes are crucial to understanding transition probabilities and decay rates. Transition probabilities provide relevant information on the elusive nuclear force as well as tests of modern nuclear models, whereas decay rates can provide information of nuclear-astrophysics explosive phenomena (e.g. X-ray bursts or novae) as well as the age of the oldest objects in the universe such as globular clusters.

Similarly to the change in the sound frequency for a train approaching or moving away from us, the Doppler effect can be used to measure lifetimes of nuclear levels in the femtosecond - few picoseconds regime (10^{-15} - 10^{-12} s) by using gamma-ray detectors at different angles θ (Belgya *et al.*, 1996). As illustrated in Figure 1.3, the energy of the gamma ray de-exciting the level of interest shifts depending on the detection angle as a function of cos θ. Simply, the higher the statistics and the larger the angular coverage the better the fit to the data. Here lies the importance of the new GAMKA array with up to 18 HPGe clover detectors covering at

least five angles and the new DSAM lifetime set up recently commissioned at iThemba LABS (Principal Investigator: Smarajit Triambak). The current AFRODITE (AFRican Omnipurpose Detector for Innovative Techniques and Experiments) array only allows the coverage of three angles, 45, 90 and 135 degrees. An additional advantage at iThemba LABS is that one can easily run heavy-ion reactions with bombarding beams at about 10% the speed of light. This feature allows a more accurate measurement of lifetimes as the stopping powers, or how the nucleus slows down in the nuclear medium, are better known at faster beam velocities.

A modified version of the Doppler effect can be used to measure nuclear lifetimes. In Figure 1.3, the energy of the de-exciting gamma ray shifts depending on the scattering angle, θ, for gamma-ray detection is shown. This shift allows a measurement of nuclear lifetime ranging from femtoseconds (10^{-15} s) to a few picoseconds (10^{-12} s) (Orce *et al.,* 2008). This upper limit depends on the velocity of the recoiling nuclei in the nuclear medium, i.e. the target. The accuracy of the measurements depends on the knowledge of the stopping powers, or how the recoiling nucleus slows down travelling along the target material. Electronic stopping powers are very well known for high recoiling velocities, where most of the slowing down arises from electronic interactions. At low recoiling velocities, the nuclear stopping powers also have to be taken into account, which generally adds a 15% uncertainty to the lifetime measurement (Orce *et al.*, 2006; Orce *et al.*, 2008; Pasternak *et al.,* 2009). Precise lifetimes can therefore be measured by accelerated heavy beams, which have higher recoil velocities, in inverse kinematics.

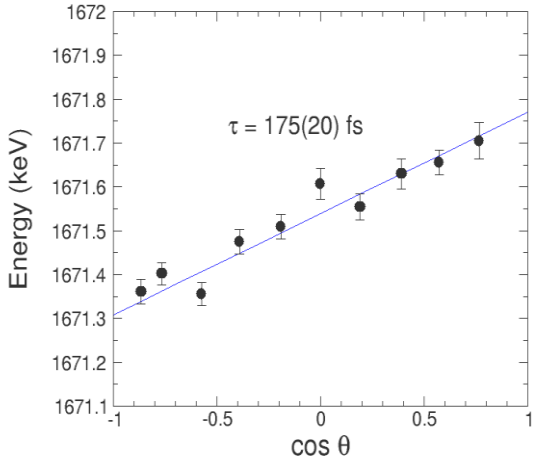

Figure 1.3: *An accurate fit to the nuclear lifetime depends on statistics and the number of data points, i.e., detectors at different angles. The energy of the de-exciting gamma-ray shifts depending on the scattering angle (θ) for gamma-ray detection (Orce et al., 2008).*

1.3.2 Nova nucleosynthesis

Classical novae are explosive events that take place in binary star systems such as the one shown in Figure 1.4, on the surface of the white dwarf star as a result of a thermonuclear runaway. It is during such short-lived and explosive events that many of the proton rich elements are formed. The production of the ^{22}Na radionuclide can be then be predicted by hydrodynamic simulations from such events (ONe novae). The reasonably short half-life of ^{22}Na makes it ideal to identify possible nova sites by gamma-ray space telescopes or via detection of a 1275 keV line from the beta decay of ^{22}Na. However, such a signature is yet to be observed (Seuthe *et al*., 1990). It has been mentioned (D'Auria *et al*., 2004) that at nova peak temperatures, the dominant mechanism for the destruction of ^{22}Na could arise from certain proton capture resonances on ^{22}Na that compete with a beta decay in the reaction cycle. Presently there exists a discrepancy in the measured strength of these resonances that could be resolved by lifetime measurements of relevant states in ^{23}Mg (Kirsebom, 2016). The development of a new scattering chamber at iThemba LABS would allow a measurement of these lifetimes in the near future. However, such a measurement would require a ^{24}Mg beam, in order to produce the states of interest using a one-neutron removal reaction. This is yet another new beam that can be produced with enriched ^{24}Mg metallocene via the MIVOC method.

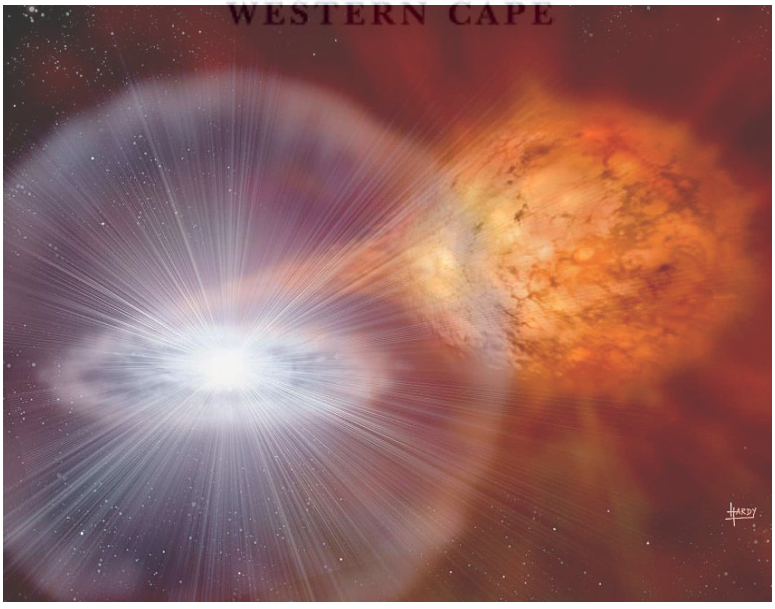

Figure 1.4: *An artist's impression of a nova explosion. Image by Hardy, 2006*.

1.3.3 Nuclear shapes

A remarkable feature of atomic nuclei is their ability to adopt different shapes for a small cost in excitation energy compared to their total binding energy, see Figure. 1.5 (Andreyev *et al*., 2000). Nuclear shapes are important to understand phenomena such as beta decay, shape coexistence or collective nuclear motion. And can be measured using Coulomb-excitation reactions at energies well below the Coulomb barrier. The spectroscopic quadrupole moment, or the nuclear charge distribution in the laboratory frame, of excited states with angular momenta J # 0, 1/2 can be determined using the reorientation effect (RE), which generates a time-dependent hyperfine splitting of the nuclear levels (Andreyev *et al.*, 2000).

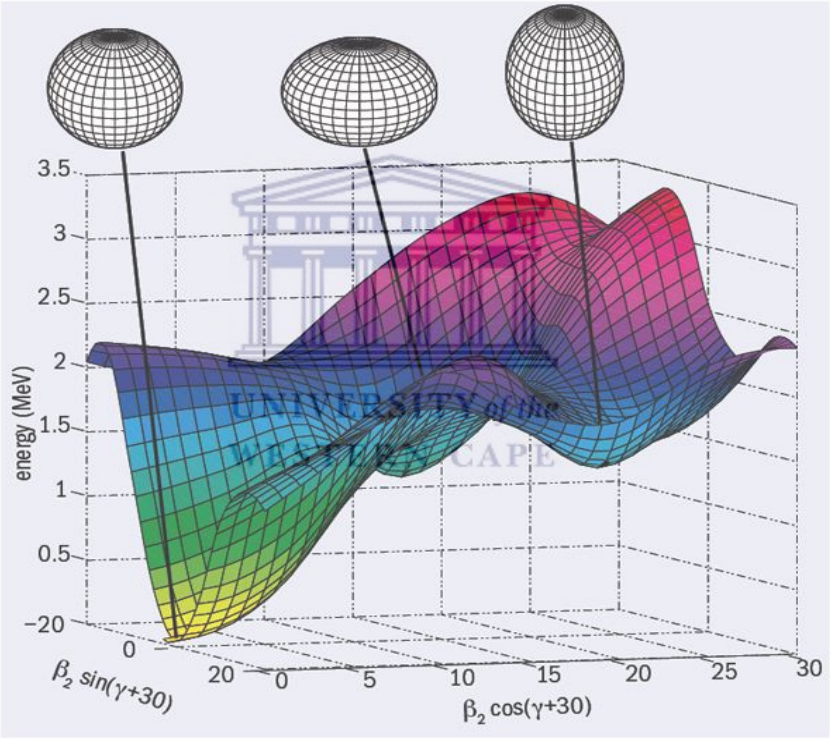

Figure 1.5: *A sketch illustrating the ability of atomic nuclei adopting different shapes for a small cost in energy compared to their total binding energy (Andreyev et al., 2000).*

The population of different magnetic sub-states through the time-dependent electric-field gradient of the target changes with the spectroscopic quadrupole moment, either enhancing or inhibiting the asymmetry of the angular distribution of the de-excitation gamma-rays. This

change in the angular distribution provides a spectroscopic probe for a measurement of the spectroscopic quadrupole moment. The relevant point for the current study is that for accelerated ions the use of high-Z targets enhances the RE, which is proportional to $\frac{Z\ target}{Z\ beam}$. Also the use of beams onto a heavy target enhances the population of high-lying states, particularly when heavy ions are involved. The combination of accelerated beams of physical interest and heavy targets thus allows more sensitive measurements of nuclear shapes. Alternatively, the study of the nucleus of interest bombarded on light targets such as ^{12}C favours the determination of reduced transition probabilities, or B(E2) values. Hence, the relevance of developing new beams to accommodate new and exciting nuclear physics research at iThemba LABS.

1.4 Outline of this thesis

For most nuclear physics experiment conducted at iThemba LABs using the separated sector cyclotron, one of the most important components is the beam of particles. For this thesis, we explore methods to manufacture nickelocene from natural nickel, thereafter synthesis nickelocene with ^{60}Ni and ^{62}Ni isotopes. In chapter 2 that follows, the background of these class of metals, referred to as metallocenes will be discussed. This will begin with their history, chemical properties and finish with the discussion on the nickelocene compound. In chapter 3, beam production at iThemba LABS facility is introduced including the various possibilities that are available to supply the requested beam to the users.

Nickelocene compounds synthesis and characterisation is discussed in chapter 4. In these characterisations, the following methods XRD, FT-IR and ^{1}H NMR were used. This is followed in chapter 5 by the results of the nickelocene characterisation. Chapter 6 provides illustrations and first tests for beam productions using the synthesised nickelocene, and then thesis summary and conclusions are provided in chapter 7.

Chapter 2 Metallocenes Background

Although the study focuses on the nickelocene complex which belongs to the family of organometallic compounds, it is of interest to discuss other available metallocene materials in literature. This is important for future research proposals at iThemba LABS, whereby more enriched particle beams using organometallic materials via the MIVOC method will be produced. The significance of metallocenes through their applications in general is also highlighted to give full scope of these complexes. The periodic table of elements is attached on the appendix for the reference of all elements discussed in the metallocenes of group elements, transition metals, lanthanides and actinides elements.

2.1 Organometallic compounds history

The birth of organometallic chemistry started in 1760 when Cadet's fuming liquid, organoarsenic compound, was accidentally formed in the organic laboratory (Thayer, 1966; Astruc, 2007). Cadet's liquid is explained by Thayer (1966) as "liquid arises from the heterogeneous fusion of potassium acetate with arsenic trioxide giving various organometallic compounds along with numerous organic and inorganic by-products" (Thayer, 1966). More studies were done by various chemists on this compound to find out what it was composed of until the discovery of Zeise´s salt, K [$PtCl_3$ (η^2-C_2H_4)], another organometallic compound. This discovery posed various questions again from chemists regarding the structure of the compound which was proposed by the founder, Zeise (Hunt, 1984; Crabtree, 2005; Astruc, 2007). Since then, many compounds were discovered, organochlorosilanes, metal carbonyl derivatives and binary metal-carbonyl compounds.

The field of organometallic chemistry provided useful ideas to industry, medicinal and organic chemical synthesis. Organometallics are favourable in industry where catalysis is applied because their catalysts are capable of forming one enantiomer of a chiral product. The field also formed links with biochemistry whereby organometallics are used as biological catalysts. For example, in the chemistry of materials for the deposition of metals organometallics are used as precursor materials with the metal of interest to be deposited. Nanoscience also benefited as organometallics are involved in the production of

nanoparticles which are used in applications like electronics, magnetic and optical devices or in sensors (Grunes *et al.*; 2003; Zhang *et al.*, 2007). Another example is the rodium and iridium based catalyst of the organometallics which are famously used to convert methanol to acetic acid without any by-products produced after the reaction. And this brought hope as to consider organometallic chemistry as a way forward for a possible solution when climate change becomes severe (Zhang *et al.*, 2007; Cantrill, 2012).

A proposed structure of benzene by the principal formulator of the theory of chemical structure, Kekule (1865), brought some insights and theories in the field of organic chemistry but those could not be proven and ended up being neglected. Some of the open questions remained about the kind of compounds that could exist in the cyclic family and the kind of reactions these compounds could undergo. For instance, the angle strain theory regarding the cubic carbon-based molecules that were thought to be unstable because of the sharp 90° angle. Surprisingly, the cubic carbon cyclic compounds so called cubanes were discovered which are much stable and has many application in industry and in pharmaceutical purposes. In addition to the cubanes, cyclopropanone and benzyne also form part of the cyclic-stable compounds with angles less than 105° (Johnson, 1977; Crabtree, 2005; Astruc 2007). Another hypothesis which was found to be impossible was the chemical bond between carbon and transition metals, however this theory was also proven to be incorrect and swept away after the discovery of Ferrocene, a stable compound in air and at temperatures above 300 °C (Johnson, 1977; Robertson, 2012; Bacher, 2016). Ferrocene, $(C_5H_5)_2Fe$, was the first metallocene to be discovered and published by Kealy and Pauson (1951), and its chemical structure was later published in the following year by Wilkinson *et al.* (1952). The compound was accidentally discovered, the aim of the research study was to synthesise the fulvalene compound, $C_{10}H_{10}$ (Robert & Caserio, 1977) The ferrocene name came after empirical calculation of the formula by the IUPAC and was the first transition metal compound containing carboxylic rings as ligands that are coplanar to each other to form a sandwich structure with a metal. This was one of the ground-breaking moments in the organometallic field as researchers worked tirelessly to synthesise more metallocene compounds and their derivatives (Salzer, 1999; Takahashi, 2004; Robertson, 2012; Bacher, 2016). Crabtree (2005) however mentions that several chemists have noted at the beginning of the 1950s a very stable orange compound powder that is formed when cyclopentadienyl is passed through iron tubing but these studies never published any information about the compound (Crabtree, 2005). Since then, a variety of bicyclopentadienyl complexes of other transition metals and

their derivatives were synthesised. To mention a few, materials like nickelocene, cobaltocene, nickelocenium cation, titanocenedibromide, vanadocene, ruthenocene, chromocene, magnesocene and manganocene were synthesized (Salzer, 1999; Takahashi, 2004).

Ferrocene has the unusual properties of an organoiron compound, being stable at more than 500 ^{0}C and able to be dissolved in and recovered from concentrated sulphuric acid. Kealy and Pauson (1951) work started a storm of research on transition metals in general an area between organic and inorganic chemistry, which has flourished ever since and has led to an improved understanding of important biochemical processes (Robert & Caserio, 1977; Vassylyev, 2005). More research studies were conducted for compounds containing hydrogen, carbon and iron which were still believed to be not feasible at that time. For example, Miller *et al.* (1952) further synthesised ferrocene a year after discovery of ferrocene via a different approach by reacting reduced iron with cyclopentadienyl in nitrogen. At the time, it was still believed that direct replacement of hydrogen on carbon by iron was not possible. After this discovery, another door for organometallic compounds was open which are defined as materials which possess direct, more or less polar bonds between metal and carbon atoms (Yamamoto, 2001).

Most organometallic compounds resemble organic compounds in their physical properties rather than inorganic compounds that they form reactions with. As a result, organometallic compounds exist as low melting crystals, liquids or gases because of the distinct molecular structures that can be formed by these compounds. One of the chemical behaviours of these complexes is that they are soluble in a wide variety of weakly polar solvents (Pugmire, 2001). As a result, organometallics with cyclic structures are preferred in many applications and mostly as homogeneous catalysts in processes where all the reacting partners are present in one phase, usually the liquid phase. Homogeneous enantioselective catalysts that selectively react to give the desired product are the most studied compounds in the field of organometallic chemistry, especially the metallocenes, because of their special character in catalysis reactions. The advantage of using the metallocenes catalysts especially in polymer production applications is that they produce homogeneous polymers. This is due to the single active site in the metal of the metallocenes. The electronic and stereochemical location of the metal is controlled by the organic ligand shell as a result; each metal centre has the same ligand environment. These conditions are not possible when using other contour part catalysts (Carnahan & Jacobsen, 2000; Shamiri *et al.*, 2014). For example, palladium is one of the

most studied metals in organometallic chemistry because it is versatile and catalyses a number of organic reactions (Tsuji, 2004; Colacot, 2012; Hickman & Sanford, 2012). Another application of organometallic compounds is the use of degraded products of metallocenes to manufacture fibres for high quality formation of fibre structures upon calcination of electrospun fibres, fibre mats or membranes (Liard, *et al.*, 2001; Pugmire, 2001; Rezola, 2002; Takahashi, 2004). Refractory materials like tungsten carbide film for microelectronics and tribological applications can be obtained via organometallic chemical vapour deposition. This is considered as the clean method in the deposition of refractory materials as deposition via other methods requires high temperatures which yield contaminations (Lai and Lamb, 1995).

2.2 Metallocenes

Metallocenes are defined or described in various ways depending on their applications. Originally metallocenes compounds were initially considered as sandwich complexes of bis-cyclopentadienyl and the metal. However, with wider usage and developments in the field of metallocenes, other cyclopentadienyl complexes were identified as half sandwich and multidecker sandwich (multicyclopentadienyl) complexes as well as complexes with additional substitution at the metal centre. In addition, the metallo-prefix from the name metallocene is restrictive again when one considers more development of complexes involving non-metallic elements such as boron, silicon or arsenic (Jutzi & Burford, 1998). Therefore in consideration of this, metallocenes can be referred to as any compounds containing a metal that is bonded to the π-cloud of a cyclopentadienyl (Cp) or similar substituent (Macdonald, nd). This comes after considering that some of the p-block elements that form or could form complexes with cyclopentadienyl are not metals.

2.2.1 The structural bonding of metallocenes derivatives

Cyclopentadienyl ligands are bound in various ways, and this coordination is referred to as hapticity, η (Cotton, 1968). In a typical normal sandwich structure both of the cyclopentadienyl (Cp), a pentahapto, η^5, coordination is experienced. This is the most occurring and uniform binding of the central metal atom of all 5 carbon atoms at the same metal-carbon distances, see Figure 1.1. There are other structural elements with coordination

of monohapto, dihapto, trihapto and tetrahapto that do exist but are much less common. In addition, metallocenes sandwich structures typically exist in the form of various oxidation states with the number of valence electrons (NVE) between 14 and 20. Complexes with 18 NVE are said to be stable as compared to the ones with NVE of less or above 18. This rule is typically applied to predict the stability of the organometallic compound. It is stated by Royo and Ryan (1998) and Astruc (2007) that organometallic molecules or complexes are particularly stable when the valence electrons of the metal plus the bonding electrons which are contributed by the ligand are in a total of 18. The high stability of ferrocene, cobaltocenium and rhodecenium cations is due to the 18-electron rule. All three molecules are commonly isoelectronic and have 18 valence electrons except for a low spin rhenium anion that has 17 valence electrons. The reactivity of rhodocene and cobaltocene can be also explained as both complexes have 19 valence electrons; as a result they are easily oxidised. Although the 18 electron rule is useful in predicting the stability of the organometallic complexes, however it is not universal when it comes to explain the bonding and structure in organometallic complexes (Astruc, 2007). This will further be discussed in section 2.3.

2.2.2 Stability of metallocenes derivatives

The chemistry of metallocenes, bis (cyclopentadienyl) metal derivatives has been developed for most d-elements (Royo & Ryan, 1998). The stability of metallocenes differs and depends on the metal and its oxidation state, for instance ferrocene, ruthenocene and osmocene are particularly stable because in each compound, the metal involved achieves the electronic configuration of an inert gas. In addition, some metallocene ionic compounds are more stable than their metallocenes. For instance, the cobaltocenium ion is resistant to oxidation in a way that it can be recovered from boiling aqua regia (mixture of hydrochloric acid and nitric acid). In cobaltocenium ions, the metal has the 18 outer shell electrons, the characteristic similar to that of a noble gas krypton electron configuration. Many other unsaturated organic compounds as well can form π complexes with transition metals. For example, a substance that in some ways is comparable to ferrocene is the complex of two benzene molecules with chromium metal, called dibenzenechromium as shown in Figure 2.1 (Royo & Ryan, 1998). The bonding structure of the compound raised some questions as to whether it involves a π or σ bonding. It is reported that the bonding involves zero-valent chromium and the π electrons of the two benzene rings; this was reported by Royo and Ryan (1998). Nevertheless, Rayon

& Frenking (2003) did a further study on dibenzenechromium bonding and found that the σ bonds contribute more significantly in dibenzenechromium than in ferrocene. Thus it was concluded that dibenzenechromium is a σ-bonded molecule (Rayon & Frenking, 2003). Because of the compound stability it was explained that, in dibenzenechromium, the electronic configuration of chromium atom is similar to that of krypton (Seyferth, 2002). Although dibenzenechromium is thermally quite stable, however, the stability decreases at 285 ˚C and the complex breaks down to give benzene and chromium. Furthermore, it is said that the compound appears to lack the aromatic character of either benzene or ferrocene as judged by the fact that it is destroyed by reagents used for electrophilic substitution reactions (Rayon & Frenking, 2003).

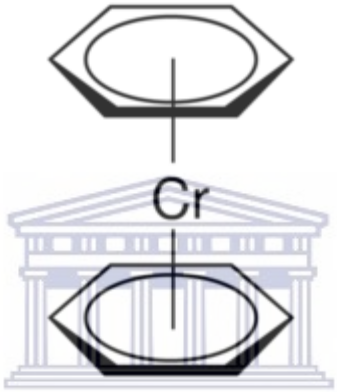

Figure 2.1: *The structure of dibenzenechromium with the bonding that involves zero-valent chromium and π electrons of the two benzene rings (Royo & Ryan, 1998; Seyferth, 2002).*

Several transition metal complexes of cyclobutadienyl have been reported to be prepared and are thought to be extraordinary because of the parent hydrocarbons that are prepared from are not stable in general. Cyclobutadienly is known for oligomerisation, which shows how instable the compound is. Reactions that logically should lead to cyclobutadienyl give dimeric products instead. Furthermore, metallocene derivatives are known of other conjugated cyclic polyenes. Examples are bis (cyclooctatetraene) uranium, uranocene, and bis (pentalenylnickel). Russian chemist, Vol'pin (1972), discovered that unusual reactivities and reactions could be formed by some of the metallocenes. For instance, titanocene undergoes a reaction that forms a complex compound that can be easily reduced to form ammonia during the absorption of dinitrogen, (N_2), (Vol'pin, 1972; Royo & Ryan, 1998).

2.2.3 Metallocenes of the s and the p-block elements

The size of the atom plays a significant role in the bonding of metallocene complexes formed within the group metallocenes. Metallocene complexes are known of going through the π bonds reactions with a few exception compounds that have σ bonds. The π bonds tend to be weak which is the reason of having instable metallocene compounds in most of the cases. Starting with the alkali metal metallocenes of group 1 and 2 are considered as vital compounds as they are used during the synthesis of other metallocenes of any element from the periodic table. These ionic compounds present simple molecular formulae but their chemical structures are interesting (Williams *et al.*, 1990; Jutzi & Burford, 1998; Macdonald, n.d). Different structures within the group are contributed by the charge distribution of the anion of each element as a result the alkali metal compounds are being either linear super sandwich or zig-zag structures (Figure 2.2). This variation in structure is mostly contributed by the mass of the atom and the media where these compounds are at. For example, in solution, the alkali metal cyclopentadienyl compounds can adopt a variety of structural forms that can be reflected as pieces of the super sandwich structure. Similarly to the alkaline metallocenes, the alkaline earth metallocenes are useful reagents for the synthesis of other metallocenes. In addition structural properties of some of the group 2 metallocenes compounds are quite different to those of same the group metallocenes.

The heavier analogues are highly ionic and contain large cations, thus they can also form polymeric structures similar to those found for the heavier group 1 metallocenes (Jutzi & Burford, 1998; Bachmann *et al.*, 2016; Macdonald, n.d). For instance, Ca and Ba form polymeric structures of metallocenes. In general, in main group metallocenes, metallocenes interacts in with either π-central bonding or peripherally bonding. If those conditions cannot be met, then slip-sandwich structures are formed. Beryllocene and boronocene cation structure are the examples of metallocenes compounds that do not have such bond. As a result, their structures stand out from other metallocenes structures. However, beryllocene caught attention to many, and findings related to this behaviour are explained by Beattie and Nugent, (1992). The structure was studied by various ways using X-rays and computational methods. The reasons came up from those investigations were the small size of the Be^{+2} ion

which contributes to the offset of the bonding angle. Another reason that caused a slip of the rings of the compound is a shallow potential energy surface found in beryllocene, as a result the steric requirements of the Cp ligands changes and give rise to the observed geometrics shown in Figure 2.3 (Chiu & Schäfer, 1977; Nugent *et* al., 1984; Jemmis & Reddy, 1990; Margl & Schwarz, 1994; Jutzi & Burford, 1998; Bacher, 2016; Bachmann *et al.*, 2016).

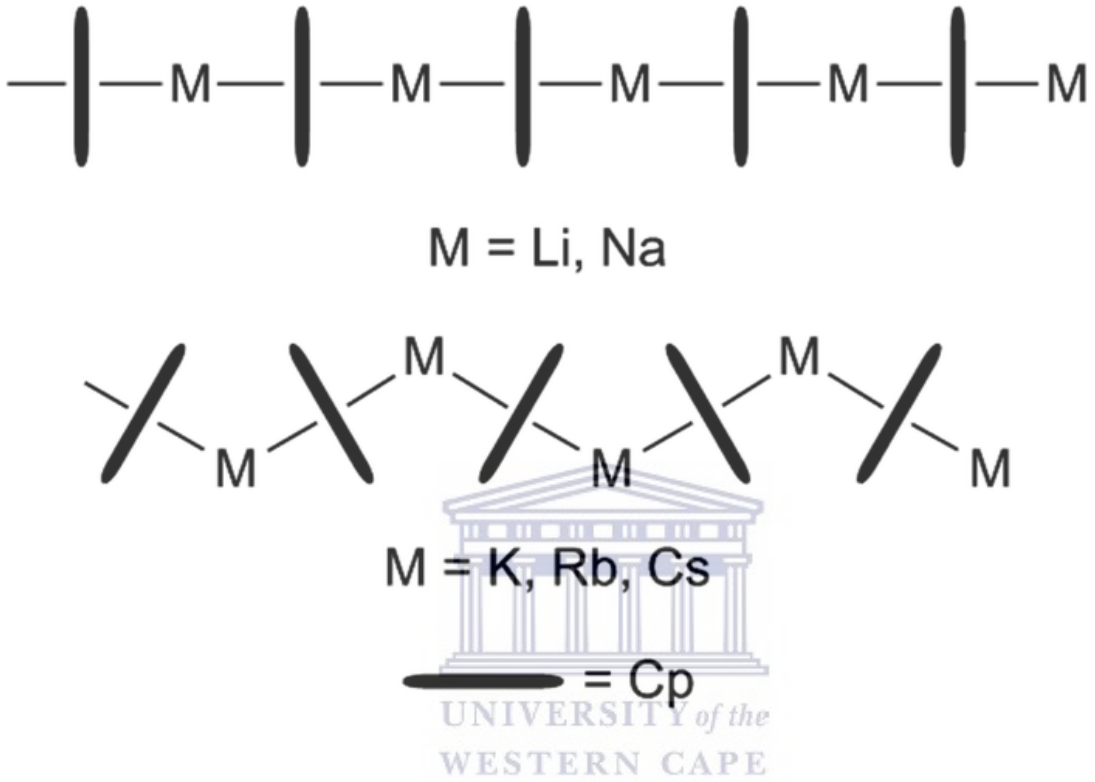

Figure 2.2: *Alkali metal cyclopentadienyl compound sandwich illustrating linear structure for lighter metals of Li and Na (top) and zig-zag structures found on heavier metals from group 1 (K, Rb and Cs) (bottom) (Pugmire, 2001; Fernandez & Carmona, 2005; Bachmann et al., 2016).*

The p-block metallocenes present a greater variety of covalent bonding and form stable compounds as opposed to the metallocenes of the s-block. This variation of bonding within the group 14 compounds is contributed by the variety in atomic size of the group 14 elements. For example, the group 15 solid M-Cp structures are σ-bonded on their Cp^* rings and this type of bonding is found on P and As. However, the observed ^1H NMR spectrum of As has one signal, and this is indication that the bonding is no longer σ on the Cp^* and this change is said to be contributed by the rapid 1, 2 rearrangement of atoms in the complex (Jutzi & Burford, 1998; Macdonald, n.d). The π-bonded Cp^* rings in the solid state are

however formed in the Sb and Bi analogues. Again this type of bonding is due to the size of the larger atoms and their coordination spheres. In this group, cationic metallocenes are favourable because they form stable complexes which are composed of combined chemical bond interaction of σ- and π-donor properties of the η-bonded Cp ligand. These compounds can be synthesised via halide abstraction using strong Lewis acid or by metathesis reactions (Macdonald, n.d).

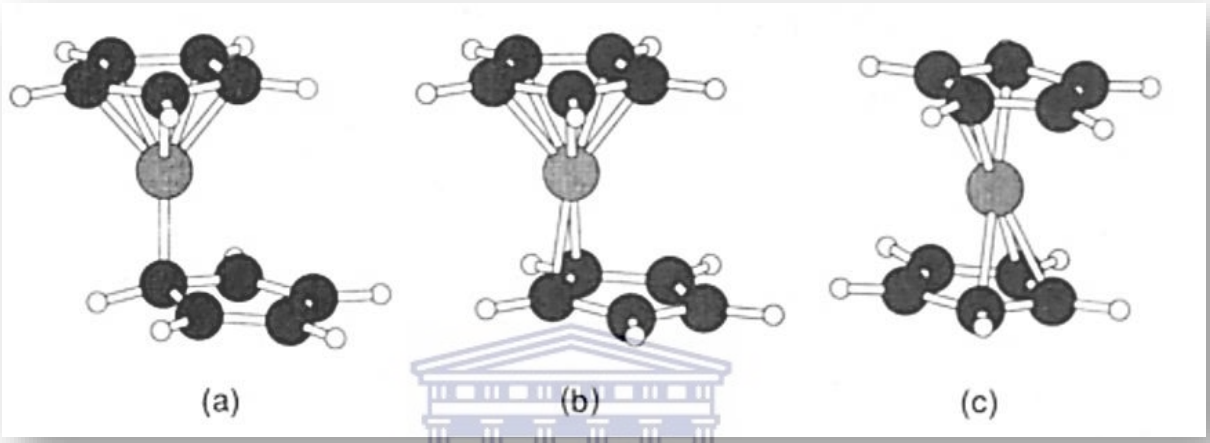

Figure 2.3: *Slip-sandwich conformation of beryllocene for C_s symmetry and gas phase where: (a) represents ground state geometry (η^1/η^5) whereas (b) and (c) transition states for the intramolecular transformation of beryllocene of the η^2/η^5 and η^3/η^3 bonding modes respectively (Almenningen et al., 1979; Margl, & Schwarz, 1994).*

The group 14 sandwiches represent the most extensive series of isolated main group metallocenes and present interesting structures. Metallocenes compounds of group 14 form either σ − or π-bonded structures as well (Burkey & Hanusa, 1995). This time the bonding of the metallocenes is determined by the oxidation state of the element as well as opposed to the metallocenes of group 13. In the high oxidation state elements, σ −bonded compounds are preferred while low oxidation state elements have a tendency or preference to form π-bonded Cp' groups. Compounds formed within the group are germanocene, stannocene and plumbocene and are easily accessible in various forms of compounds (Armstrong *et al.*, 1997; Jutzi & Burford, 1998). For example, the lead (Pb) compounds are often polymeric or

oligomeric in the solid state and this is because of the large size and low electronegativity of the atom (Stone & West, 1986; Beswick *et al.*, 1998; Jutzi & Burford, 1998; Layfield *et al.*, 2002; Thayer, 2010; Macdonald, n.d). Figure 2.4 shows a typical polymer structure of plumbocene. Monomeric gaseous phase structures of plumbocene can be obtained by substituting Cp groups in a polymer structure (Stone & West, 1986). Similar polymer compounds are also found in heavy s-block compounds, for example Cp_2Ba. Silocene is however an exception within the group 14 metallocenes as it has one known isolated derivative, Cp_2^*Si. This is attributed to the difficulties associated with the stabilisation of a divalent silicon centre. This compound could have bent or parallel rings in the same crystal whereby the latter structure is due to the small size of Si. Cp_2^*Si is found to be a very reactive metallocene and has a rich insertion and oxidation chemistry with both main group and transition metal compounds. In almost every case, the reaction is driven by the need for the Si(II) to become oxidised to Si(IV) (Jutzi 1989; Macdonald, n.d).

Group 13 cationic metallocenes have isoelectronic slip-sandwich structures similar to the neutral s-block metallocenes of the group 2. Various structures of these metallocenes have been synthesised along the group and diverse structural behaviours in cationic structures of B, Al and Ga among the group are reported (Kwon & McKee, 2001, Macdonald *et al*., 2008). Again all this variation in structures among the group 13 is also attributed to the oxidation state of the element. (Dohmeier *et al.*, 1993). Because of the vacant valence orbitals on high oxidation state of group 13 centres, one would presume that the metallocenes bonding of these elements will support the π-coordination of Cp' ligands. However, this is not the case. Only σ-bonded cationic metallocenes compounds are reported which are somehow stable at certain conditions. For example, Bochmann & Dawson (1996) reported the parent aluminocenium cation metallocene from oxidation state 3 (MIII), and this cationic metallocene is known in industry as an effective initiator for olefin polymerisation of isobutane. The compound is however only stable at low temperatures (Bochmann & Dawson, 1996; Pugmire *et al*., 2001).

Another interesting cationic of this group is boron (B), which has an interesting bonding structure. This brought interest to researchers in the field to conduct intensive structural investigation on B analogue using technologies such as NMR and crystallographic. Findings from the results confirmed that the Cp^* of the ring have σ-Cp, π-Cp interactions (Jutzi & Burford, 1998; Voigt *et al.*, 2000; Macdonald, n.d). This type of interaction was predicted to

occur in the beryllocene structure which was not the case. Such ring interactions were not expected to occur for this metallocene since it has smallest ring-ring distance as compared to any bis Cp' compound in the periodic table. Voigt and the team even refer to it as "the most tightly squeezed metallocenes" (Voigt *et al.*, 2000). The gallocenium (Ga) cation is much more difficult to synthesise in the group 13 analogues (Jutzi & Burford, 1998; Macdonald, n.d). But the compound of gallocenium cation also has σ-Cp, π-Cp structure like borocenium cation as opposed to the D_{5d} type structure observed in Cp_2^*Al. The high electronegativity in Cp_2^*Ga contributes to this slip-sandwich structure (Robert & Caserio, 1977).

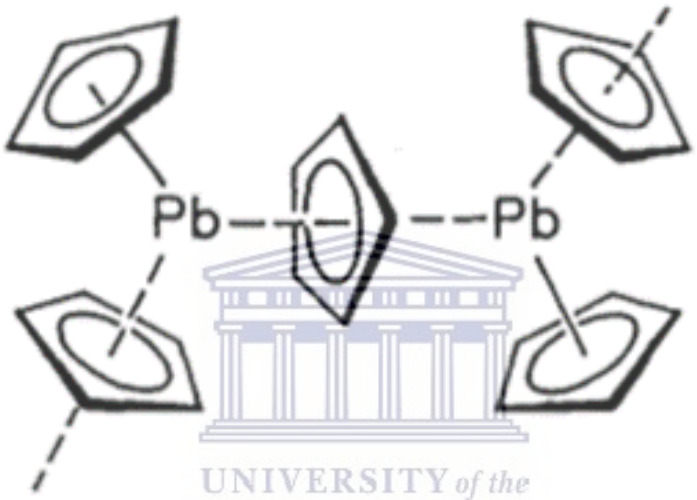

Figure 2.4: *The branched polymeric structure observed in the solid state for the sandwich metallocene of Cp_2Pb. The structure reveals a tricoordinate environment for each lead centre composed of two μ- π-Cp ligands (dashed lines) and one terminal Cp ligand (solid line) (Stone & West, 1986; Jutzi & Burford, 1998; Layfield et al., 2002).*

2.2.4 Transition metal and rare earth metallocenes

The first recorded metallocenes in the history of organometallic chemistry is ferrocene synthesised from the transition element, Fe. This resulted in a series of investigations and synthesis of metallocenes compounds from the transition metals (Chirik & Bercaw, 1998). These developments of metal cyclopentadienyl ligands compounds extended the scope of the organometallics for their application in many fields. For example, in the group 3 metallocene,

organoscandium compounds were less favourable until the soluble metallic ring compounds of Sc were developed (Melson, 1975; Arnold *et al*., 1998; Mountford & Ward, 2003; Henderson *et al.*, 2004). From the lanthanide elements, the only stable divalent metallocene are those of the elements of Sm, Eu and Yb (Arnold, 1998).

Group 3 metallocene complexes have been reported and prepared in various methods. Metal vapour synthetic techniques have afforded a variety of reactive, low valent organometallic complexes of group 3 and the lanthanide elements. This technique remains the only route to zero-valent molecular lanthanide complexes. Another, promising possible reported method of synthesis is the cyclisation reactions undergone by 2,2-dimethylpropylidynephosphine at metal atoms during co-condensation reactions. The choice of metal in this route of synthesis clearly dictates the nature of ring or rings to be formed. For example, the cyclisation method has been applied to the synthesis of vanadium complex five phosphaalkyne units, resulting in the isolation of sandwich complexes such as [V(η^5-$P_3C_2Bu^t_2$) (η5-$P_2C_3Bu^t_3$)]. Scandocene complexes have been prepared in similar procedure as the vanadium complexes by condensation of electron beam vaporised scandium with an excess of Bu^tCP. This is followed by flash sublimation for separation of a dark purple microcrystalline [Sc (η^5-$P_2C_3Bu^t_3)_2$]. And by repeated sublimation and removal of by-product, this yielded the forest-green triple-decker complex [(η^5-$P_3C_2Bu^t_2$) Sc (μ-η^6: η^6- $P_3C_3Bu^t_3$)Sc(η^5-$P_3C_2Bu^t_2$)]. The compound is presented in Figure 2.5 (Arnold, 1998; Chirik & Bercaw, 1998; Mountford & Ward, 2003; Henderson *et al.*, 2004). Rogers *et al.*, (1981) reported that the first Cp_3Y, was prepared by Birmingham and Wilkson. Cyclopentadienyl derivative of yttrium with the crystal structure of the THF adduct, (THF)Cp_3Y, has since been reported as well. The lanthanum (La) complex can also be synthesised in a similar manner in a THF adduct structure and has been identified as a zig-zag polymeric material in which metal ion is coordinated in the η^5 fashion to three Cp ligands and η^2 –coordinated to a fourth Cp ring (Rogers *et al.*, 1981; Chirik & Bercaw, 1998).

Unfortunately, the sterically hindered tris(cyclopentadienyl) complexes do not offer much opportunity for catalytic activity, more attention has been devoted to the preparation of bis (cyclopentadienyl) complexes of yttrium (Chirik & Bercaw, 1998; Bochkarev, 2004). Alkyl and hydride derivatives have received the most attention, due to their function as homogeneous catalysts. Unlike for the organoscandium analogues, use of the sterically demanding pentamethylcyclopentadienyl ligand generally does not produce monomeric

yttrocenes free of coordinated salts or Lewis bases. For instance, reaction of YCl_3 with 2 equivalents of KCp^* in THF results in the formation of $Cp_2^*YCl_2K(THF)_2$ (Eppinger *et al*., 2000; Hou & Wakatsuki, 2003). The neutral metallocenes alkyl and hydride derivatives of the group 3 are mostly used in the investigations of the mechanisms of chain initiation, propagation and transfer without the co-catalysts such as methylalumoxane (MAO) and the possible complications of ion pairing effects in the process. As a result, detailed studies into the rates, enantioselectivities and α agnostic assistance for olefin insertion have been performed with group 3 and rare earth metallocenes (Chirik & Bercaw, 1998; Eppinger *et al*., 2000).

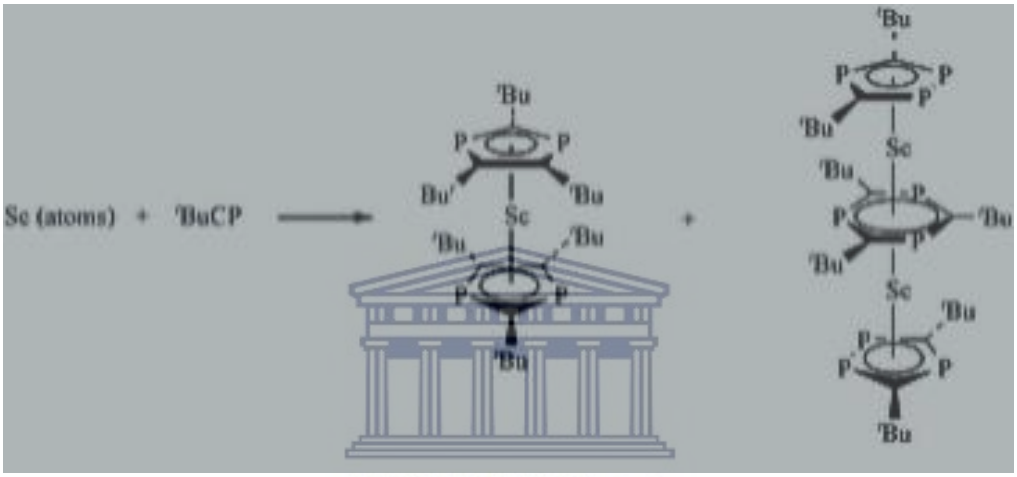

Figure 2.5: *An image of dark purple microcrystalline scandocene complex [Sc (η^5-$P_2C_3Bu^t_3)_2$] and a triple decker scandocene complex obtained after repeated sublimation [(η^5-$P_3C_2Bu^t_2$) Sc (μ-η^6: η^6- $P_3C_3Bu^t_3$) Sc (η^5-$P_3C_2Bu^t_2$)] (Arnold, 1998; Royo & Ryan, 1998; Mountford & Ward, 2003; Bochkarev, 2004).*

The fact that the olefin polymerisation is initiated at titanium–carbon bond increased the importance of the chemistry of this class of compounds. In addition titanium is favourable because of its distinction in Ziegler–Natta catalysis. Organozirconium compounds have received attention later after some developments (Wailes *et al*., 1974) in olefin polymerisation. In many cases titanium and zirconium form similar types of compounds, but these compounds differ in their chemical behaviour. Methyl derivatives of zirconium, for example, are far more sensitive to hydrolysis than the corresponding compounds of titanium, whereas the latter are more sensitive to thermal decomposition. Other differences have been noted in the cyclopentadienyl derivatives. For instance in zirconium, the oxygen-bonded ligands in compounds of the type $Cp_2Zr(OR)X$ (where Cp is π-cyclopentadienyl), are to

effect a decrease in the stability of one of the cyclopentadienyl groups to such an extent that solvolysis or insertion of SO_2, NO, etc., can occur. No such effect is noted with the corresponding titanium compounds even under the same conditions. Coming to hafnium although it has not received little attention, it seems that the chemistry of its organo derivatives is as closely related to that of zirconium as its inorganic chemistry.

The thermal instability of alkyl transition metal compounds was originally attributed to natural weakness in the metal–to–carbon bond. Thermodynamic and spectroscopic data suggests, however, that there is no reason that transition metal–to–carbon bonds are any weaker than bonds from main group metals to carbon (Wilkinson, 1973). It was concluded that the instability of transition metal alkyl and aryl derivatives is contributed by superficial decomposition by low activation energy pathways (Arnek & Zetterberg, 1987) such as α and β elimination of metal hydride, homolysis, or coupling of ligands at the transition metal atom. Cyclopentadienyl derivatives of titanium and zirconium were among the first of this type to be prepared (Wailes *et al*., 1974). As a result bis (cyclopentadienyl) titanium and zirconium halide have been available since then and the organometallic chemistry of these metals is reported to be evolved in these compounds. In bis (cyclopentadienyl) derivatives of titanium, zirconium and hafnium, the angle subtended at the metal atom by the centres of gravity or centroids, of the cyclopentadienyl rings are normally around 130˚. The structure of these compounds is therefore essentially tetrahedral. Typical structures of tetrahedral of these compounds have been found in the tetracyclopentadienylzirconium and that of hafnium.

Wilkinson and Birmingham (1954) reported bis (η^5- cyclopentadienyl) dihalozirconium complexes [Zr (Cp_2) X_2, X=Cl, Br] as some of the earliest examples of organozirconium compounds. Today, zirconium is one of the most widely used transition metals in organic synthesis, although it still lags behind copper and palladium in terms of versatility and frequency of use. However, the chemistry of organohafnium compounds has proved to be useful for the investigation of the structural and mechanistic aspects of both organozirconium and hafnium compounds (Negeshi & Takahashi, 2003). Negeshi and Takahashi (2003) compiled various known and possible organozirconium and organohafnium compounds according to:

- "The nature of Zr–C and Hf–C bonds, i.e. π– and/or σ–bonding and hapticity".

- "The formal oxidation state of zirconium and hafnium metal. Since many of these compounds contain more than one type of carbon ligand, the complexes are prioritised according to which of their ligands have the highest hapticity and the organisation is independent of the M–L bond being formed. Besides, the majority of well-known organozirconium and organohafnium compounds are derivatives of zirconocene and hafnocene, respectively".
- "As with many organometallic compounds, several methods are also applicable to the preparation of organozirconium and hafnium compounds. Those most frequently used are synthesis by complexation with neutral donors or π-donors (oxidative complexation), by transmetalation, hydrometalation, or carbometalation and oxidative addition (Negeshi & Takahashi, 2003) ".

Generally free titanocene [Cp_2Ti] is a 14 electron species and is too reactive to be isolable and due to this, it forms *ansa* titanocene complexes (Liard *et al.*, 2001). The chemistry of titanium is characterised by its multiple oxidation states and the available oxidation states of titanocene are +2, +3, +4 (Figure 2.6). Organometallic compounds of Ti(III) are said to be paramagnetic and are reported to be used in wide applications. They are used in applications like in water splitting to hydrogen and oxygen for neutral carbon energy supply (Beckhaus, 1998; Godemann *et al.*, 2015).

It is reported that the bright green titanocene was firstly obtained by Wilkinson and Fischer in 1956 from the reaction of $TiCl_2$ with NaCp which marked the discovery of one of the most extensively utilised complex systems in organotransition metal research (Freitag & Gordon, 2002). Ever since the titanocene complexes are currently synthesised by introducing the Cp ligands using the salt metathesis reaction. Their common derivatives of titanocenes, e.g. [Cp_2TiCl_2] are available by various reported possible synthetic methods (Wailes *et al.*, 1974; Beckhaus, 1998):

- Higher yields of up to 65% were reported somewhere else (Sazler, 1999) via $TiCl_3$ treated with Cp^*Na or Cp^*Li in dimethoxyethane solution and then further oxidised with hydrochloric acid.
- The use of cyclopentadienyl-substituted tin compounds to prepare monocyclopentadienyl transition metal complexes for the synthesis of $CpTiCl_3$ and

related compounds (. The very same method is used for selective and high yielding preparations of mixed ring complexes such as [Ti (η^5-C_5H_5) (η^5-C_9H_7)Cl_2] and [Ti(η^5-C_5H_5)(η^5-$C_9H_4Bu^t$)Cl_2].

- The use of lead dichloride ($PbCl_2$) as an oxidising agent for the preparation of mixed L_2TiCl_2 or substituted derivatives showing functionalised side arms. $PbCl_2$ is used as a reagent to oxidise a wide variety of tetravalent [Cp_2^* TiR] complexes to their tetravalent analogues.
- Amine elimination reactions from titanium amides and Cp-H for the synthesis of [$CpTi(NMe_2)_3$] from [$Ti(NMe_2)_4$] and Cp-H (Wailes *et al.*, 1974; Beckhaus, 1998).

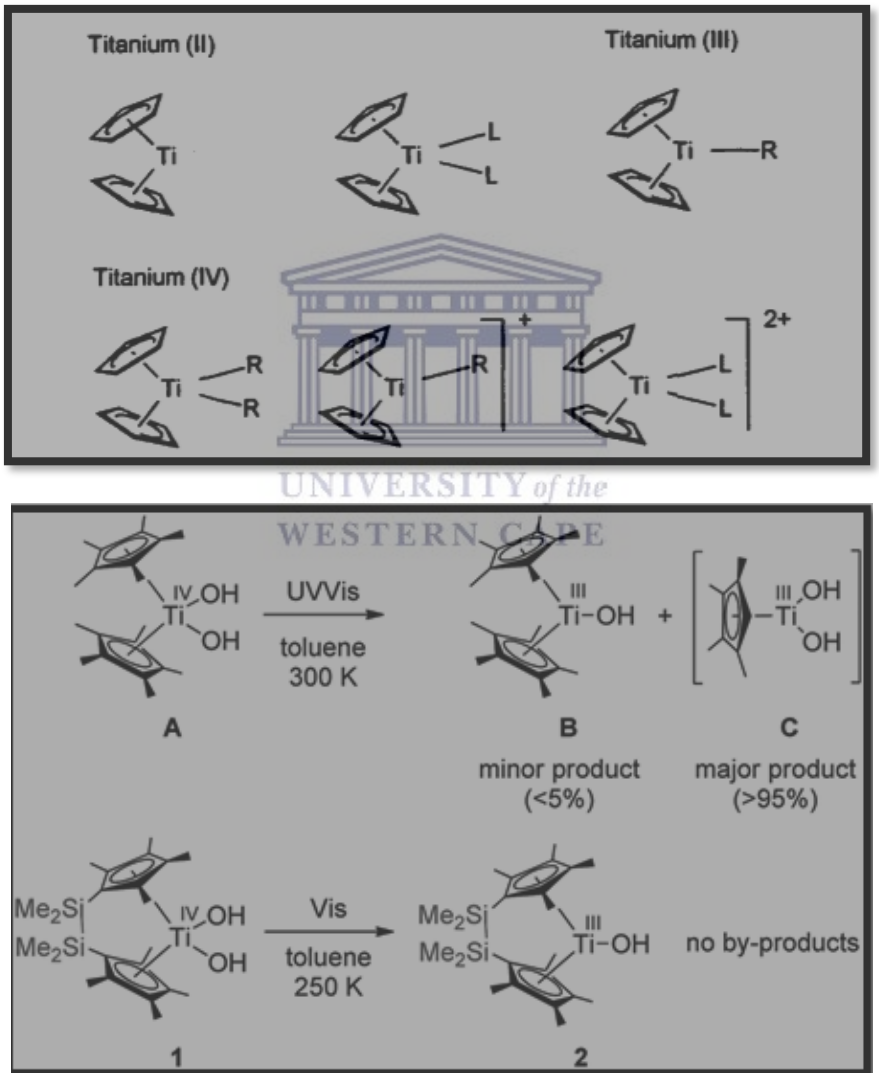

Figure 2.6: *General ligand and structure type of titanocene complexes of +2, +3 and +4, (top) (Beckhaus, 1998). Titanocene compounds of oxidation states +3 and +4, (bottom) (Godemann et al., 2015).*

2.2.5 Group 5 and group 6 metallocenes

Metallocenes in general are sandwich metal complexes with two parallel cyclopentadienyl rings coordinated to a central atom. In other cases cyclopentadienyl rings are not parallel but slightly bent due to attractive van der Waals forces between the rings. There are those metallocene compounds that coordinates with one or more additional substituents to form bent bis (cyclopentadienyl) complexes (Royo & Ryan, 1998). Group 5 metallocene have not received much attention as group 4 metallocenes. Among the group 5, vanadocene complexes have received much attention the same way as the group 4 metallocenes while niobium and tantalum compounds have received less attention. Group 5 organometallic compounds are considered as being reactive compounds as they obtain 15 electrons as oppose to 18 electron rule (Royo & Ryan, 1998; Galletti & Pampaloni, 2010). Niobium and tantalum are the most reactive compounds of the group when compared to vanadium which is much less reactive. The viable method for the synthesis of neutral metallocenes in group 5, for example, is through metathesis reaction of vanadium (II) halides using alkali cyclopentadienides to transfer the cyclopentadienyl rings (Royo & Ryan, 1998). Niobium and tantalum metallocenes are also synthesised through the same method (Royo & Ryan, 1998). It has also been mentioned that application of group 5 metallocenes is limited especially in catalytic polymerisation due to their low catalytic activity especially for Nb and Ta complexes (Galleti & Pampaloni, 2010). Galletti and Pampaloni (2010) have done some work on niobimium cyclopentadienyl complexes (half sandwiched complexes) as catalytic precursors for polymerisation of olefins and they also experienced the low activity in polymerisation as reported before.

Royo and Ryan (1998) reported possible complexes of group 5 and 6 metallocenes and their synthesis. In group 5 metallocenes, vanadium (II) species are normally produced by reducing $[VCl_3(THF)_3]$ with agents such as Li $[AlH_4]$, Zn or the alkali metal cyclopentadienide when used in excess under reflux. Other vanadium (II) compounds such as $[VCl_2(THF)_6]$ or $[V_2Cl_3(THF)_6]_2[Zn_2Cl_6]$ have also been used. The reported vanodocenes include compounds containing variously substituted cyclopentadienyl rings such as C_5H_5, C_5D_5, C_5H_4R (R=Me, Pr^i, Bu^n, Bu^t, Et) etc. The dinuclear bis (fulvalene) derivative $[V_2(fulvalene)_2]$, a dark purple pyrophoric solid and complexes containing mixed cyclopentadienyl rings [VCp (C_5H_4R](R=

CMe_2Ph, CHMePh) have been isolated. All of these complexes were reported to be thermally stable, air sensitive, red to purple oils or crystals; those containing substituted rings had lower melting points and were more soluble and more air sensitive. The niobium and tantalum derivatives were found to be less stable when compared with other vanadium complexes. For example, the reactive niobocene complex was formed by H abstraction from H_2 reductive elimination reaction of $[NbCp_2H_3]$ and by the reduction of $[NbCp_2Cl_2]$ with sodium naphthalenide (Royo & Ryan, 1998).

Group 6 metallocene have 16 electrons and through the redox reaction of the neutral compounds of group 6 metallocene, anionic and cationic metallocene are produced. Beginning with the chromium metallocene synthesis, the 16-electron neutral chromocene derivatives are obtained by reaction of a previously reduced chromium (II) species such as $CrCl_2$ or $[Cr_2 (\mu\text{-}OAc)_4]$ with alkali metal cyclopentadienides (Figure 2.7). Similar reactions with appropriate alkali cyclopentadienide salts have been used to prepare the ring–substituted, indenyl, and fulvalene dinuclear derivatives and related complexes containing bridged bis (cyclopentadienyl) ligands (Royo & Ryan, 1998). The chromium derivatives, obtained as red solids, are more accessible since they are thermally stable and less reactive than those of the heavier metals. Heavier metallocenes from W and Mo are reported to be synthesised via photochemically induced elimination of neutral ligands from $[MCp_2(CO)]$ (M=Mo, W) and $[WCp_2(C_2H_4)$ or similar reductive elimination from $[MCp_2H_2]$ or $WCp_2(CH_3)H]$ (Royo & Ryan, 1998).

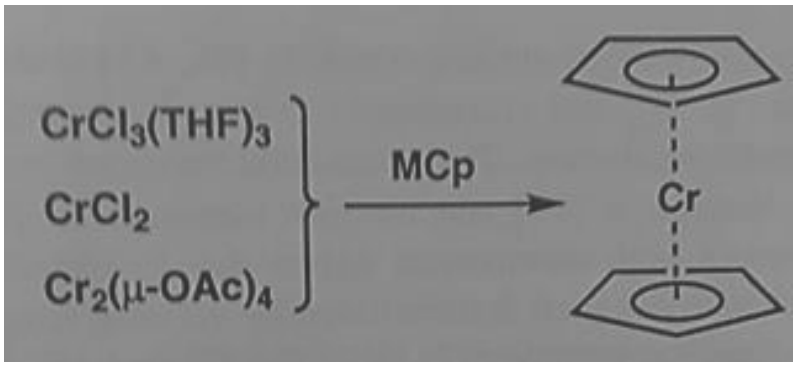

Figure 2.7: *The structure showing the synthesis of a neutral 16-electron chromocene derivative (Royo & Ryan, 1998; Togni & Halterman, 1998).*

2.2.6 Lanthanocenes and actinocenes

Lanthanocenes are considered to be trivalent compounds whereas actinocene are tetravalent compounds (Liu *et al.*, 1997; Green, 2000). The organometallic chemistry of the lanthanocenes and actinocenes, the *f* elements compounds has attracted the attention of both the experimentalists and the theoreticians due to their so called bis[8] annulene metal sandwich complexes M(C_8H_8) ((Liu *et al.*, 1997). Actinocene have not found that much attention, for example uranocene since there are no application for the complex.

The organolanthanide chemistry genesis started when Wilkinson and Birmingham (1954) described the tris (cyclopentadienyl) lanthanide complexes, $L_n(C_5H_5)_3$, from a reaction of YCl_3 and NaCp. However, the development of this area of organometallic chemistry was relatively slow due the instability of organolanthanide compounds towards moisture and oxygen (Edelmann, 1998). Edelmann (1998) reported the synthesis lanthanocene (II) compounds via different routes. Beginning with the ammonium route since most of the rare earth metals can be dissolved easily in liquid ammonia. Eu $(C_5 H_5)_2$ was first obtained by reacting the blue solution of Eu metal in liquid ammonia with cyclopentadiene (Edelmann, 1998). The base free material was obtained by heating the initial produced ammonia adduct to 200 ºC under high vacuum followed by the vacuum sublimation of the thermally highly stable product at 400 ºC. The behaviour of Eu $(C_5H_5)_2$ illustrates the typical properties of most organolanthanide complexes. The compound is thermally extremely stable while it rapidly decomposes in the presence of traces of oxygen. Yb $(C_5 H_5)_2$ too has been prepared by adopting the same ammonia route (see reaction 2.1) (Edelmann, 1998).

$$Ln + 3C_5H_6 \xrightarrow[2.\ subl.]{1.\ NH_3(l)} Ln(C_5H_5)_2 + C_5H_8 \qquad (2.1)$$

Other synthetic routes of lanthanocene (II) complexes are using THF solution which yields $Ln(C_5H_5)_2THF$ adducts (reaction 2.2) (Edelmann, 1998). For this route, an elegant transmetallation reaction starts with the metal powders of (L_n=) Sm, Eu or Yb which are treated with Hg $(C_5 H_5)_2$.

$$Ln + Hg(C_5H_5)_2 \xrightarrow{THF} (C_5H_5)_2Ln(THF)_n + Hg \qquad (2.2)$$

Similarly, Yb reacts with $Tl(C_5H_5)_2$ in DME solution to give $(C_5H_5)_2$ Yb (DME) (reaction 2.3) (Edelmann, 1998).

$$Yb + 2\,TlC_5H_5 \xrightarrow{DME} (C_5H_5)_2\,Yb(DME) + 2Tl \quad (2.3)$$

The most straightforward access to $Sm(C_5H_5)_2$ involved the reaction of SmI_2 with two equivalents of sodium cyclopentadienide (reaction 2.4) (Edelmann, 1998).

$$SmI_2 + 2Na(C_5H_5)_2 \xrightarrow{yields} Sm(C_5H_5)_2 + 2NaI \quad (2.4)$$

The actinocene synthesis were not much developed until the late 1960s where Streitwieser and Müller-Westerhoff (1968) prepared the first linear sandwich of cyclooctatetraene uranium, $(Cot)_2U$ complex, uranocene, of the f element (Streitwieser & Müller-Westerhoff, 1968; Berthet *et al*., 2013). Seyferth (2004) reported that other actinocene of actinides were also synthesised successfully in laboratories in the USA and Europe since then. The transuranium research laboratory at Oak Ridge National Laboratory extended the research further on to transuranium radioactive elements of berkelium and californium tricyclopentadienyl complexes. The preparation method used for the synthesis was radiochemical for Np tricyclopentadienly complex (Seyferth, 2004). A different approach was used for the synthesis of tricyclopentadienylplutonium which reported to find the extensive use during the synthesis of other transuraniun metal cyclopentadienyls. The reaction for the method used is displayed in reaction 2.5.

$$2PuCl_3 + 3(C_5H_5)_2\,Be \rightarrow 2(C_5H_5)_3\,Pu + 3BeCl_2 \quad (2.5)$$

2.2.7 Industrial application of metallocenes

Metallocenes have found uses in a wide variety of chemical and industrial applications since their discovery in 1951 and some of the uses have been mentioned in the beginning of this chapter (Cliffton & Carter, 1989; Hamielec & Soares, 1999). Around all the fascinating organometallic chemical aspects in metallocene catalysis, the key aspect which earned them their enormous industrial research focus is their use of group 4 metallocene catalysts. One of the remarkable examples of metallocenes catalysis is the polymerisation of cyclic olefins

without ring opening (Janiak, 1998). Therefore, bis (cyclopentadienyl) group 4 metal complexes are currently introduced in industry as a new generation of Ziegler-Natta catalysts for the polymerisation of olefins. Ziegler-Natta catalyst means the rapid polymerisation of ethane and α-olefins with the aid in the coordination sphere of a metal catalyst, operating at low pressure and low temperatures (Cossee, 1964; Boor, 1979, Janiak, 1998). Among the group IV metallocenes of titanium, zirconium and hafnium, the zirconocene complexes deserve the most interest, academically and industrially. For instance the titanocene catalysts are unstable at conventional polymerisation temperatures while the hafnium systems are too expensive. Hence, the so called metallocene catalysts are mostly zirconocene derivatives with zirconocene dichloride being the parent system. Their development as useful polymerisation catalysts in industry, serve as the first large scale industrial application for the long recognised and well developed class of metallocene complexes (Togni & Halterman, 1998).

For example, ferrocene is used as an anti-knock addictive in motor fuels as well as a catalyst in reactions such as commercially important production of polyethylene. Furthermore, metallocenes derivatives can also serve as monomer units for production of various metallocene polymers and copolymers. Recently, interest has been spurred by their proposed application as sources for metallisation particularly by chemical vapour deposition methods (Pugmire *et al.*, 2001). However, there are several constraints placed on a material in order for it to be effective source for the selective area deposition of metal where the selectivity is control by electron or photon stimulated deposition. The material serving as the metal-source must desorb molecularly from the surface in the absence of incident radiation to ensure deposition in desired areas only.

In the case of metal deposition from organometallic precursors, where organic ligands are used to volatilise the metal for transport to the substrate, the unbound ligands should be stable and easily desorbed both in the substrate material and on the deposited metal. If they do decompose on the substrate, their deposition products should desorb cleanly under mild conditions. This will allow for the production of contaminant–free metal features. For example, nickelocene has many favourable properties that give it good potential as a viable chemical vapour deposition (CVD) and selective–area CVD source. It is less toxic than many of its alkyl counterparts and is much less toxic than nickel tetracarbonyl which is commonly used for CVD of nickel. Furthermore, nickelocene is solid at a room temperature making it

easy to handle, purify and is stable to 573 K in an inert atmosphere (Togni & Halterman, 1998; Pugmire *et al.*, 2001).

Room temperature and vapour pressure for metallocenes are sufficient enough to allow effective transport of source material to the substrate. Due to this behaviour, nickel has been deposited in microscale patterns on silicon, silver and copper with photo or electron assisted decomposition. In the study report by Pugmire *et al.* (2001), scanning transmission electron microscopy was used to deposit Ni from nickelocene in 10 nm wide lines on a thin carbon film demonstrating that very fine control over spatial deposition can be exercised. When information on the composition of the nickel-deposition surface has been reported, use of nickelocene in CVD processes generally has been observed to include some carbon contamination within the metal film except in the case of threshold photolysis. While a number of studies have been reported on metal deposition using metallocenes as precursors, very little is known about the surface chemistry of metallocenes at the molecular level. A good understanding of the metallocenes surface properties is necessary in order to maximise the controllability of decomposition, minimise contamination and tailor precursors and conditions to optimum deposition efficiency. A very important piece of information in the understanding of nickelocene surface chemistry is the role that substrate reactivity plays in order to answer:

- "What effects does surface reactivity play on the thermally induced metal-ligand bond cleavage of adsorbed nickelocene (Pugmire *et al.*, 2001)?"
- "Does surface reactivity affect the fragmentation, if any, of the cyclopentadienyl, or of its decomposition fragments (Pugmire *et al.*, 2001)?"

As much as cyclopentadienyl compounds (metallocenes) have been used successfully for CVD but sometimes their high volatility makes them less favourable candidates for the method. This high reactivity and thermal stability make them favourable for atomic layer deposition (ALD), whereby high reactivity is reported that it can be controlled by sequential pulsing of the precursor material (Putkonen & Niinistö, 2005). Organometallic precursors, especially the metallocene compounds have been reported also by Putkonen and Niinistö (2005) as precursors for ALD for thin film growth. This finding is considered as the advancement of the CVD method. Group II and IV metallocene derivatives and

tricyclopentadienyl compounds of lantanthanides have been utilised on ALD for the synthesis of thin films.

Ferrocenetriazole derivative are one of the systems that have potential applications in the field of nanoscience, conducting polymers, electrochemical detection and sensing, medical chemistry as a biosensing probes and a host guest chemistry. A ferrocene moiety is generally a preferred choice for electrochemical monitoring and organic hybrid devices due to its extensive stability and versatility in functionalisation (Kaminsky, 1998; Ganes *et al.*, 2011; Komero *et al.*, 2011; Francois, 2013). Metallocenes have found wide use in medicine, for example, they are used as anti-tumor drugs (Gomez-Ruiz *et al.*, 2012). Organometallics have a great structural variety, ranging from linear to octahedral and even beyond and by rational ligand design, provide control over key kinetic properties such as hydrolysis rate of ligands. Furthermore, they are kinetically stable, usually unchanged, and relatively lipophilic and their metal atom is in low oxidation state. Because of these fundamental differences compared to classical coordination metal complexes, organometallics offer ample opportunities in the design of novel classes of medicinal compounds, potentially with new metal–specific modes of action. Organometallics such as metallocenes, half-sandwich, carbine, CO, or µ-ligands also found application in medicinal chemistry. For example ferroquine is used for antimalaria, bent metallocenes of the transition metals used as anti-cancer complexes, as well as half sandwich complexes of Os (II) used as antitumor drugs (Koleros *et al.*, 2010; Gasser & Metzler–Nolte, 2011; Kaluderović *et al.*, 2011). The second-order optical nonlinearity metallocenes are reported to be used in devices for telecommunications, optical computing, optical storage and optical information processing (Calabrese *et al.*, 1991).

2.3 Determining the properties of organometallic ligands

2.3.1 The crystal and ligand field theory

The crystal field theory (CFT) provides a way of determining the electrostatic respects on how the energies of the metal ion orbitals will be affected by the set of surrounding atoms or ligand. This theory has been used to describe various spectroscopies of transition metal coordination complexes, in particular optical spectra (colours). CFT positively interprets

magnetic properties, colours, hydration enthalpies, and spinel structures of transition metal complexes, but it does not describe bonding (Cotton, *et al.*, 1986; Hartwig, 2010; Aguayo, 2016). CFT was combined with molecular orbital theory to form a ligand field theory (LFT), which delivers understanding into the process of chemical bonding in transition metal complexes. In the other hand, the ligand field theory refers to an entire body of hypothetical apparatus used to understand the bonding and linked to electronic properties of complexes and other compounds formed by the transition elements (Cotton, *et al.*, 1986; Hartwig, 2010). There are, however, two things that set the study of the electronic structures of transition metal compounds apart from the remaining body of valence theory. One is the presence of partly filled *d* and *f* shells. This leads to experimental observations unlikely possible in other cases, the paramagnetism, visible absorption spectra, and apparently irregular variations in thermodynamic and structural properties as some of the cases. Second is that the crystal field theory provides a powerful yet simple method of understanding and connecting all of those properties that arise from the presence of the partly filled shells. The metallocene comes to a 2-1-2 split: the orbitals in the xy plane (d_{xy} and $d_{x^2-y^2}$) barely occur in interaction with the Cp ligands and so are energetically favoured. The d_{z^2} orbital occurs only with a small quantity in the interaction and is in the middle. And the most destabilising orbitals d_{xz} and d_{yz} show entirely to the rings (Crabtree, 2005).

2.3.2 Molecular orbital theory

The crystal picture gives a qualitative understanding and molecular orbital theory (MO) gives an understanding of electronic structure widely by theoretical calculations (Mulliken, 1966; Crabtree, 2005). MO it further describes the photochemical behaviour of a molecule (Mulliken, 1966). For example, the properties of ferrocene, in terms of structure and stability could be fully described through molecular orbital theory. In the molecular orbital theory, as in the crystal and ligand field theory, interactions between the metal orbitals with the ligand orbitals are considered (Crabtree, 2005). As in the crystal field theory, the energy splitting of the orbitals is from the interactions between metal and ligand orbitals. This result to a molecular orbital diagram containing bonding, non-bonding and antibonding orbitals and this is shown in Figure 2.8, the MO diagram for ferrocene. From the diagram, if a ligand orbital of a Cp ring and a d-orbital of the metal interact, it creates two new molecular orbitals which splits into energetically bonding and an antibonding molecular orbitals. The strength of

splitting is said to be greater when the interaction between the ligand and the orbital is stronger. If there are no interactions, the corresponding energy orbital does not change and there is non-bonding orbital. Even with molecular orbital theory, the orbitals pointing toward the ligand are most affected. The more binding molecular orbitals are occupied with electrons, the stronger the bond between the metal and the ligand, and the resulting complex is stable. In 18-valence electrons, all bonding molecular orbitals are occupied and the complex has the highest stability (Royo & Ryan, 1998).

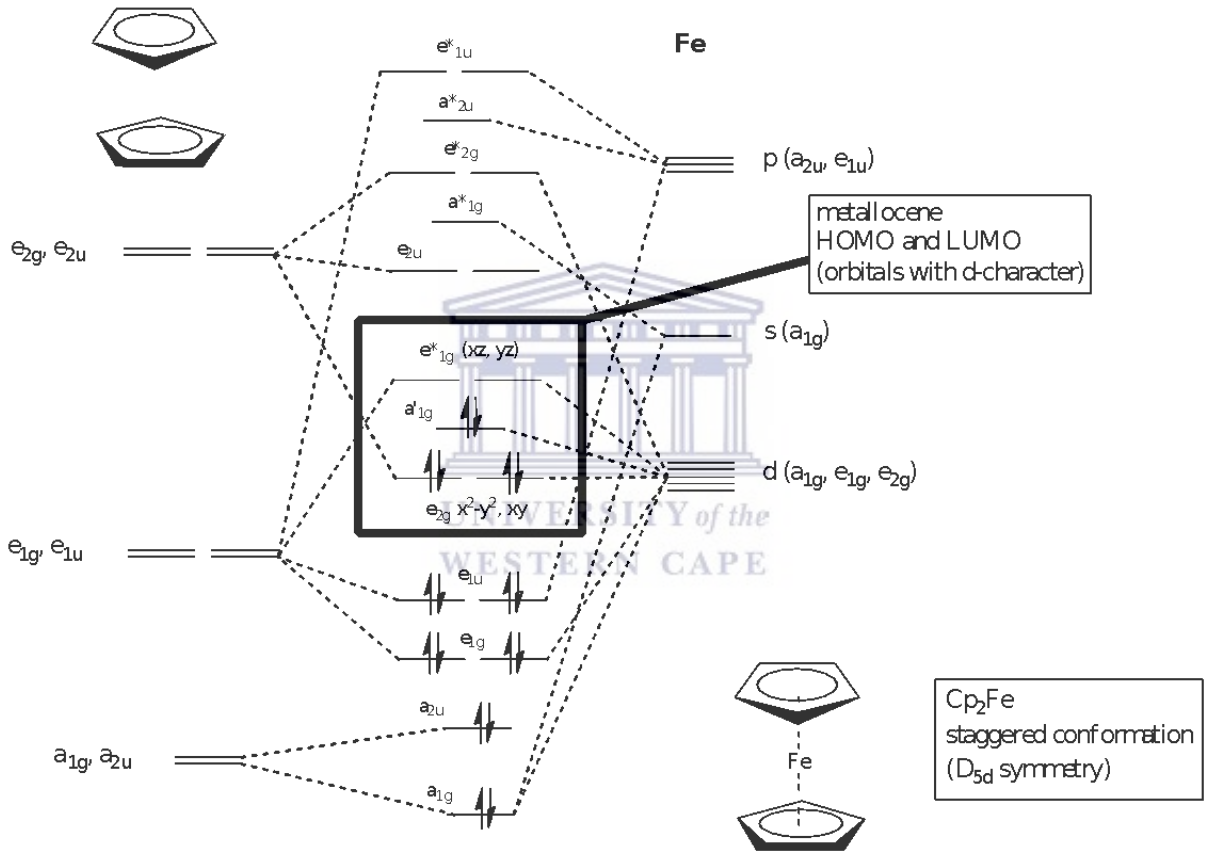

Figure 2.8: *The molecular orbital diagram of ferrocene (NPTEL, 2016).*

2.3.3 Organometallic chemistry of nickel

The organometallic chemistry of nickel started back during the preparation of nickel carbonyl [$Ni(CO)_4$] for the use in the Mond process for refining of nickel metal (Jolly & Wilke, 1974;

Kubiak, 1995). Nickel is the only metal which reacts significantly with CO at STP. In general, the chemistry of Ni is dominated by the divalent Ni^{II} and zerovalent Ni^{0} oxidation states although examples of Ni^{I}, N^{III} even Ni^{IV} are known. In the case of Ni^{I}, there is a tendency of disproportionation ($2Ni^{I}Ln^{+} \rightarrow Ni^{II}Ln^{2+} \rightarrow Ni^{0}Ln$). The strong tendency of nickel to form complexes with alkenes and alkynes has also led to the development of important organometallic processes for their oligomerisation (Kubiak, 1995). Although the organometallic chemistry of metal carbonyls is widely used, but the chemistry of zero-valent metal cyanide compound is much more limited. Many nitrogen donor ligand complexes of Ni^{0} are known. The addition of amine and pyridine–type ligands generally leads to unstable species. However, the use of chelating nitrogen donor, ligands such as 1,10-phemathroline or 2,82-bipyridine leads to stable complexes.

Nickelocene, Ni $(\eta^{5}\text{-}C_5H_5)_2$, is of central importance in the organometallic chemistry of cyclo-pentadienylnickel compounds. In addition, nickelocene is the only metallocene to have a 20-valence electrons configuration (Crabtree, 2005). The complexes of nickelocene have been prepared by a variety of methods but the convenient, famous laboratory synthesis are based on the addition of sodium cyclopentadienide to anhydrous nickel halides or alternatively the treatment of cyclopentadiene with hydroxide in the presence of Ni^{II} salts. As one of the chemical properties, nickelocene is soluble in most non-polar organic solvents and only in solutions where it is significantly sensitive to oxygen. The structure of nickelocene is reported to involve staggered cyclopentadienyl rings at low temperatures, although like most of the metallocenes, the actual structure is probably dependent on temperature and crystal structure packing (Jolly & Wilke, 1974; Seiler & Dunitz, 1980).

Differences in structural geometries of nickelocene versus ferrocene and cobatocene are the interplanar separation between cyclopentadienyl rings. In nickelocene it is 3.60 Å which is significantly longer than those found in ferrocene (3.32 Å) or cobaltocene (3.40 Å) (Seiler & Dunitz, 1980). All these differences are because of the electronic structure of nickelocene which places the two extra electrons into molecular orbitals of the nickel–cyclopentadienyl ring anti-bonding character. The anti-bonding orbital is doubly degenerate (e_{1g}) and hence nickelocene is a ground state triplet (μ_{eff} = 2.8913 m). The known rule of metallocenes having 18 valence electrons is that are stable and any NVE above 18 or below from the complex are instable. This fact explains why nickelocene oxidises easily, the NVE in nickelocene structure is 20 (Crabtree, 2005). The weak nickel-cyclopentadienly ring bonding

influences the chemistry of nickelocene. This is liberated by displacement of cyclopentadienyl ring. An extensive organometallic chemistry of nickel has been developed upon the displacement of the cyclopentadienyl rings. For example, the reaction of the two equivalents of nickelocene with Lewis or Bronsted acids results in the displacements of one cyclopentadienyl ring and the formation of the triple decker sandwich, Figure 2.9. Additionally, when nickelocene is treated with NO it results in the formation of the stable 18-valence electron complex, Ni (η^5-C_5H_5) (NO), a red liquid complex (Lauher *et al.*, 1976; Crabtree, 2005).

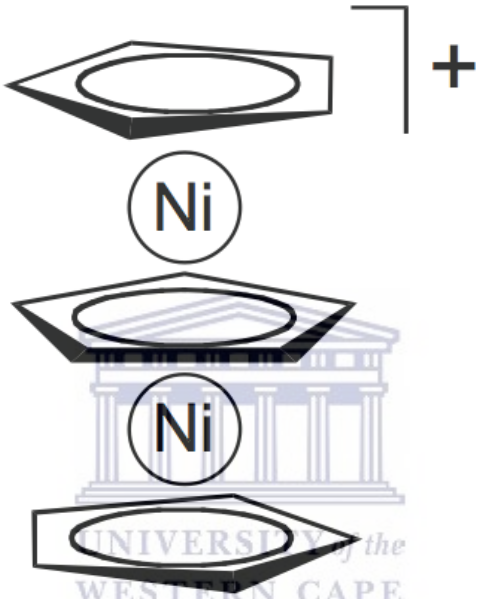

Figure 2.9: *Triple decker sandwich of nickelocene resulted after the reaction of two equivalents of nickelocene with Lewis or Bronsted acids (Lauher et al., 1976).*

This chapter covered metallocene complexes that could be formed from main group elements, transition metals, lanthanides and actinides. Since the MIVOC method uses organometallic compounds known to have high vapour pressure in room temperature. Figure 2.10 presents a modified reproduction of the periodic table illustrating which elements could be good candidates to form organometallic compounds (Leach, 2008).

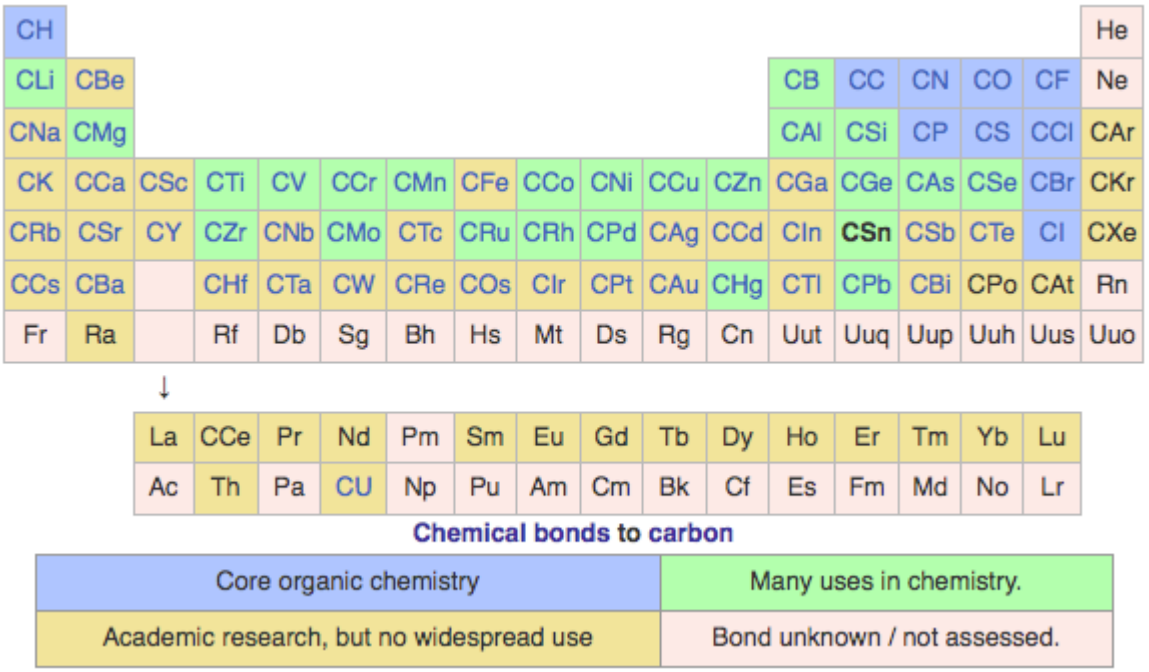

Figure 2.10: *Organometallic periodic table (Leach, 2008).*

Chapter 3 Particle Beam Production at iThemba LABS

One of the main objectives of the iThemba LABS is the operation of the Separated Sector Cyclotron (SSC) which provides beams of various ion species at energies ranging from 5 to 220 MeV/amu (Conradie, 1992). Accelerated beams are used for fundamental nuclear physics research, radioisotope production and medical physics applications.

The SSC is supported by two pre-accelerators which are solid pole cyclotron, referred to as SPC1 and SPC2. For the pre-acceleration of light ions, SPC1 has a maximum bending magnet power for 8 MeV protons, i.e. a cyclotron with a K-value of 8. It is equipped with an internal Penning Ionisation Gauge (PIG) source. This injector is dedicated for pre-acceleration of light ions. The second solid pole cyclotron, SPC2, with a K–value of 10 caters for heavy ion acceleration demand. SPC2 is similar to SPC1 except that it is equipped with different types of external ion sources, two Electron Cyclotron Resonance Ion Source (ECRIS) and the atomic beam source for nuclear spin polarised protons.

3.1 The Layout of the accelerator complex at iThemba LABS

Figure 3.1 gives an illustration layout of the facility of iThemba LABS. The first part of the facility is described by an example of H^+ acceleration to 66 MeV as used for neutron therapy and isotope production. A high–intensity proton beam is pre-accelerated to energy of 3.14 MeV in the light ion injector cyclotron, SPC1, and transported to the SSC through a transfer beamline with a provision for re–bunching of the beam, beam pulse length definition, beam emittance definition and energy selection. The beam is horizontally injected into the SSC and accelerated to energy of 66 MeV. The 66 MeV beam is directed with bending magnets and focused transversely with quadrupole magnets to a horizontal and vertical beam target station for the production of radioisotopes. The same beam is also directed to a vault for neutron therapy treatments. The intensities of the beam are typically 100 µA to 250 µA for isotope production and 30 µA for neutron therapy. Furthermore, for medical proton therapy the

particles are pre-accelerated in SPC1 to energy of 8 MeV and to a final energy of 200 MeV in the SSC.

The SPC2 injector cyclotron pre-accelerates beams of nuclear spin polarised protons or heavy ions. After acceleration in the SSC the beams are directed to nuclear physics experimental research vaults. Nuclear physics vaults consist of scattering chamber, the K600 magnetic spectrometer, the AFRODITE γ–ray spectrometer and a beamline for the production of neutron beams.

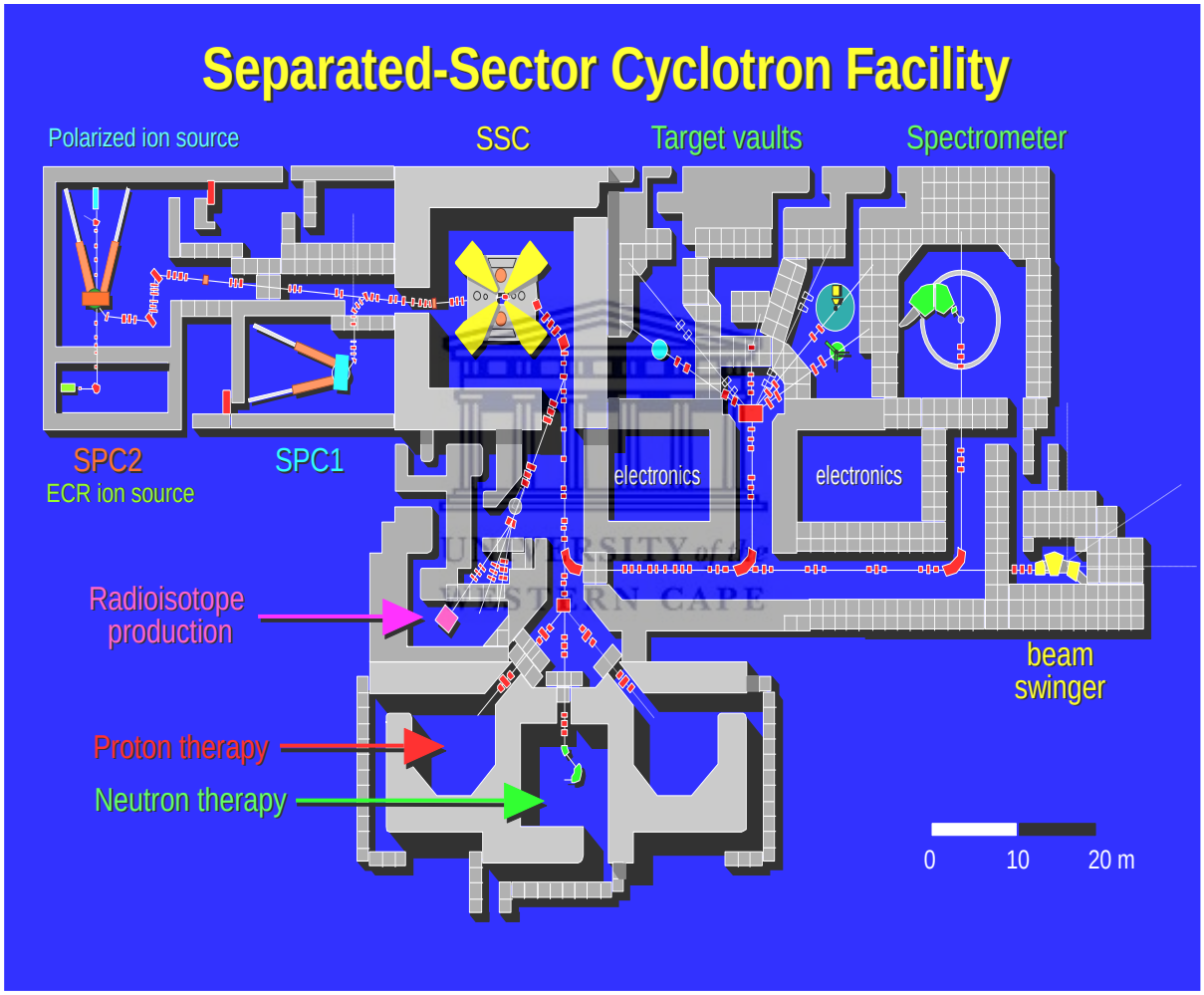

Figure 3.1: *The layout of iThemba LABS cyclotron facility. Light ions are pre-accelerated in the first solid-pole injector cyclotron (SPC1) for medical therapy and radioisotope production. The second solid-pole injector cyclotron (SPC2) is used for pre-acceleration of heavy ions and polarized protons.*

3.2 Electron Cyclotron Resonance Ion Source

This study focuses on the production of exotic beams at iThemba LABS, therefore further discussions and background on the ECR ion sources will follow. Ion beams have found wide application in scientific research to study the structure of matter, particle of interests and investigation of wide range of natural and exotic phenomena under laboratory conditions. They are also used in medicine for radiation therapy, in industrial material processing and analysis as well as radiation hardness testing of electronics (Geller, 1996; Brown, 2004). New developments in scientific research require higher beam energies and new ion species to expand the range of phenomena available for research studies. Higher beam currents are also required to make the observations of rare, low cross section reactions possible. Therefore, these requirements are a driving force for continuous ion source research and developments.

Nuclear physics uses a variety of isotopic ion beams to explore the properties of nuclei through accelerator driven nuclear reactions. These beams are accelerated after being produced in a dedicated ion source (Rubert, *et al.*, 2012). Electron Cyclotron Resonance Ion Sources (ECRIS) are favourable among other sources because of their reliability and long life time span between maintenance (Geller, 1996). In addition, most ion beams for experiments that are relevant for research in nuclear and atomic physics can be provided. Furthermore, they can deliver ions with high ionisation degree which is important for efficient acceleration.

In an ECR ion source ions are produced inside a plasma confined in an external magnetic field, and sustained with microwave radiation. Higher plasma density is one of the requirements to produce higher beam currents. The required electron energy for ionisation lies between 100 eV to 50 keV (Geller, 1996). In order to produce desired species, elements to be ionised need to be introduced into plasma volume to undergo ionisation and followed by subsequent extraction. Gas and liquid species can be introduced directly to the plasma for ionisation without difficulties. However, production of metallic beams is more difficult than producing the gaseous beams from materials. This is due to the fact that metals need to be vaporised or sputtered off before they are introduced into the plasma (Lu *et al.*, 2012). Based on this, the selection of the best method to feed the solid into the ECR ion source strongly depends on specific properties of materials (Rubert *et al.*, 2012; Bogomolov *et al.*, 2015).

There are several methods to provide solids and metals in gaseous form for ECR ion source production. Methods like oven heating, plasma sputtering; pulsed excimer laser and MIVOC are used for formation of gaseous elements for ECR ion source (Cheng, 1995; Cao *et al*., 2007).

3.3 The MIVOC method for the conversion of organometallic material

For the materials to be ionised in ECR ion source applications, some need to be prepared prior to their introduction in the plasma of the source. Other materials can be introduced directly to the plasma of the ECR ion source, known as direct plasma contact method. There are also available heating methods of materials to their vapour state that are currently used in ECR ion sources. These methods are oven heating and sputtering. The heating methods are however dependent on the physical and chemical properties of the materials to be heated. These methods have limitations and could not cover the whole scope of the materials to be used in ECR ion sources. For example, beams produced from transition metals are impossible to be produced with the aforementioned methods since these elements melts and vaporises at high temperatures. Problems with unstable beam are also encountered especially in plasma contact method since the metallic oxide materials are used for this method as the source of metal. The end results are the amount of uncontrollable oxygen ions in the plasma source. The downfall of the sputtering method is low beam intensities that are achieved with this method that are not more than 5 μA. Full descriptions of the methods are described in detailed by Cao *et al.* (2007) and Cavenago *et al*. (2009) including their advantages and disadvantages. The limitations mentioned, implied that alternative method to produce exotic beams from low vapour pressure metals at iThemba LABS are required and nickel as one of them. Nickel atoms are relatively challenging to produce by heating nickel substrate. This is due to nickel high melting temperature and low partial pressure at temperatures below 1000 ^{o}C. This problem could be circumvented by forming a metallocenes which can prevent the strong metallic binding of the Ni atoms and produces a sufficient vapour pressure at room temperature. Therefore, the focus of this research study is on MIVOC method as a technique for ECR ion source applications for the production of nickel beams.

The MIVOC technique was first developed in Finland for ECR applications (Koivisto *et al*., 1994; Cao *et al.*, 2007). Advantages of the MIVOC method for beam production are that it allows the production of most difficult beams that are impossible with other methods (Rubert *et al.*, 2012). For example, beams from metals like vanadium, chromium, cobalt and nickel can be produced with this method (Leherissier *et al.*, 2007). The reason being that in the MIVOC technique, solid state volatile metallic compounds produce vapour gas having metallic atoms even at room temperature (Bogomolov *et al.*, 2015). The technique involves a separate container which is loaded with the volatile compound and taken to 10^{-5} mbar to get rid of moisture and decomposed components. The vapour pressure of the metallocene is typically 10^{-5} to 10^{-4} mbar, which is sufficient for the molecules to enter the plasma chamber. Here, they are dissociated and ionised allowing extracting an intense beam of metallic ions. Beams with higher currents compared to other methods can be obtained with this method (Cao *et al.*, 2007). Furthermore, the MIVOC method has been demonstrated as very efficient to produce highly charged ion beams at the lowest consumption of the material (Sasaki, 2002; Rubert *et al.*, 2012). Nakagawa *et al*. (1997) did some comparison on beam intensities produced from precursor compounds using metallocenes and hexacarbonyls organanometallics. Metallocenes seem to produce higher beam currents than hexacarbonyls because of the six bonds on metal compared from hexacarbonyl which only has two bonds from the rings of the metallocenes (Nakagawa *et al*, 1997).

The challenge with the MIVOC method is that the organometallic precursor materials with a metal of interest are commercially available only for natural materials. As a result, isotopes with small abundances cannot be produced with sufficient intensities with natural material. Isotopically enriched organometallic materials have to be synthesised in small scale in the interested laboratories to produce isotopic metallic beams. Such exotic materials have been produced somewhere else with enriched metals like nickel, iron, vanadium, chromium, cobalt and ruthenium, etc., and have been used for beam production via the MIVOC method (Koivisto *et al*, 1994; Koivisto *et al.*, 1996; Koivisto *et al.*, 2002; Leherissier *et al.*, 2007; Rubert *et al.*, 2012). In the periodic table shown in Figure 3.2, the beam particles that are produced to date through the ECR ion source with organometallic materials using the MIVOC method are highlighted in cyan. Some of the enriched metal ion beams produced in

JYFL (Finland), GANIL (France) and JINR[1] (Russia) using metallocenes are also presented in Table 3.1.

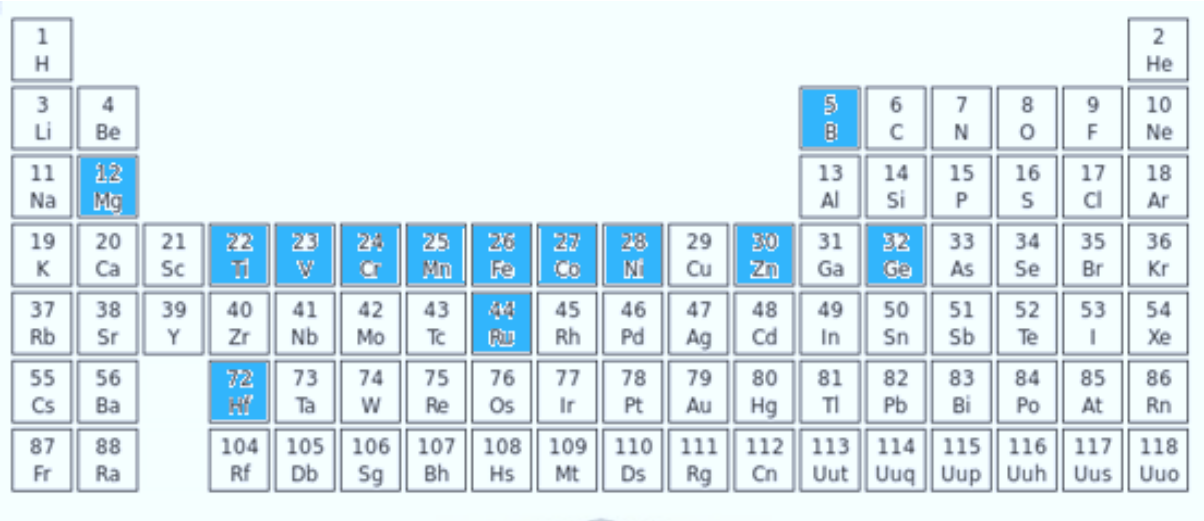

Figure 3.2: *Metallic beams produced via the MIVOC method to date are highlighted in turquoise in the periodic table of elements (Koivisto et al., 1994; Koivisto et al., 1996; Nakagawa et al., 1997; Koivisto et al., 2002, Cao et al., 2007; Leherissier et al., 2007; Rubert et al., 2012; Bogomolov et al., 2015).*

Table 3.1: *Some of the metallic ion beams poduced via MIVOC method using organometallic material with the enriched metal.*

Organometallic material	Beam	Institute	References
Ferrocene	^{54,56}Fe	JYFL	Leherissier *et al.*, 2007, Koivisto *et al.*, 1996
Magnocene	^{24,26} Mg	GANIL	Leherissier *et al.*, 2007, Koivisto *et al.*, 1996
Nickelocene	^{58,60}Ni	JYFL	Koivisto et al, 1994
Titanocene	^{48,50}Ti	FLNR, GANIL, JYFL,	Koivisto *et al.*, 2002,
Ruthenocene	^{102}Ru	GANIL	Leherissier, *et al*, 2006, status report

[1] JYFL: Department of Physics (JYFL), University of Jyväskylä in Finland; GANIL: The Grand Accélérateur National d'Ions Lourds, or Large Heavy Ion National Accelerator, in France; FLNR-JINR: Flerov Laboratory of Nuclear Reactions – Joint Institute for Nuclear Research in Russia

3.4 Electron Cyclotron Resonance Ion Sources at iThemba LABS

The acceleration of ion beams at iThemba LABS is achieved by using two dedicated types of ion sources whereby the ionisation of elements take place. The ionised elements are then extracted and pre-accelerated at either the first solid pole injector cyclotron (SPC1) or (SPC2) before being transferred to the SSC. The full description of the SSC is given by Conradie (1992). The current study is about the MIVOC method development for the vaporisation of metal species before being transported to the SPC2 solid pole injector shown in Figure 3.3. This is part of an upgrade for ECR ion sources in order to increase the number of ion beam species to be produced at iThemba LABS. ECR ion sources used at iThemba LABS for the production of ionised particles are the ECRIS4 and the Genoble Test Source GTS.

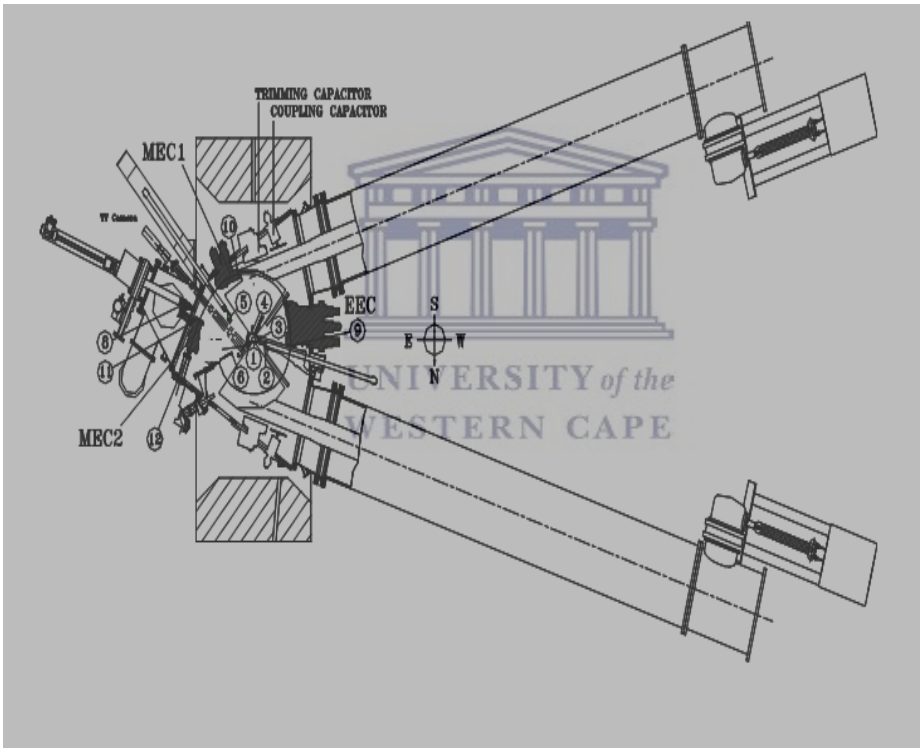

Figure 3.3: *The layout of the SPC2 pre-accelerator of iThemba LABS. 1: Inflector 1; 2: Probe 1; 3: RADAX slits; 4: Radial slit; 5: Probe 2; 6: Axial slit; 8: Harp; 9: Electrostatic extraction channel; 10: 1st magnetic channel; 11: 2nd magnetic channel; 12: Deflection magnetic channel.*

The Electron Cyclotron Resonance Ion Source 4 (ECRIS4) source has been used at iThemba LABS for beam production since June 2008 (Thomae *et al*., 2009). This source was

originally built at GANIL (Sortais, 1995) for the Hahn Meitner Institute (HMI) in Berlin, Germany (Waldmann & Martin, 1995). It was later donated to iThemba LABS (Thomae *et al.*, 2009). This source consists of a water cooled plasma chamber with a length of 18 cm and a diameter of 7 cm. The chamber is surrounded by FeNdB permanent magnets which produce a hexapole field of 1 T at the wall of the chamber for radial plasma confinement. Two solenoid coils produce an axial field which confines the plasma axially. The field on the axis typically varies from 0.4 to 1.1 T. The microwave power is coupled into the source via a wave guide and the coaxial coupling system. The generator can deliver up to 2 kW of microwave power at a frequency of 14.5 GHz. This is the ion source that will be used for beam production experiments in this research.

In addition to ECRIS4, the Genoble Test Source GTS in Figure 3.4, is another modern room temperature ECRIS used at iThemba LABS. The source is coupled to a 14.5 GHz and 18 GHz microwave generator. It has a provision for two ovens. The axial field can be varied between 0.5 T and 1.2 T by means of three solenoid coils and the radial field has a value of 1.3 T using FeNdB permanent magnets (Thomae *et al.*, 2009).

The arrangement of the two sources in the vault is shown in Figure 3.4. It allows for the simultaneously operation, i.e. the required beam for cyclotron acceleration will be delivered from one source while the other source can be used for beam development. The beam line for the ECRIS4 consists of a solenoid which focuses the beam extracted from the source into the focal position in front of the double-focusing 90° bending magnet. Two steerer pairs allow for adjusting the beam with respect to the axis. Behind the magnet the beam is focused by means of Einzellens into the Q-transfer beam line.

3.5 Ion particle beams at iThemba LABS

Ion beams at iThemba LABS are subject to certain limitations regarding particle energy and intensity. Due to:

- the frequency range which can be adjusted for the cyclotron resonators,
- the RF (radio frequency) voltage which can be stably generated in the acceleration gaps,
- the magnetic induction which can be achieved in the magnet poles and

- the charge state of the ion to be accelerated obtained in the ion source,

The energy range is limited to approximately 10-200 MeV/amu depending on the mass over charge state of the ion question. Another limitation is the beam intensity which can be delivered to the target. Whereas in earlier experiments, intensities of tens of particle nano amperes (pnA) were sufficient, nowadays much larger intensities in the range of 10 pμA are requested.

The beam transmission of the transport and acceleration chain is known to be as follows: approximately 10 % of the intensity extracted from the ion source can be accelerated with SPC2 and transmitted into the SSC. These losses are mainly due to the intrinsically limited longitudinal acceptance of the RF acceleration cavities, the limited transverse acceptance of the inflector and extraction channel and instabilities during acceleration in the injector cyclotron. The injection, acceleration and extraction of the main accelerator, SSC, accounts for another reduction by a factor of 5. Furthermore, to deliver a low emittance beam onto the target (to avoid unwanted background) the slits of the high energy beam line have to be closed to a certain amount accounting for a further reduction in beam intensity. Adding together, a minimum beam intensity of at least 1 to 2 pμA must be extracted form ion source. Whereas this is not a problem for light elements, for heavier elements, e.g. Ni, which require charge states of 4+ to 12+ for successful acceleration requirements, this is more difficult to fulfil.

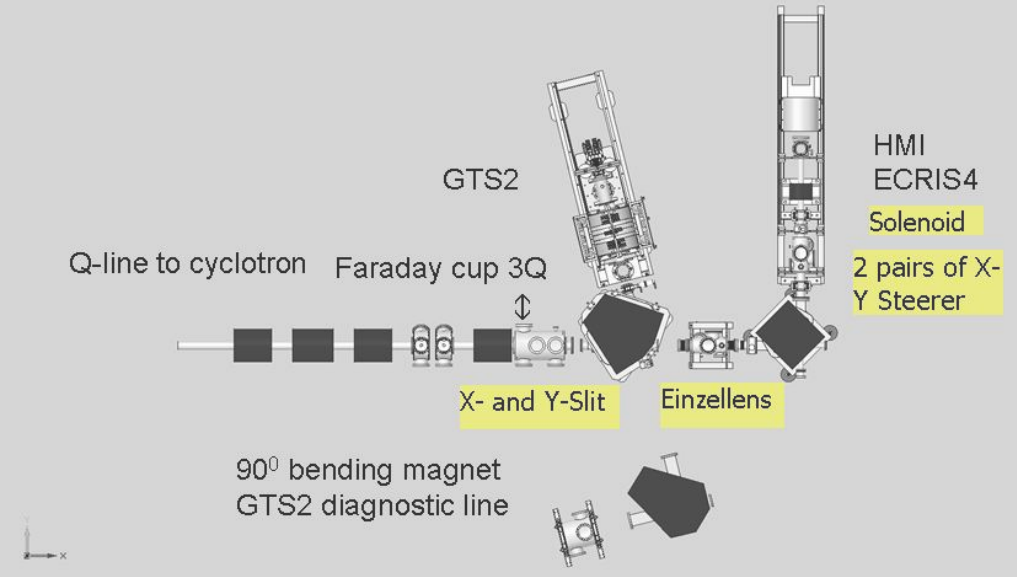

Figure 3.4: *The schematic Layout of the ECR vault for HMI ECRIS4 and GTS2. The schematic shows the positions of the solenoid, the two pairs of horizontal and vertical steerers, the einzellens and the Faraday cup 3Q.*

Chapter 4 Synthesis of nickelocene using nickel isotopes

In this chapter the procedure for the synthesis of nickelocene complexes using natural nickel and the isotopes of ^{60}Ni and ^{62}Ni is described. The main aim of the study is to synthesise the nickelocene with the enriched ^{60}Ni and ^{62}Ni isotopes. The ^{nat}Ni in the sandwich complex of metallocene was used to develop the method before using enriched isotopes of nickel for cost saving. The final product of enriched nickelocene $^{60}NiCp_2$ and $^{62}NiCp_2$ will be used for metallic beam production of ^{60}Ni and ^{62}Ni. These metallic beams will then be used in the fundamental nuclear physics experiment, more details in chapter 1 whereby the motivation of the study is described. In addition, in this chapter, characterisation methods used on synthesised nickelocenes for the investigation and determination of the structure of nickelocene complexes are described in detail. Techniques used for characterisations were Infrared Spectroscopy (IR), X-ray Diffraction (XRD) and Proton Nuclear Magnetic Resonance (^{1}H NMR). This chapter begin with the background where the behaviour of nickelocene is highlighted in order for the reader to understand all the step by step synthesis undertaken to the final product of the enriched nickelocene.

4.1 Synthesis of nickelocene

4.1.1 Background of nickelocene complex behaviour

Nickelocene is an organometallic compound that has 20 valence electrons which exceeds the normal number of 18 electron count as seen for many organometallic compounds as discussed in chapter 2. The extra two electrons are in orbitals that are weakly metal–carbon antibonding and as a result the complex undergoes reactions in which metal – carbon bonds are broken to a stable electron count at the metal centre to 18. Considering the instability of the complex, there should be measures that need to be exercised in order to keep the complex in its original 20 electron count, and this is achieved by storing the complex under inert environment.

Metallocenes in general are prepared following the methods as described by Jolly & Wilke (1974):

- Direct reaction between metallic nickel and cyclopentadiene.
- Reaction of main group metal cyclopentadienide and nickel salt.
- Deprotonation of cyclopentadiene by an inorganic base in the presence of nickel salt.

In this study, the preferred method to synthesise nickelocene was the second mentioned method above, reaction of metal cyclopentadienide and nickel salt.

Isotopic materials are costly and supplied in small quantities. In addition, the cost of the material also depends on the abundance of the isotopic material and the methods used to separate during the production. Thus, to minimise the cost during method development of nickelocene, natural nickel was initially used to develop the method before the enriched isotopic nickels could be considered.

The setup for the synthesis of metallocenes was assembled in the Target Laboratory at iThemba LABS. The following equipment and chemicals (listed in Table 4.1) were available for use including the characterisation equipment not available at the current laboratory facility, however sourced externally:

- Analytical weighing balance
- Buchner funnel and Buchner flask
- Condenser
- Cold finger
- Glass vials
- Hot plate with magnetic stirrer
- Oil free vacuum pump
- Ultrasonic bath
- Test tubes with arms
- Vacuum boxes
- SMP10 Stuart melting point apparatus
- Bruker's X-ray Powder Diffraction

- ^{1}H NMR spectroscopy
- Infrared (IR) spectroscopy
- Thermometer
- Fume hood

Table 4.1: *Table listing the chemicals and nickel materials being used, supplier and the purity or isotopic enrichment.*

Chemical	Supplier	Purity (%)/ concentration (M)	Isotopic Enrichment (%)
Nickel powder	Cerac	99.97 %	-
Hydrochloric acid (HCl)	Sigma Aldrich	32 %	-
Ammonium hydroxide solution (NH_4OH)	Sigma Aldrich	25 %	-
Acetone [$(CH_3)_2CO$]	Sigma Aldrich	99.99 %	-
Chloroform ($CHCl_3$)	Sigma Aldrich	≥99 %	-
^{60}Ni powder	Isoflex, USA	-	99.80
^{62}Ni powder	Isoflex, USA	-	98.02
Sodium Cyclopentadienide in THF (C_5H_5Na)	Sigma Aldrich	2. 0 M	-
Argon gas (Ar)	Air products	99.99 %	-

4.2 Nickelocene method development

Nickelocene synthesis in this research involves multi-step synthesis which comprises the following steps: (a) synthesis of nickel chloride, (b) hexaaminenickel (II) chloride and (c) sublimation of the nickelocene complex. Only enriched nickel powder (isotopic nickel) material was available, not in an oxide form. Therefore, the method was initiated by using a natural material of nickel for the method development using the steps as specified in the next subsections.

4.2.1 Nickel (II) chloride hexahydrate ($NiCl_2{\cdot}6H_2O$)

The method used was adapted from the one used at the Department of Physics in the Jyväskylä accelerator laboratory (Rubert *et al.*, 2012) and also referred by Crabtree (2005). The process was initiated by synthesising hydrous nickel chloride. This was achieved by:

- Dissolving 300 mg nickel (Ni) powder into 25 ml concentrated 32% hydrochloric acid (HCl) and the reactants were placed into ultrasonic bath set at 80º C to speed up the reaction until nickel powder dissolved completely and the light green nickel chloride in solution was formed (Lee *et al*., 1998), as shown in Figure 4.1(a).
- The solution was then heated on the hot plate to dryness until the characteristic yellowish brown colour was obtained, reaction 4.1, which is anhydrous nickel chloride ($NiCl_2$), Figure 4.1(b).

$$Ni\ (s) + 2HCl(aq) \xrightarrow[\uparrow H_2]{\Delta H} NiCl_2(s) \qquad (4.1)$$

All processes were conducted under the fume hood for better ventilation as HCl fumes are toxic when inhaled.

4.2.2 Hexaaminenickel(II) chloride [$Ni(NH_3)_6Cl_2$]

Anhydrous nickel chloride ($NiCl_2$) powder was dissolved in approximately 2 ml of deionised water and the green solution of nickel chloride hexahydrate was formed ($NiCl_2{\cdot}6H_2O$), following,

$$NiCl_2(s) + 6H_2O(l) \rightarrow NiCl_2 \cdot 6H_2O(aq) \qquad (4.2)$$

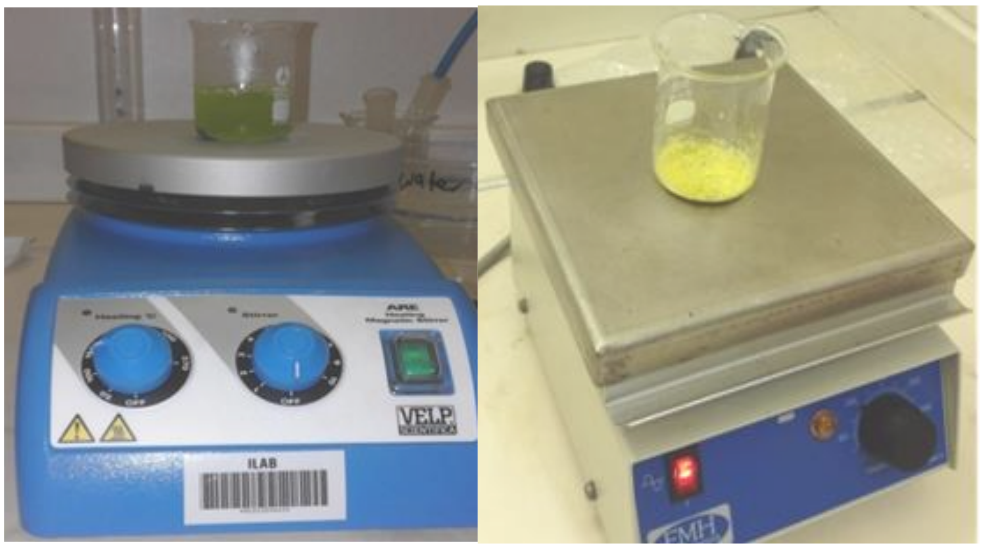

(a) (b)

Figure 4.1: *(a) Pictures showing the set up for synthesis of hydrous nickel chloride and (b) the anhydrous dried nickel chloride, yellowish brown powder.*

- Hexahydrate nickel chloride complex is composed of six water molecules bonded to nickel chloride crystals. This complex can easily form coordination complexes because of the weak link between nickel chloride and the water molecules. Therefore, ammonia was added to the complex to displace ammonia water molecules as it forms stronger bond with nickel chloride than water (Girolami *et al*., 1999). Then, about 10 ml ammonia solution (NH_3) was slowly added to nickel chloride hexahydrate, this was achieved by adding a drop NH_4OH at a time and swirling to allow the solution to cool down as the reaction releases heat. Addition of ammonia solution was done until a deep blue solution of hexaaminenickel(II) chloride was obtained, see Figure 4.2 (a) and refer also to reaction 4.3 below.

$$[Ni(H_2O)_6]Cl_2(aq) + 6NH_3(aq) \rightarrow [Ni(NH_3)_6Cl_2](aq) + 6H_2O(l) \qquad (4.3)$$

- The solution was let to stand in air for about 5 minutes to allow further cooling.
- Then the hexaaminenickel(II) chloride was extracted from the solution by adding acetone until the lavender precipitate was formed at the bottom of the glass beaker, Figure 4.2(a).
- It should be noted that, acetone and HN_4OH used were kept in the refrigerator a night before being used in order to achieve a better yield of the complex.
- The complex was then placed in ice bath for 30 minutes until the precipitate settled; see the image in Figure 4.2(b).

Figure 4.2: *Hexaaminenickel (II) chloride (a) solution cooling down to ambient temperature and (b) in ice bath for further precipitation.*

- The resultant precipitate was collected on Whatman no.5 filter paper after vacuum filtration. The vacuum filtration process was done using a Buchner funnel and a Buchner flask which was connected to an oil free vacuum pump to assist the filtration.
- The filtration process was done until the complex was dry, Figure 4.3(a). Filtration was stopped when the green colour started to develop on the sides of a filter paper. The green colour indicates the evaporation of ammonia out of the complex since ammonia is volatile. The filtration process lasted for about 30 minutes.
- The complex was then, scrapped off from the filter paper, weighed and transferred to a vial wrapped with parafilm to keep the complex intact and the vial was stored under vacuum using a vacuum desiccator for 4 days for further drying, as shown in Figure 4.3(b).

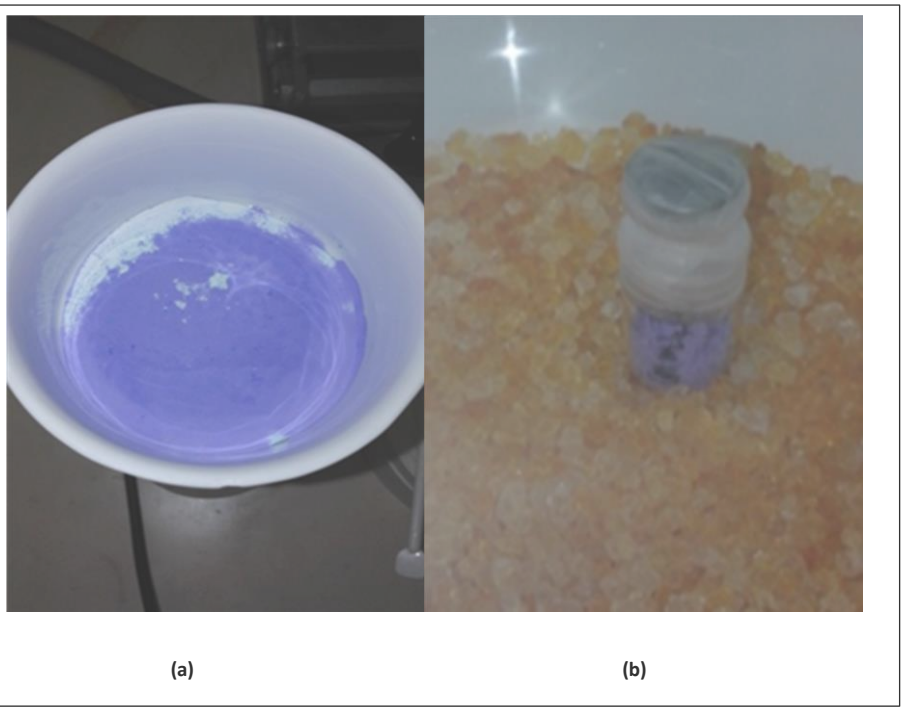

Figure 4.3: *(a) Images showing the vacuum dried hexaaminenickel (II) chloride in Buchner funnel and (b) the hexaaminenickel (II) chloride in a vile stored in a vacuum desiccator for further drying.*

4.2.3 Synthesis and sublimation of nickelocene

For the synthesis and sublimation of nickelocene the set up used in this study is shown in Figure 4.4. All the used glassware was oven dried for 3 days at 100 ℃ before use for safety precautions. The sodium cyclopentadienide in tetrahydrofuran (THF) reacts vigorously when in contact with water and moisture, which might result into fire. It was then allowed to cool in a desiccator. The experimental set up glassware was first purged with argon gas for 3 to 5 minutes for complete dryness and to create the inert atmosphere before the addition of reactants. Thus the synthesis of nickelocene was carried out as follows:

- Dried hexaaminenickel-(II) chloride prepared above was transferred to reaction tube in Figure 4.4 which was followed by adding 5 to 8 ml of 2 M sodium cyclopentadienide in THF, (refer to reaction 4.4). During the heating, the temperature of the oil bath where the reaction tube was immersed was kept at 75 ℃ in order to

achieve the reaction temperature at 60 °C and at this temperature the green nickelocene solution was formed.

$$2\ \mathrm{Na}C_5H_5(aq) + [Ni(NH_3)_6Cl_2](\mathrm{s}) \rightarrow \mathrm{Ni}(C_5H_5)(s) + 2NaCl(s) + 6NH_3(g) \quad (4.4)$$

- After 2 hours, the oil bath temperature was increased to 85 °C for 10 minutes to ensure that ammonia evaporates completely before sublimation of the nickelocene. The argon flow was also stopped during the 10 minutes of evaporating ammonia from the product.
- It should be noted that throughout the reaction process, argon gas was allowed to flow slowly in the reaction chamber.

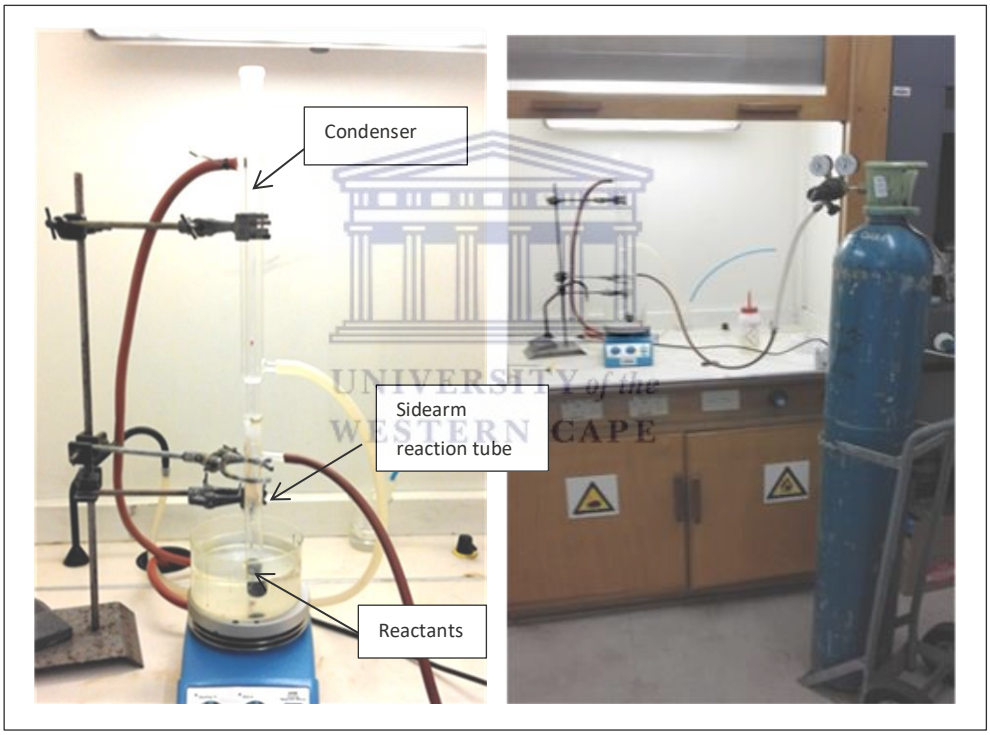

Figure 4.4: *The set-up used during the formation of crude nickelocene.*

- The final step in the synthesis of nickelocene was sublimation. The purpose of sublimation is for purification of the crude nickelocene. This was achieved by removing the condenser from the reaction chamber and coupling the cold finger to the reaction chamber as shown in Figure 4.5.

- Since the nickelocene begins to sublime around 80 °C, the temperature of the oil bath was increased to 120 °C. When the temperature was just above 110 °C the sublimation begun but the nickelocene was not collected on the cold finger only but sublimed at the walls of the test tube as well. The length of the test tube was shortened to minimise the distance in between the bottom part of the test tube where the crude nickelocene is at and the cold finger to ensure that most of the purified nickelocene is collected on the cold finger.
- Figure 4.6 shows the collected nickelocene after modifications. The final product was collected and stored in normal glass vials and some in headspace vials and stored under inert atmosphere. Samples were weighed under the nitrogen filled glove box.

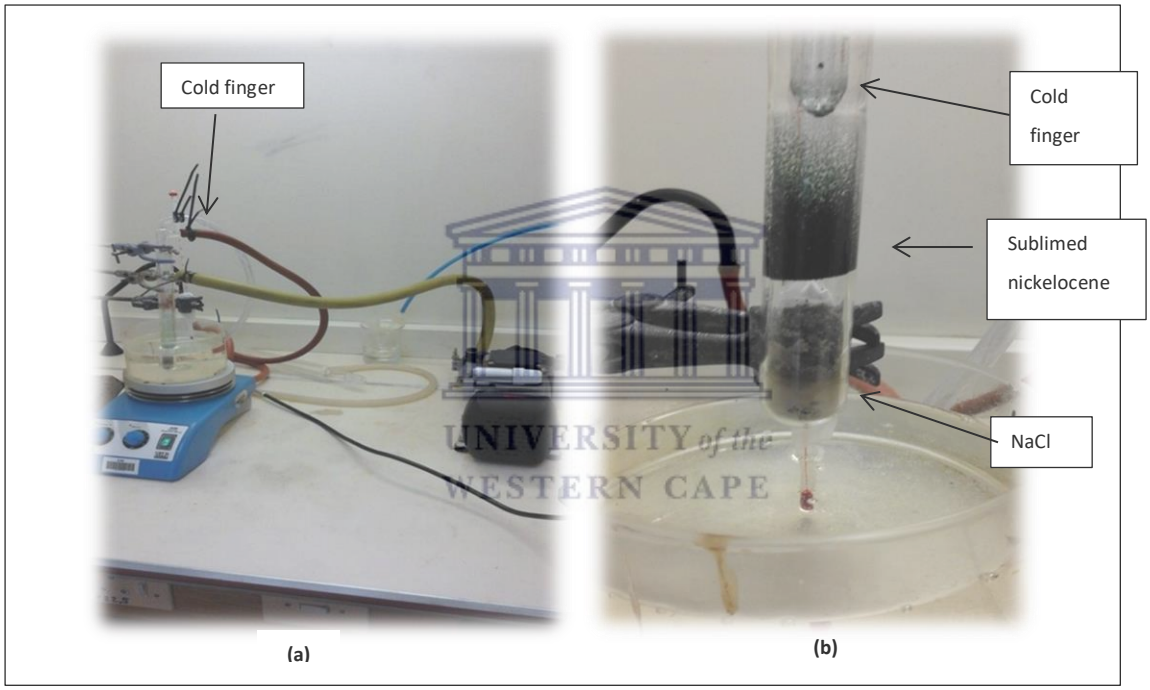

Figure 4.5: *The sublimation set up, shows unmodified test tube with cold finger coupled on as a collector of nickelocene during deposition process. Image on the left (a) is before deposition and the one on the right (b) is for when the nickelocene deposited on cold finger and the sides of the test tube.*

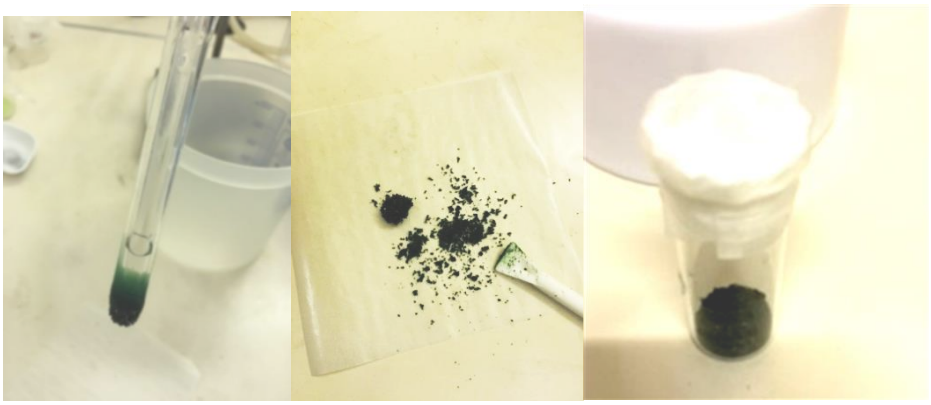

Figure 4.6: *(a) An image of green crystalline of nickelocene on deposited on cold finger when modified test tubes were used, (b) the collected product in a weighing paper and (c) stored in a sealed vial for further storage.*

4.3 Characterisations

Crystal structure and the compound unique structure information were collected using XRD, ^{1}H NMR and FTIR techniques after determining the melting point of the synthesised materials. All the identification of nickelocene samples that are discussed in this section are as follows: Samples 1 to 7 are nickelocene samples with natural nickel ($^{nat}NiCp_2$) and then nickelocenes with enriched ^{60}Ni and ^{62}Ni ($^{60}NiCp_2$ and $^{62}NiCp_2$). A commercially acquired nickelocene sample from Sigma Aldrich was used as a reference sample in this study. The tables with sample identities are presented in Chapter 5.

4.3.1 Melting point determination

All the synthesised nickelocene samples were physically characterised by testing their melting point in the target laboratory of iThemba LABS. The melting point was conducted by inserting the synthesised crystal powder to capillary melting point tubes as the sample holder and the melting point was determined using SMP10 Stuart digital melting point apparatus shown in Figure 4.7.

Figure 4.7: *Melting point apparatus used for determination of synthesised nickelocene samples melting point.*

4.3.2 X-ray diffraction (XRD) analysis

The crystal structure and the orientation of synthesised nickelocene were investigated by the X–ray diffraction method. Analysis were conducted using the equipment available at the Materials Research Department (MRD) of iThemba LABS. X-ray diffraction is based on constructive interference of monochromatic X–rays and crystalline sample whereby X-rays are generated by a cathode X-ray tube, as shown in Figure 4.8. The process involves filtering the X–rays first to produce monochromatic radiation, followed by concentrating them by use of collimators to be finally directed to the sample (Girolami *et al*., 1999). In the X–ray tube, electrons are emitted from the cathode filament and accelerated towards the anode plate. The anode is typically fabricated from high purity metals of copper, chromium, molybdenum, iron, cobalt, nickel or silver. The electron current between the filament and the anode may be adjusted by tuning the filament current in the range of 10 mA.

When electrons impinge on the anode, they are decelerated by their interaction with the target plate atoms leading to the emission of X–rays. The acceleration voltage in kV must be greater than the energy of the characteristic radiation required by the experiment in keV (Birkholz, 2006). Diffraction effects are observed when electromagnetic radiation impinges on periodic structures with geometrical variations on length scale of the wavelength of the radiation. The interatomic distances in crystals and molecules amounts to 0.15 to 0.4 nm and this corresponds in the electromagnetic spectrum with the wavelength (λ) of X-rays having photon energies between 3 and 8 keV. This equivalence in energy leads to interactions so that

the electrons of an atom will primarily be responsible for the scattering of X–rays. The number of electrons in a given volume of space determines how strongly an atom scatters X–rays. The interference of scattered X–rays leads to a general occurrence of diffraction (Ewald, 1962; Birkholz, 2006; Van Holde, *et al*., 2006).

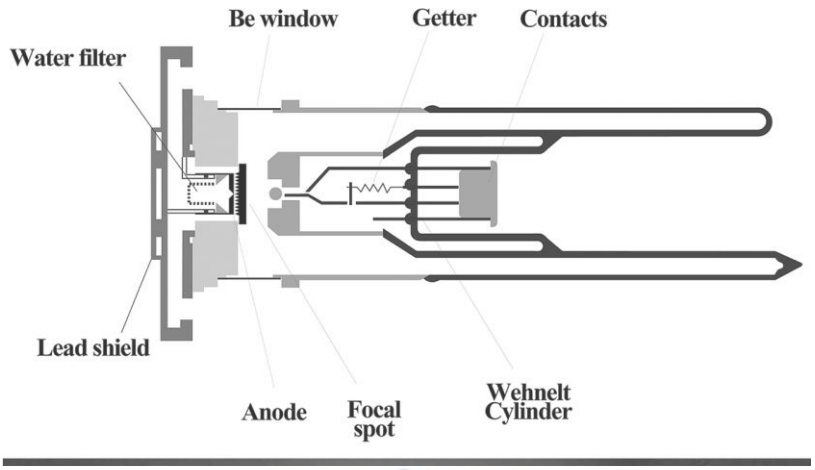

Figure 4.8: *Schematic showing the conventional X–ray tube (Birkholz, 2006).*

Constructive interference happens only under specific crystalline orientation conditions. For instance, when a crystal is placed in a monochromatic beam it can generate a diffraction signal only if its orientation in a beam satisfies the Bragg's condition for a given lattice plane (Sarrazin, *et al.*, 2005). Bragg's equation (Equation 4.5) may be obtained geometrically as shown in Figure 4.9 and also explained in details by Birkholz (2006) and Van Holde *et al.* (2006). The Bragg's equation is written as;

$$n\lambda = 2d \sin\theta \qquad (4.5)$$

where n is the reflection order., λ is the wavelength of the X-rays, d interplanar distance and θ the incident angle. Essentially, when a set of crystallographic lattice planes with distances d_{hkl} is irradiated by plane wave X–rays impinging on the lattice planes at an angle θ, it causes a relative phase shift of the wave depending on the atom configuration. The phase shift comprises of Δ_1 and Δ_2 in which their sum equals to $2dsin\theta$ for any arbitrary angle θ. The

reflected wave after the constructive interface can only be achieved when the phase shift *2dsinθ* is a multiple of wavelength.

The nickelocene crystalline commercial samples were analysed as supplied along with the synthesised nickelocene samples prepared at iThemba LABS for comparison. The characterisation of these nickelocene complexes using XRD have never been investigated at iThemba LABS before and as such no reference sample exist. To carry out the analysis, a D8 Advance Bruker X-ray diffractometer, shown in Figure 4.10 was used at iThemba LABS. The analysis of samples was conducted using CuK_{α} radiation with a wavelength of 1.5418 Å. Angular steps were incremented by 0.05º and counts were collected for 0.5 seconds per step. The data were collected at 2θ from 5º to 70º from a commercial sample and from samples 1, 2, 3 and 4. XRD data were collected at 2θ from 10º to 69º for $^{60}NiCp_2$ and $^{62}NiCp_2$. The XRD analysis results of commercial sample (Sigma Aldrich), sample 1 (iThemba LABS), $^{60}NiCp_2$ and $^{62}NiCp_2$ were further processed using the EXPO2014 program (Altomare *et al.*, 2005). All XRD results are discussed in chapter 5.

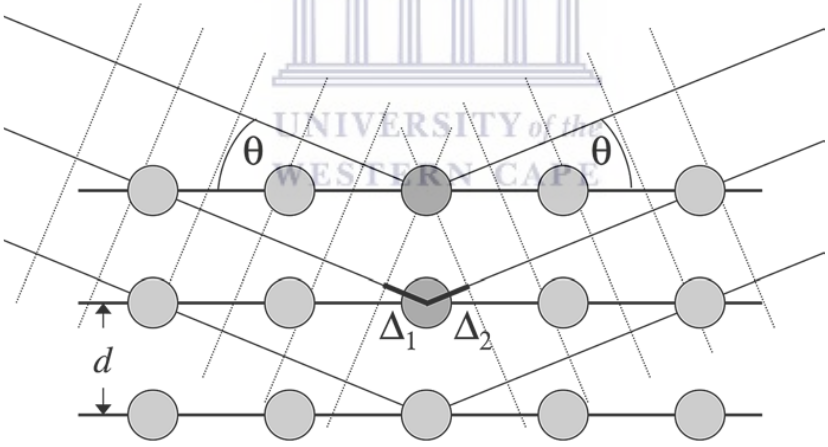

$$\Delta_1 + \Delta_2 = 2d\cos(90° - \theta) = 2d\sin\theta$$

Figure 4.9: *The schematic drawing of different sets of crystallographic planes that occur according to Bragg's condition (*Birkholz, *2006).*

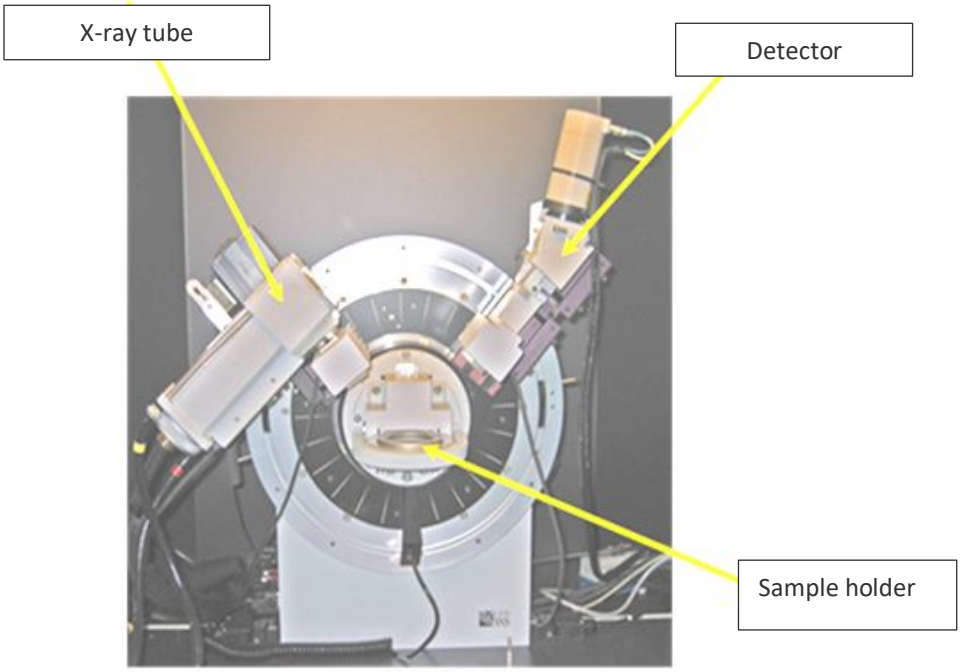

Figure 4.10: *A D8 Advance Bruker X–ray diffractometer employed during the structural investigation of nickelocene complexes.*

4.3.3 Proton Nuclear Magnetic (^{1}H NMR) Spectroscopy analysis

Nuclear magnetic resonance (NMR) spectroscopy is a technique that relies on the magnetic properties of the atomic nucleus. When a nucleus is placed in a strong magnetic field, nuclei resonate at a characteristic frequency in the radio frequency range of the electromagnetic spectrum. Slight variations in this resonant frequency provide detailed information about the molecular structure in which the atom resides (Traficante, 1996; Faust, 1997; Jacobsen, 2007). This implies that NMR absorption is a result of transition between the energy levels caused by applied radiofrequency radiation (Evans, 1995). In short, many atoms behave as if the positively charged nucleus was spinning on an axis. The spinning charge creates a tiny magnetic field. When this spinning nucleus is placed in an external magnetic field, it tries to align itself with it (Gerothanassis *et al*.,, 2002; Jacobsen, 2007). Since the spinning nucleus has angular momentum, the torque exerted by the external field results in a circular motion called

Larmor precession. The rate of this precession is proportional to the external magnetic field strength and to the strength of the nuclear magnet and is given by:

$$v_o = \gamma \frac{B_o}{2\pi} \tag{4.6}$$

where v_o is the precession rate (radiation frequency) in Hertz, γ (gyromagnetic ratio) the nuclear magnet strength and B_0 the external magnetic field strength. This resonant frequency is the radio frequency range for strong magnetic fields and can be measured by applying a radio frequency signal to the sample and varying the frequency or applied magnetic field until absorbance of energy is detected (Traficante, 1996; Gerothanassis, *et al*., 2002; Jacobsen, 2007).

The magnetic resonance phenomenon occurs as a result of the quantum mechanical property of the intrinsic spin I. The spin confers a magnetic moment onto a nucleus. The spin (I) can have values $I=0$, ½, 1, 3/2, etc. (Faust, 1997; Gerothanassis *et al*, 2002; Edwards, 2009). The gyromagnetic ratio,γ, is a proportionality constant which determines the resonant frequency of the nucleus for a given external field. In a magnetic field, a nucleus of spin I has $2I + 1$ possible orientations, given by the value of the magnetic substates m_I, which has values of $-I$, $-I+1$, …$I - 1$(e.g. for a nucleus of spin 3/2, m_I = -3/2, - ½, ½, 3/2). For example, a nucleus with spin I =-1/2 nucleus, when placed in a static field has an energy which varies with the orientation to the field. The possible energies are quantised, with the two possible values m_I (±½) corresponding to parallel and antiparallel orientations of this small magnet and the external field as shown in Figure 4.11. Then, NMR absorption is a consequence of transition between the energy levels stimulated by applied radiofrequency radiation (Traficante, 1996; Edwards, 2009).

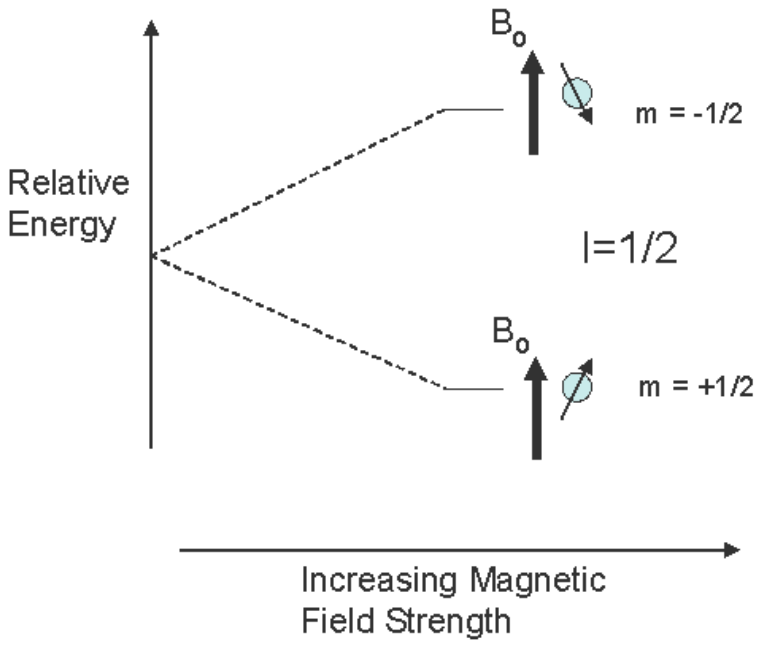

Figure 4.11: *The splitting of the degenerate nuclear energy levels in applied magnetic field (Edwards; 2009).*

The ^{1}H NMR spectroscopy investigations on nickelocene samples were conducted at Central Analytical Facilities (CAF) of Stellenbosch University. The confirmation of the ligand structure was conducted on synthesised samples of nickelocene from the target laboratory at iThemba LABS, as well as on the commercially acquired nickelocene material supplied by Sigma Aldrich. Samples were firstly dissolved in deuterated chloroform ($CDCl_3$) and aided the process by sonication. Dissolved samples were transferred to NMR tubes for analysis. The proton NMR was recorded on 600 Varian ^{unity}Inova NMR spectrometer with ^{1}H and ^{13}C frequencies of 600 and 150 MHz respectively. ^{1}H NMR spectra were obtained using a 5 mm dual channel IDpfg and the spectra were referenced to the residual solvent signal at 7.26 ppm. Samples 1, 2 and 3 including the commercial nickelocene used as a reference were analysed in this condition. The second batch of samples (commercial, sample 7 and $^{60}NiCp_2$) was dissolved in deuterated dimethyl sulfoxide-d_6 (DMSO-d_6) solvent, as rapid decomposition of samples in $CDCl_3$ solvent and turbidity during the analysis was experienced in the first batch of samples. The data was acquired as above and the residual solvent signal was observed at 0 ppm shift and regions covered were 50 to ±300 ppm. Results and discussions are presented in chapter 5.

4.3.4 Fourier Transform Infrared determination (FT-IR)

Most of the samples could be studied using IR spectroscopy, and this serve as one of the advantages for the technique. It could be liquids, solutions, pastes, powders, films, fibres, gases and surfaces all can be examined (Smith & Dent, 2005; Othmer, 2005). For a molecule to absorb IR, the vibrations or rotations within a molecule must be enough to cause a net change in the dipole moment of the molecule. Then alternating electrical field of the radiation interacts with fluctuations in the dipole moment of the molecule. If the frequency of the radiation matches the vibrational frequency of the molecule, then radiation will be absorbed causing a change in the amplitude of the molecule.

Rotational levels are quantized and absorption of IR by gases yields line spectra. However, in liquids or solids these lines broaden into a continuum due to molecular collisions and other interactions. The positions of atoms in molecules are not fixed because they are a subject to a number of different vibrations. Vibrations fall into two categories which are stretching and bending. Stretching is a change occurs in the inter-atomic distance along bond axis, whilst bending is a change in angle between two bands. There are four types of bending that are encountered in molecular vibrations: rocking, scissoring, wagging and twisting (Smith & Dent, 2005; Siebert & Hildebrandt, 2008).

Infrared analysis was performed at the Chemistry Department of the University of the Western Cape. The analysis was achieved by mixing the KBr powder with the samples. Samples were firstly grounded with agate mortar and pestle to a fine powder and subjected to die set which was later evacuated to form a disc suitable for IR analysis. The resulting transparent compressed disc was transferred to IR sample holder. FT-IR spectra were obtained with PerkinElmer Spectrum Two FT-IR spectrometer scanned at wavelengths between 400 and 4000 cm^{-1}. Samples 1, 2 and 3 were analysed as the first batch and the $^{60}NiCp_2$ and $^{62}NiCp_2$ complexes were of the second batch of analysis. In both batches, commercial nickelocene was used as the reference material. Results are presented and discussed in chapter 5.

Chapter 5 Results and Discussion

In chapter 4, the experimental procedures for the synthesis and characterisations of nickelocene samples were described in details. In this chapter, the results obtained from those activities are presented and discussed. In particular, the percentage yield of nickelocene and that of nickel present in the nickelocene complex. This chapter is divided into four sections, namely nickelocene synthesis, XRD characterisation results, FTIR characterisation results, ^{1}H NMR analysis and their discussions.

5.1 Nickelocenes synthesis

This study is mainly on the production of nickel ion (Ni^{8+}) as the end user product produced from nickelocene, the quantity and quality of Ni was determined through each step during the synthesis. The percentage yield of nickel in overall synthesis of nickelocene was also calculated. Therefore, the initial investigations were determination of the theoretical yield and the efficiency of the production of hexaaminenickel (II) chloride, the intermediate product of the reaction. The methods used for the calculations are in section 5.1.1 and the values are reported in Table 5.1.

Moreover, it should be noted that the purity of the synthesised nickelocene complexes is an important defining factor to measure the success of the reaction. The melting points of nickelocene complexes were therefore determined as the initial factor of investigation in all samples and this value was compared with the available literature value. Furthermore, the percentage yield of the nickelocene complex was also estimated from the intermediate complex of hexaaminenickel (II) chloride. Given that the hexaaminenickel (II) chloride is a limiting reactant in the reaction to produce nickelocene, therefore theoretical yields of nickelocene in terms of mass (mg) were calculated as in section 5.1.2 using the complex masses. Related results are presented in Table 5.2. The graphical representation in Figures 5.1 and 5.2 are for the masses and percentage yield, respectively. The change in mass of Ni were monitored throughout the multi-step synthesis as well in order to identify if there is any discrepancy between the initial values of nickel used from the beginning of a reaction with

that found in the final product. The results are presented in Table 5.3 and their determination is discussed in section 5.1.3.

5.1.1 Theoretical yield and efficiency of hexaaminenickel(II) chloride production

Note the molar masses of $Ni[(NH_3)_6]Cl_2$ were calculated according to the isotopic masses of ^{nat}Ni, ^{60}Ni and ^{62}Ni. Thus molar masses are as follows: 231.78 g.mol^{-1} (^{nat}Ni), 233.02 g.mol^{-1} (^{60}Ni) and 235.02 g.mol^{-1} (^{62}Ni). The procedures used for the calculations of theoretical yield and efficiency of $Ni[(NH_3)_6]Cl_2$ are shown below:

$$Theoretical\ yield\ (Ni[(NH_3)_6]Cl_2)\ (mg) = mg\ Ni \times \frac{molar\ mass\ of\ Ni[(NH_3)_6]Cl_2}{molar\ mass\ of\ Ni}$$

$$\varepsilon\ (\%) = \frac{actual\ mass\ of\ Ni[(NH_3)_6]Cl_2}{theoretical\ mass\ of\ Ni[(NH_3)_6]Cl_2} \times 100$$

The actual mass of $Ni[(NH_3)_6]Cl_2$ above (and in Table 5.1 below) refers to the masses of the synthesised product.

Table 5.1: *Initial masses of Ni and the calculated theoretical masses (mg) and efficiency (%) of $Ni[(NH_3)_6]Cl_2$.*

Sample	Mass of Ni (mg)	Theoretical yield $Ni[(NH_3)_6]Cl_2$ (mg)	Actual yield $Ni[(NH_3)_6]Cl_2$ (mg)	Efficiency of $Ni[(NH_3)_6]Cl_2$ (%)
Sample 1	300	1185	922	78
Sample 2	300	1185	1044	88
Sample 3	305	1207	800	66
Sample 4	300	1185	629	53
Sample 5	300	1185	1127	95
Sample 6	300	1185	870	73
Sample 7	300	1185	700	59
^{60}Ni	293	1139	814	71
^{62}Ni	218	827	340	41

5.1.2 Theoretical yield (mg) and percentage yield of nickelocene

The theoretical (expected) yield using the limiting reactant, $Ni[(NH_3)_6]Cl_2$, was calculated as follows: Note that the molar masses of $NiCp_2$ according to isotopic mass of ^{nat}Ni, ^{60}Ni and ^{62}Ni are: 188.88 g.mol^{-1}, 190 g.mol^{-1} and 192 g.mol^{-1}, respectively also that of $Ni[(NH_3)_6]Cl_2$ were; 231.78 g.mol^{-1}, 233.02 g.mol^{-1} and 235.02 g.mol^{-1}, respectively.

Therefore;

$$Theoratical\ yield\ (NiCp_2)\ (mg)\ = mg\ Ni[(NH_3)_6]Cl_2 \times \frac{molar\ mass\ of\ NiCp_2}{molar\ mass\ of Ni[(NH_3)_6]Cl_2}$$

The percentage yield of $NiCp_2$ was calculated as follows:

$$\%\ yield(NiCp_2) = \frac{actual\ mass\ (mg)\ NiCp_2}{theoratical\ mass(mg)} \times 100$$

Table 5.2: *The actual mass of synthesized $Ni[(NH_3)_6]Cl_2$, theoretically calculated values of $NiCp_2$ and the actual mass of synthesized $NiCp_2$ for Samples 1-7 and $^{60}NiCp_2$ and $^{62}NiCp_2$ are presented. Included also is the measured melting points of $NiCp_2$ complexes, refer also to the reported values 171 – 174 ^oC by Park & Sudarshan (2001).*

Sample	$Ni[(NH_3)_6]Cl_2$ (mg)	Theoretical Yield $NiCp_2$ (mg)	Actual mass $NiCp_2$ (mg)	% yield of $NiCp_2$ from the amount of $Ni[(NH_3)_6]Cl_2$	Melting Point (^oC)
Sample 1	922	751	260	35	173
Sample 2	1044	851	463	54	171
Sample 3	800	652	367	56	172
Sample 4	629	513	238	46	171
Sample 5	1127	918	158	17	173
Sample 6	870	709	151	21	173
Sample 7	700	570	207	36	173
^{60}Ni	814	664	349	53	172
^{62}Ni	340	278	198	71	171

Figure 5.1 shows a plot of the masses of the nickel (natural and nickel 60 and 62), intermediate product (hexaaminenickel(II) chloride) as well as the nickelocene final products as shown in Table 5.1 and Table 5.2. The consistency in terms of the production of hexaaminenickel(II) chloride is noted from the results presented in Table 5.1. Efficiency of above 90 % was achieved in sample 5. Results presented in Table 5.2 show the theoretical yield (in mg) and the actual yield (in mg) of nickelocene (samples 1–7) and nickelocene with enriched ^{60}Ni and ^{62}Ni synthesised in-house. These values in Table 5.2 show some discrepancy in the theoretical and actual mass. The discrepancy is mostly pronounced in samples 5 and 6. The measured percentage yield are on average (40 ± 20) %, with the lowest yield at 17 % and highest yield at 56 % for samples 3 and 5, respectively. The highest yield of 71 % of nickelocene was obtained from enriched sample with ^{62}Ni. However, as shown in Figures 5.2 the results showed no particular trend in the percentage yield of the nickelocene complex.

During the synthesis, the observation showed that the determining factor for the higher yield of the nickelocene complex relied on the hexaaminenickel(II) chloride complex yield and the freshness of sodium cyclopentadienide used in the final step of the synthesis. The higher the mass of hexaaminenickel(II) chloride produced, the higher the mass of the nickelocene yield except for sample 5 and 6 where the sodium cyclopentadienide was starting to deteriorate during the process. For instance, in samples 5, 6 and 7, the sodium cyclopentadienide used was mostly brown in colour as opposed to its pinkish colour when it is still fresh and good which resulted in the percentage yield below 30%. Improvement in the percentage yield was observed again when a new batch of sodium cyclopentadienide was used during the synthesis of nickelocene enriched ^{60}Ni and ^{62}Ni.

Another aiding factor that helps improving the yield is the time taken for the sublimation process of nickelocene under vacuum on the cold finger, which is the final step of the synthesis. Sublimation process longer than 2 hours yielded better amounts of nickelocene collected on the cold finger. However, sample 1 was synthesised during the initial stage of the method development of nickelocene while the optimum reaction conditions were still to be identified. The sublimation time of sample 1 was below 2 hours. The success of the synthesis also relies on the purity of starting material, Ni, and concentration of ammonia in NH_4OH.

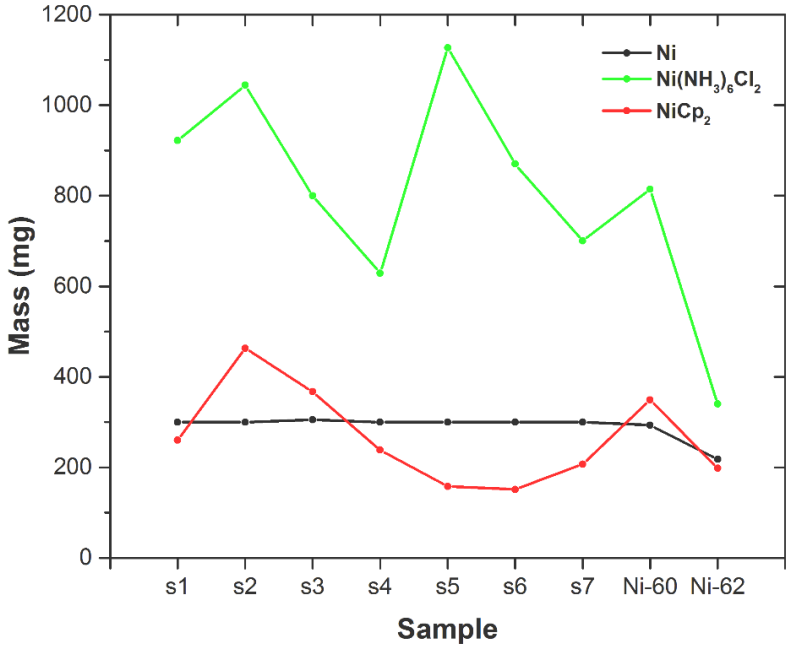

Figure 5.1: *Presentation of the mass (mg) of the starting material (Ni) for the synthesis of nickelocene from natural nickel for samples (s1 - s7), enriched nickel samples (Ni-60 and Ni-62) (black), intermediate product, $Ni[(NH_3)_6]Cl_2$ (green) and the final product, nickelocene ($NiCp_2$) (green).*

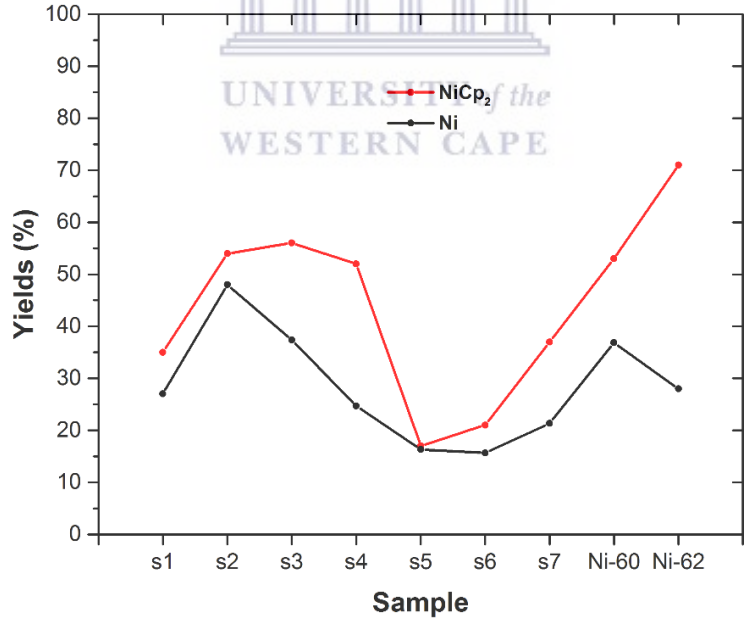

Figure 5.2: *Percentage yield of synthesized nickelocene samples and the overall amount of nickel in the products.*

Moreover, it should be noted that the calculated theoretical yields do not account for the loss of reacting materials during the synthesis. For example, the synthesis in this study required multi-step reactions, loss of material from the reactants should be expected and monitored to minimise such losses. Measured melting point in all samples were between 171 to 173 °C, which is within the range as reported from the available literature (Park & Sudarshan, 2001) and also provided by the supplier, Sigma Aldrich on the material certificate of analysis.

5.1.3 Actual yield of nickel in the nickelocene complexes

Nickel mass contents in Table 5.3 were calculated from $NiCp_2$ complexes. The efficiency of the method to produce nickel from the nickelocene was also determined. Below are the methods used for the calculations.

Actual mass of Ni from nickelocene and efficiency on the production of Ni were calculated as follows:

$$Actual\ Ni\ mass(mg) = \frac{molar\ mass\ of\ Ni}{molar\ mass\ of\ NiCp_2} \times mass\ of\ NiCp_2$$

$$\varepsilon(\%) = \frac{actual\ mass\ of\ Ni\ from\ NiCp_2}{starting\ mass\ of\ Ni} \times 100$$

Table 5.3 shows the results of the calculation of actual mass of Ni content in $NiCp_2$, the final product (samples 1, 2, 3, 5, 6, 7 and ^{60}Ni and ^{62}Ni). From the results, there is no consistency in the mass of Ni present from the nickelocene samples except for samples 3, 4 and 6 having the values of Ni of above 100 mg with sample 2 having the remaining Ni of almost 50 % from the initial mass of Ni. A great loss of Ni in the produced $NiCp_2$, of about 200 mg or more is experienced in sample 5. The high yield of the amine complex with a mass of 1127 mg with an efficiency of 94 for Ni, a high yield was expected in this sample as the Ni content was higher in this sample as compared to other samples. The low yield was most likely due to the decomposing $NaCp_2$, thus the freshness of the $NaCp_2$ play a vital role in the the product yield. In average, between 30 to 50 % of Ni yield was found in the final product from the

intermediate product in most samples with an exception in ^{62}Ni whereby about 20 % of nickel loss was observed. In conclusion from these results, it shows that Ni is lost either because of the incomplete reaction between hexaaminenickel (II) chloride and sodium cyclopentadienide or the sublimation process time was not enough to collect most the nickelocene sample during purification process. In ^{60}Nickelocene it shows that most of the nickelocene was collected during the synthesis while it was lost during the formation of the intermediate product.

Table 5.3: *Calculated masses and overall efficiencies of Ni present in $NiCp_2$ complexes synthesized.*

Sample	Mass of Ni	Actual Mass of Ni from $NiCp_2$ (mg)	Overall Efficiency of Ni produced (%)
Sample 1	300	81	27
Sample 2	300	144	48
Sample 3	305	114	37
Sample 4	300	74	25
Sample 5	300	49	16
Sample 6	300	47	16
Sample 7	300	64	21
^{60}Ni	293	108	38
^{62}Ni	218	61	29

5.2 XRD results and discussion

In Figure 5.3, the first set of results obtained after analysing four samples of nickelocene from the first batch of samples produced during the method development of nickelocene and that of commercially supplied nickelocene by Sigma Aldrich. The sample identifications are given in Table 5.1 (samples 1 to 4) and nickelocene from Sigma Aldrich as a reference and are colour coded in the spectra as shown Figure 5.3.

X-ray patterns could not be indexed in order to identify the crystal structure of the nickelocene complexes due to the unavailability of the JCPDS[2] card for the organometallic compounds at iThemba LABS XRD facility. In addition, this type of analysis on metallocenes or paramagnetic complexes was done for the first time. In this instance, the pattern obtained on commercial nickelocene was used as the reference and then compared with patterns from in-house synthesised nickelocenes. This was achieved by stacking the spectra of the analysed samples synthesised at iThemba LABS with the one obtained from analysing commercially acquired sample. In all 4 samples (see also Figure 5.3), there are resemblances in the peaks observed in the theta regions between 14 and 24. Nickelocene with the enriched ^{62}Ni was analysed and compared to commercial nickelocene, and also show the positive resemblance, see Figure 5.4. All the XRD analysis of in-house synthesised samples and the one from Sigma Aldrich were conducted under the same conditions.

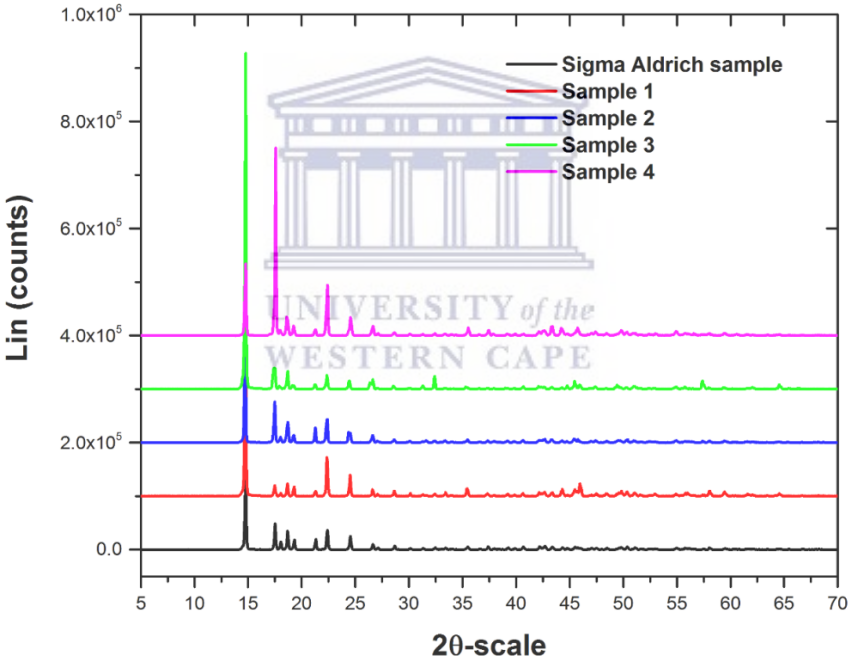

Figure 5.3: *The combined XRD patterns of synthesized nickelocene samples from in-house and commercially supplied nickel material; Sigma Aldrich (black) and other colour coded spectra are for samples 1 (red); 2 (blue); 3 (green) and 4 (purple) as in table 4.1. Note that the spectra are scaled in the vertical axis to visualize the patterns for each sample separately.*

[2] JCPDS card – Joint Committee on Powder Diffraction Standards card which provides the primary references of X-ray diffraction data.

The XRD patterns for sample1, commercial nickelocene, $^{60}NiCp_2$ and $^{62}NiCp_2$ obtained from MRD XRD analysis were further analysed by EXPO2014 software (Altomare *et al.*, 2013) and refined by PIRUM within the program (Cernik *et al.,* 1991; Altomare *et al.*, 2004, 2005 & 2007). This program which is available online was used since the estimation and analysis of the patterns could not be performed at MRD where the characterisations were done. The XRD structural analysis after investigated with EXPO2014 was found to be monoclinic for both (commercial and iThemba LABS) nickelocene prepared with natural nickel. Results for enriched complexes, $^{60}NiCp_2$ and $^{62}NiCp_2$ revealed triclinic structure instead. The detailed results in Table 5.4, about four plausible cells were estimated in $^{nat}NiCp_2$ and commercial $^{nat}NiCp_2$, only one cell was found on enriched nickelocenes, ^{60}Ni and ^{62}Ni complexes. In the four cells found on nickelocenes with natural nickel two crystal structures were confirmed, monoclinic and triclinic. The triclinic structure was only found in one of the four cells in both nickelocene complexes. Thus the structure was concluded to be monoclinic.

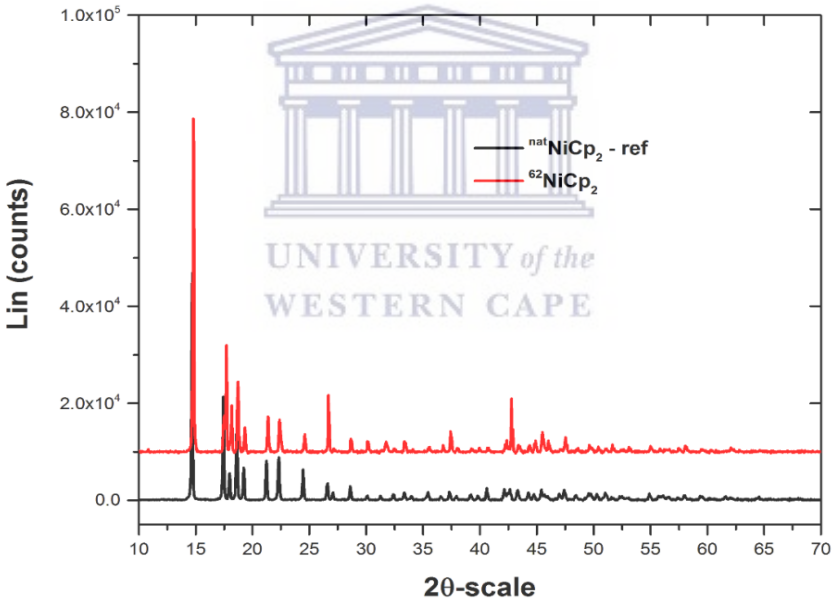

Figure 5.4: *The combined XRD patterns of synthesized nickelocene samples; (black) reference sample ($^{nat}NiCp_2$) and (red) $^{62}NiCp_2$. Note that the spectra are scaled in the vertical axis to visualize the patterns for each sample separately.*

A triclinic structure was confirmed in both nickelocene with enriched ^{60}Ni and ^{62}Ni. The space group were confirmed to be P2/m for $^{nat}NiCp_2$ and P-1 for both $^{60}NiCp_2$ and $^{62}NiCp_2$ by the EXPO2014 program (Altomare *et al.*, 2013). These results of the enriched complexes

contradict the conclusions by Seiler and Dunitz (1980) that nickelocene has only one crystal structure, i.e. monoclinic (Seiler and Dunitz, 1980). Note that ^{nat}Ni contains the following isotopes, ^{58}Ni (68.1 %), ^{60}Ni (26.2 %) ^{61}Ni (1.1 %), ^{62}Ni (3.6 %) and ^{64}Ni (0.9 %) (Valley, 1941, Rosman & Taylor, 1998) and this could possibly explain the variation in crystal structure for the natural material and enriched materials. Further investigation will be required to fully understand this behaviour between the enriched materials to the natural material, possibly starting with the dominant isotope, ^{58}Ni (68.1%) for example. Moreover, all samples should be characterised at the same time for consistency, with similar background parameters and settings of the XRD system.

Table 5.4: *The table representing the XRD lattice parameters and the crystal structures of nickelocene ($NiCp_2$) samples obtained after analysis with an EXPO2014 program (Altomare et al., 2013).*

Sample	**^{nat}NiCp$_2$ (commercial)**	**^{nat}NiCp$_2$ (iTL)**	**^{60}NiCp$_2$ (iTL)**	**^{62}NiCp$_2$ (iTL)**
Crystal system	Monoclinic	Monoclinic	Triclinic	Triclinic
Space group	P2/m	P2/m	P-1	P-1
a (Å)	9.177(3)	9.182(4)	13.459(8)	7.633(3)
b (Å)	7.883(2)	7.886(3)	8.934(4)	6.662(2)
c (Å)	5.924(3)	5.933(4)	6.416(3)	5.999(4)
α (º)	90	90	90.25(3)	103.44(4)
β (º)	91.93(3)	92.05(6)	102.98(3)	93.46(3)
γ (º)	90	90	106.86(6)	90.45(7)
Volume (Å^3)	428.3(3)	429.3(4)	717.4(7)	296.1(2)

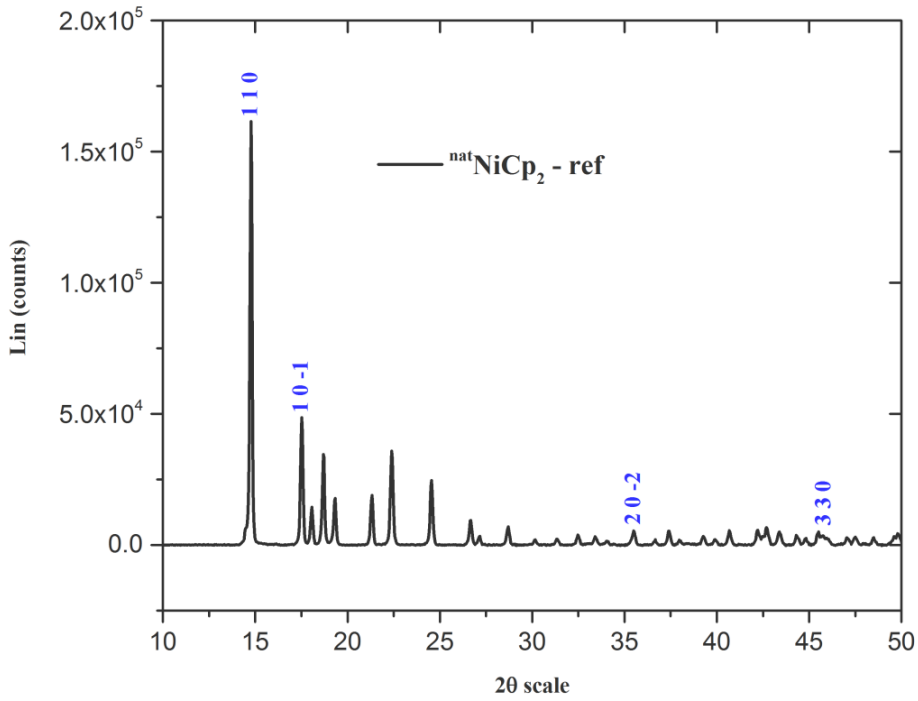

Figure 5.5: *The indexed XRD pattern of commercial $^{nat}NiCp_2$ used as a reference sample.*

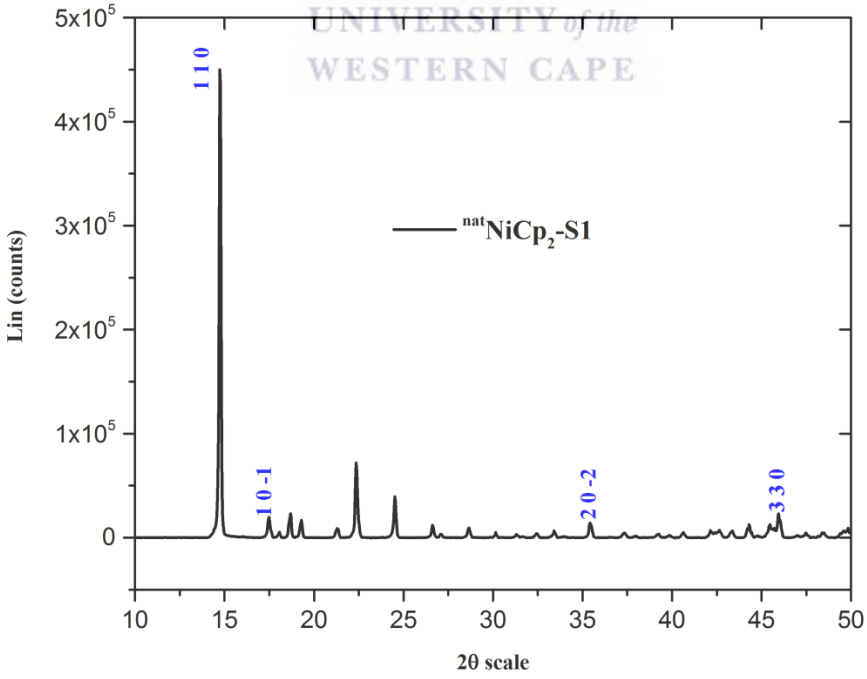

Figure 5.6: *The indexed XRD pattern of $^{nat}NiCp_2$ (sample 1) synthesized at iThemba LABS.*

These results are comparable to the one obtained for ferrocene having two crystal structures, monoclinic and triclinic, which was the initial assumption by Seiler and Dunitz of ferrocene and nickelocene being isostructural (Seiler & Dunitz, 1980). The only difference with the current results is that the phase change to triclinic on ferrocene only occurred at lower temperatures and not at room temperature as it is with the natural and enriched nickelocene (Seiler & Dunitz, 1979). The XRD patterns with indices obtained using EXPO2014 software (Altomare *et al.*, 2013) are shown in Figures 5.5 to 5.8. Only four peaks were labelled for their rotations (at 2θ approximately 15°, 18°, 35° and 45°). These 2θ angles were randomly chosen due to their intensities and also to compare with recent results on nickelocene by Gonzalez-Garcia *et al.* (2017). The rotations for natural material ($^{nat}NiCp_2$) between the commercial and the in-house synthesized nickelocene sample on the chosen 2θ angle are comparable (1 1 0; 1 0 -1; 2 0 -2 and 3 3 0). Rotations for $NiCp_2$ with the enriched ^{60}Ni and ^{62}Ni are different from the rotations obtained for natural nickelocenes as labelled in the Figures 5.7 and 5.8. The EXPO2014 data file for the analysis of $^{62}NiCp_2$ is attached on appendix (A.3) for further referencing

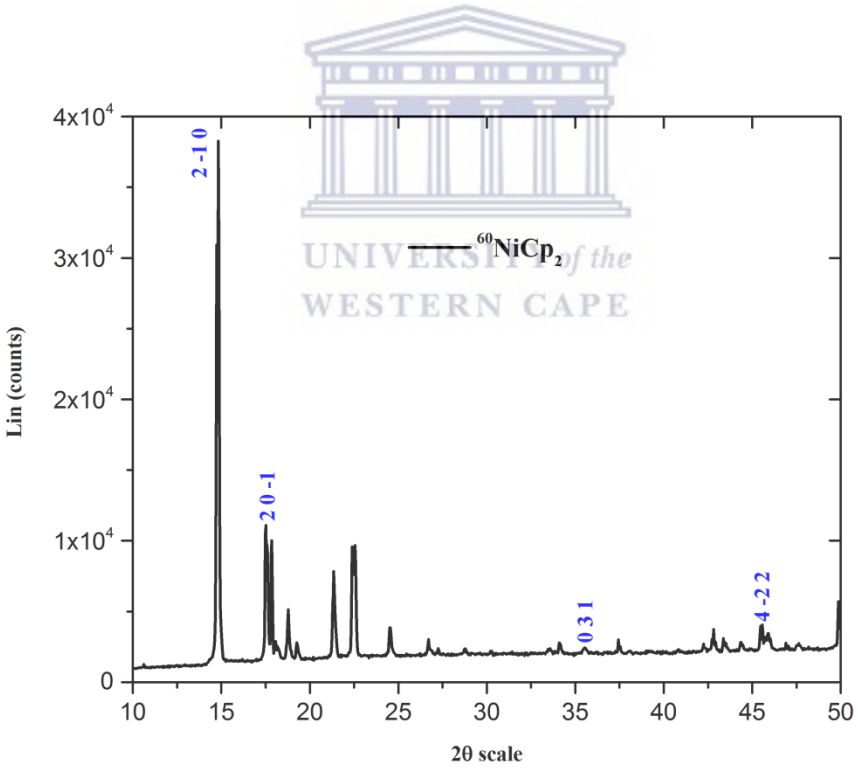

Figure 5.7: *The indexed XRD pattern of $^{60}NiCp_2$ which was synthesized at iThemba LABS.*

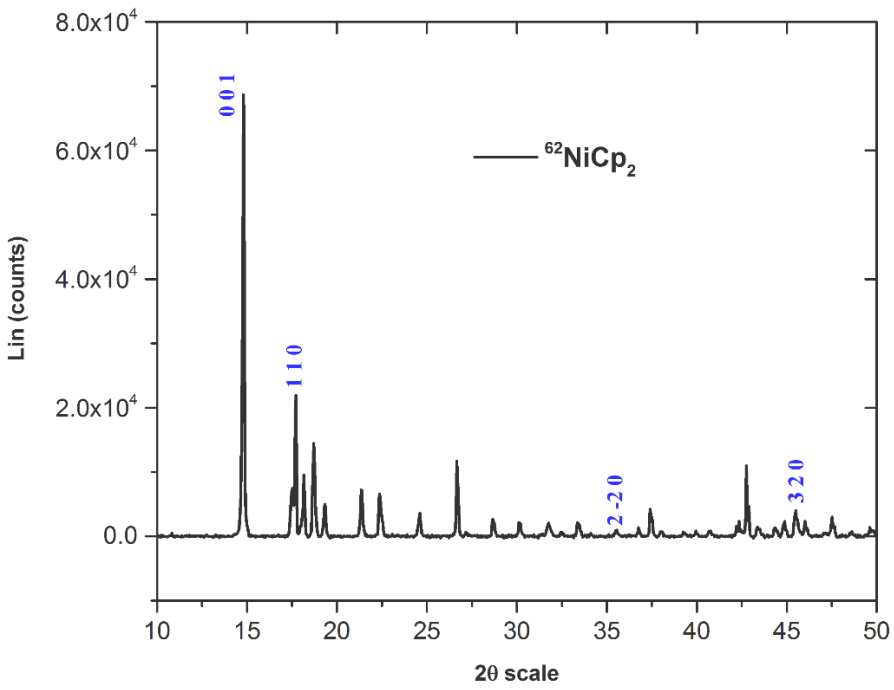

Figure 5.8: *The indexed XRD pattern the $^{62}NiCp_2$ which was synthesized at iThemba LABS.*

5.3 Fourier Transform Infrared Spectroscopy (FT-IR) results and discussions

Centrally π bonded complex which represent one of the largest groups of metal π-complexes, exhibit infrared spectra in regions almost similar to those of the centrally σ–bonded derivatives. However, these compounds are characterised by metal-ring vibrations as well as other skeletal vibrations in the far IR region (Mehrotra & Singh, 2000). The FT-IR analysis was performed using PerkinElmer equipment available at the University of the Western Cape (UWC). The results are presented in Figures 5.9 to 5.15. Tables 5.5 and 5.6 presents the functional groups, type of vibrations and the characteristic absorptions of the spectra represented in Figures 5.9 to 5.12. The FT-IR sample preparation and characterisations of these spectra were conducted at UWC.

Table 5.4: *The table showing the FT-IR frequencies of the first batch of nickelocene samples prepared in-house using natural nickel and the commercially supplied by Sigma Aldrich.*

Sample ID	V(C-H) cm^{-1}	V(C=C) cm^{-1}	s(CH) cm^{-1}	π (CH) cm^{-1}	Ni-Cp
$^{nat}NiCp_2$, Sigma Aldrich	3000	1421	1043	819	Not observed
$^{nat}NiCP_2$-1	3000	1405	1000	790	Not observed
$^{nat}NiCP_2$-2	-	-	-	-	-
$^{nat}NiCP_2$-3	3129	1535	1033	793	Not observed

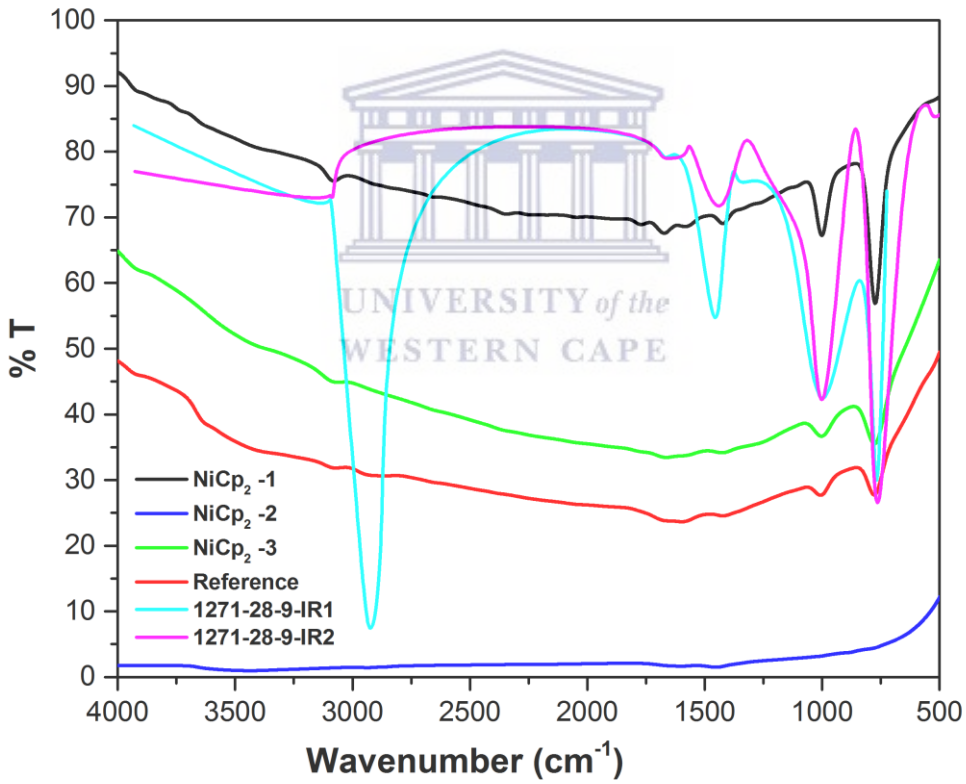

Figure 5.9: *This combined IR spectra of nickelocenes sample 1-3 ($NiCp_2$ 1-3) synthesised in-house and nickelocene supplied by Sigma Aldrich (reference) stacked to two nickelocenes spectra from the NIST database (Chemical book, 2016), sample IDs 1271-28-9-IR1 and 1271-28-9-IR2 supplied by Sigma Aldrich.*

The assigned bands presented in Table 5.5 showed the weak stretching intensities bands of C-H at wavelength regions of 3000 cm^{-1} in all samples. The spectra for the samples were fitted in FT-IR spectrum supplied by NIST on their website for nickelocene. The ID number of the given on the website is 1271-28-9 (Chemical book, 2016), see also Figure 5.9. At 1535 - 1421 cm^{-1} frequencies, the C=C is observed. The C-H in plane bending was observed at the frequencies 1043 - 1000 cm^{-1} and the C-H out of plane bending were observed in 819 - 793 cm^{-1} frequencies. The bands assigned for the metal–ring stretches were not detected because KBr FT-IR was used and is not sensitive in the regions below 500 cm^{-1}, assigned region for metal ring-stretches and tilts (Mehrotra & Singh, 2000).

Table 5.5: *The table presenting the results from the FT-IR analysis of the second and third batch of the synthesized nickelocene complexes at iThemba LABS.*

Sample ID	V(C-H) cm^{-1}	V(CH) cm^{-1}	V(C=C) cm^{-1}	V(C-C) (ring breathing mode) cm^{-1}	s(CH) cm^{-1}	π(CH) cm^{-1}
$NiCp_2$ Sigma Aldrich	3076	2978	1426	1160	1000	767
$^{60}NiCp_2$	3085	2924	1421	1109	1000	770
$^{62}NiCp_2$	3082	2969	1423	1111	1003	772

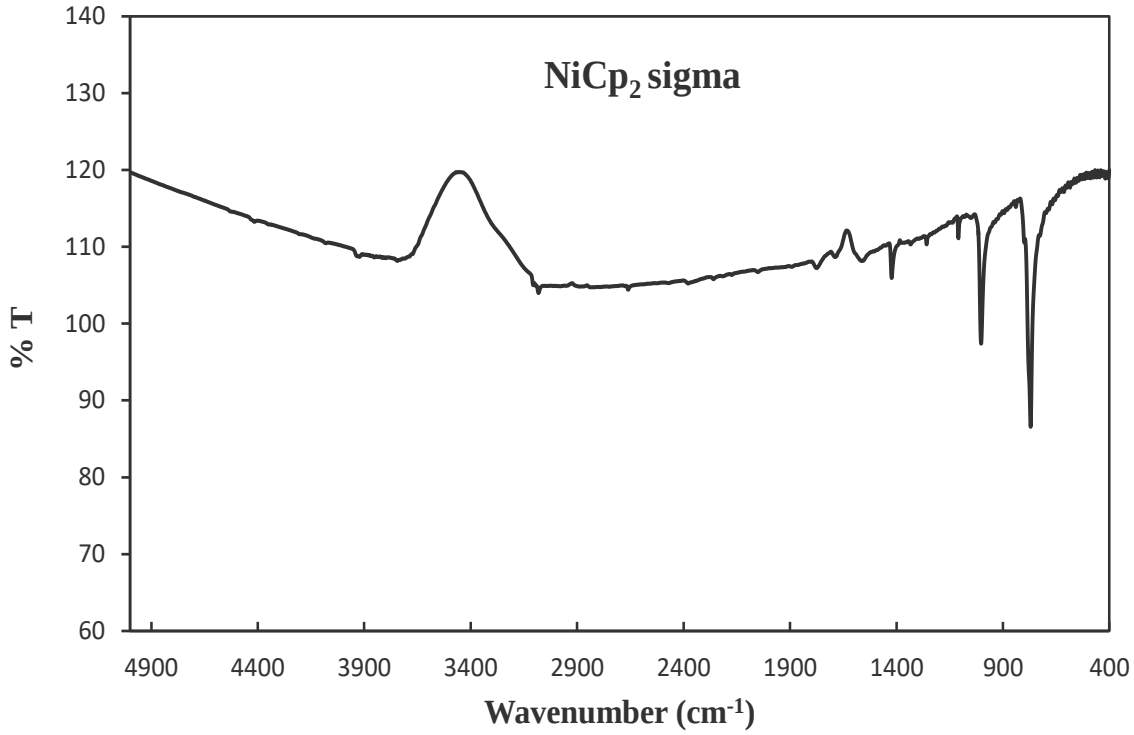

Figure 5.10: *FT-IR spectrum obtained after analysing nickelocene supplied by Sigma Aldrich used as a reference material in this study.*

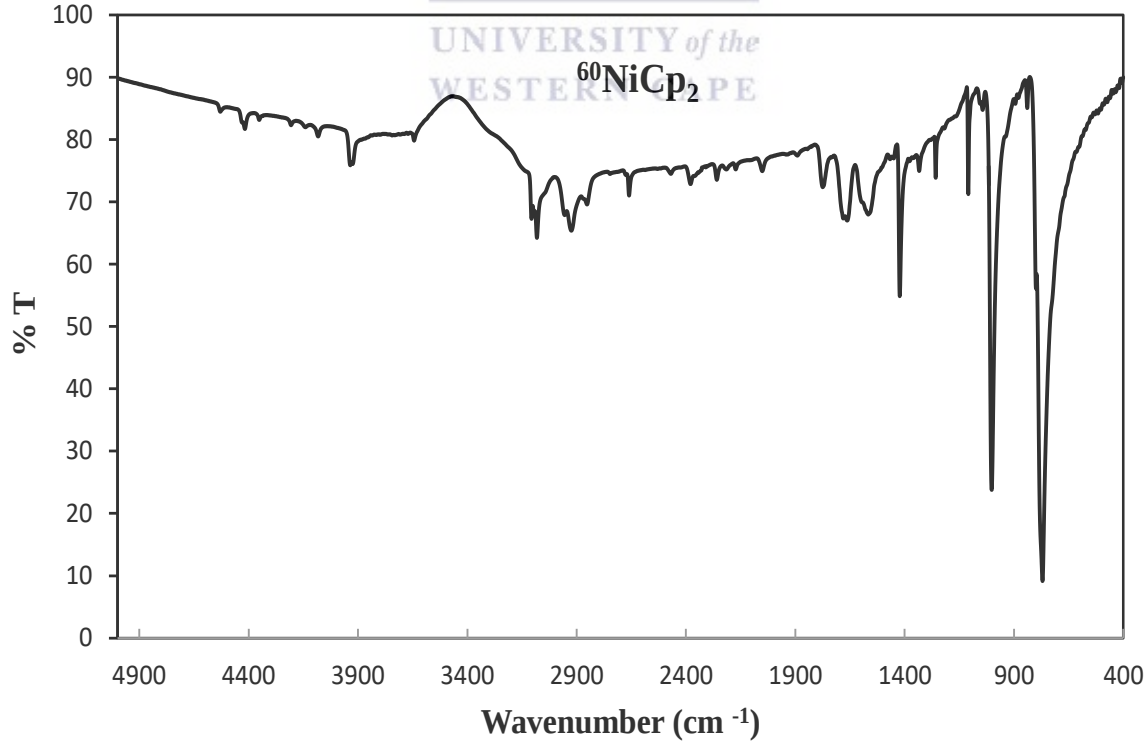

Figure 5.11: *The nickelocene with the enriched 99 % of enriched ^{60}Ni isotope FT-IR spectrum.*

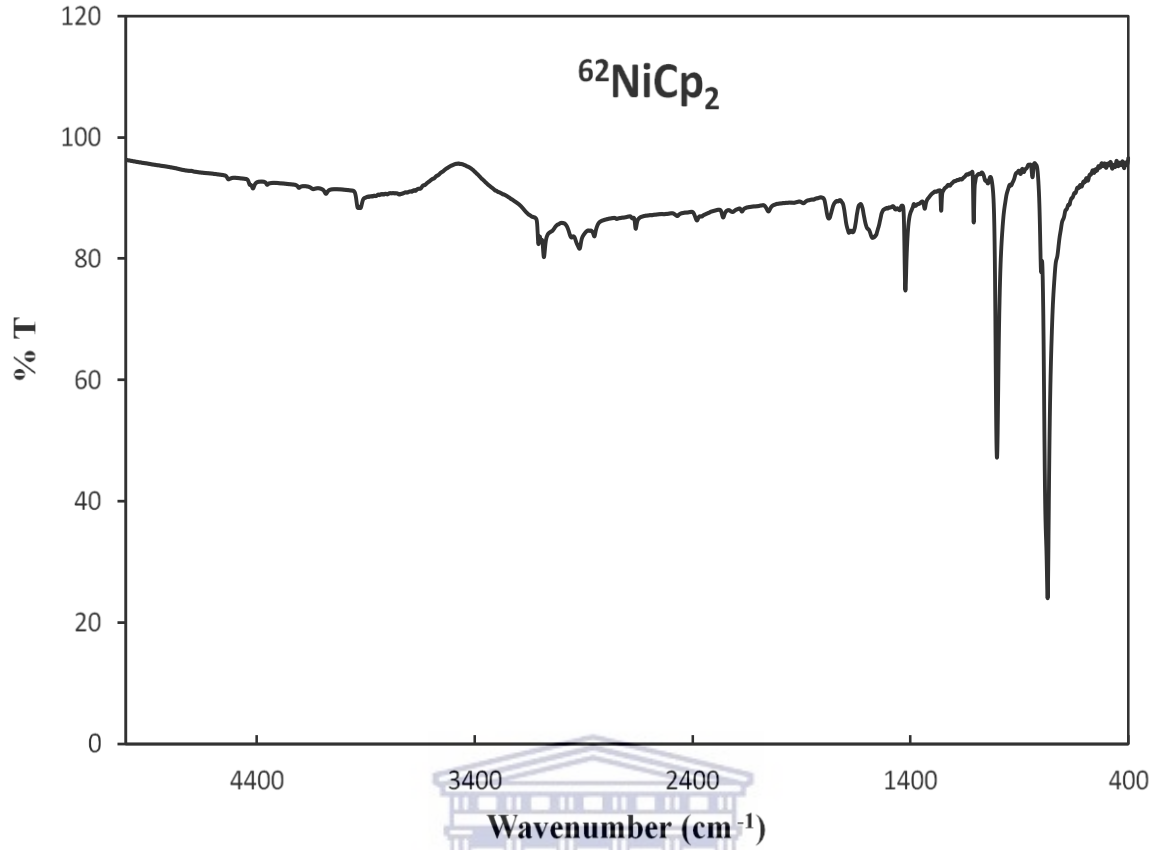

Figure 5.12: *The FT-IR spectrum obtained from the analysis of nickelocene complex with the enriched ^{62}Ni isotope.*

The FT-IR results shown in Figures 5.10 to 5.12 were obtained from the commercial nickelocene and the locally synthesised nickelocenes with enriched isotopes of ^{60}Ni and ^{62}Ni. Peaks are assigned and listed in Table 5.6. Three strong peaks were observed in all 3 samples in frequency region of 1423 to 760 cm $^{-1}$. Weak bands observed in a region of 3085 to 3070 cm^{-1} are due to C-H stretching vibrations and the C-H bands are also assigned for frequencies at 2978, 2969 and 2924 cm^{-1}. Weak bands are also observed in a region of 1100 cm^{-1} and are assigned for asymmetric ring breathing mode. The in plane CH bending was observed in 1003 and 1000 cm^{-1} frequency regions and the out of plane CH bends are in 772, 770 and 767 frequency regions. The metal–ring stretch is supposed to be seen at a region between 400 - 350 cm^{-1} as described by Mehrotra and Singh (2000). However, the stretching and bending vibrations (below 500 cm^{-1}) could not be observed due to the out of the instrument range that was used during the analysis as a result metal ring stretching was not observed.

5.4 Proton Nuclear Magnetic Resonance (^{1}H NMR) analysis results and discussion

^{1}H NMR analysis was conducted on nickelocenes produced from natural nickel and the one containing enriched ^{60}Ni. The first batch of samples which contained nickelocene with natural nickel including the reference sample were characterised at the Central Analytical Facility (CAF) of the University of Stellenbosch using solvent NMR. Deuterated chloroform ($CDCl_3$) was used as a solvent however the solubility was poor in all four samples. Combined spectrum of the analysis is shown in Figure 5.13. Samples also started to decompose during the characterisation and the analysis had to be stopped. As a result, the expected peak at the region of interest for nickelocene was not observed. The chemical shift observed at 7.26 ppm in all 4 samples is for $CDCl_3$. Results discussed below show that a bad sample can yield incorrect results. After this experience, solid state NMR was considered but the CAF facility was not equipped at the time to perform the experiment using solid state NMR. Then, other solvents were tried out and the results are presented in Figures 5.17 to 5.19.

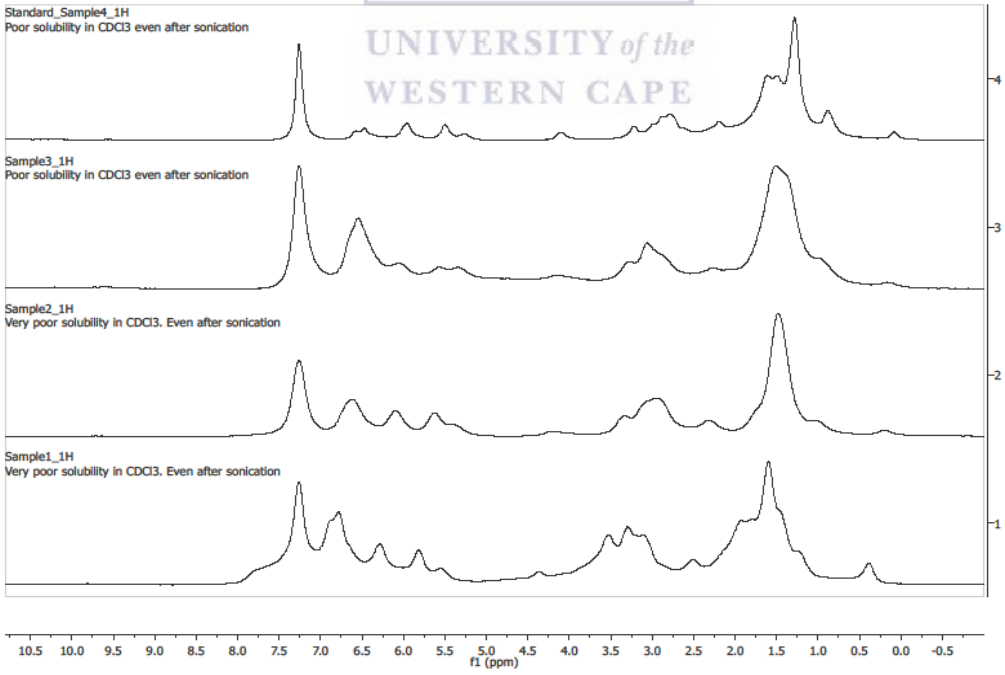

Figure 5.13: *Combined solvent ^{1}H NMR spectra of the analysis of the first batch (samples 1 to 3) of nickelocene samples and nickelocene from Sigma Aldrich. The solvent used was $CDCl_3$.*

The spectra shown in Figures 5.14 - 5.16 were all acquired on solvent proton NMR using the isotopologue deuterated dimethyl sulfoxide-d_6 (DMSO–d_6) as a solvent. DMSO was chosen instead of deuterated chloroform due to problems explained above. Figures 5.14 to 5.16 are for spectra of the commercial nickelocene and the in-house synthesised nickelocene using natural nickel and the enriched ^{60}Ni isotope. A chemical shift with a sharp intensity observed near zero in all three samples is for DMSO. Wide chemical shifts with broadened signals are observed around -250 ppm. Martin and Austin (2016) also reported the chemical shifts of nickelocene theoretically and experimental at -254 ppm. Isotropic signal shifts of nickelocene at -257 ppm are also reported for solid proton NMR (Heise *et al.*, 2001; Martin & Autschbach, 2015; Martin & Autschbach, 2016).

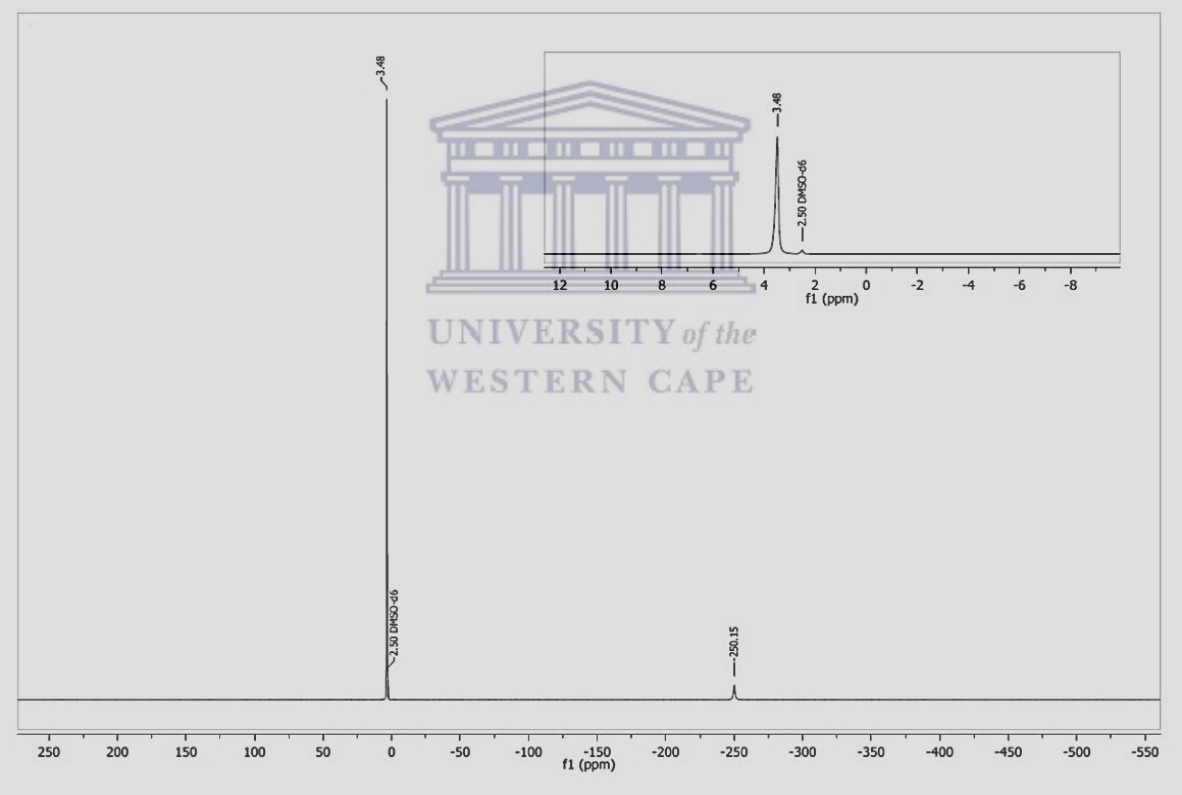

Figure 5.14: *The ^{1}H NMR of the characterisation of $NiCp_2$ acquired from Sigma Aldrich. The blown peak is for a DMSO solvent used to dissolve a complex.*

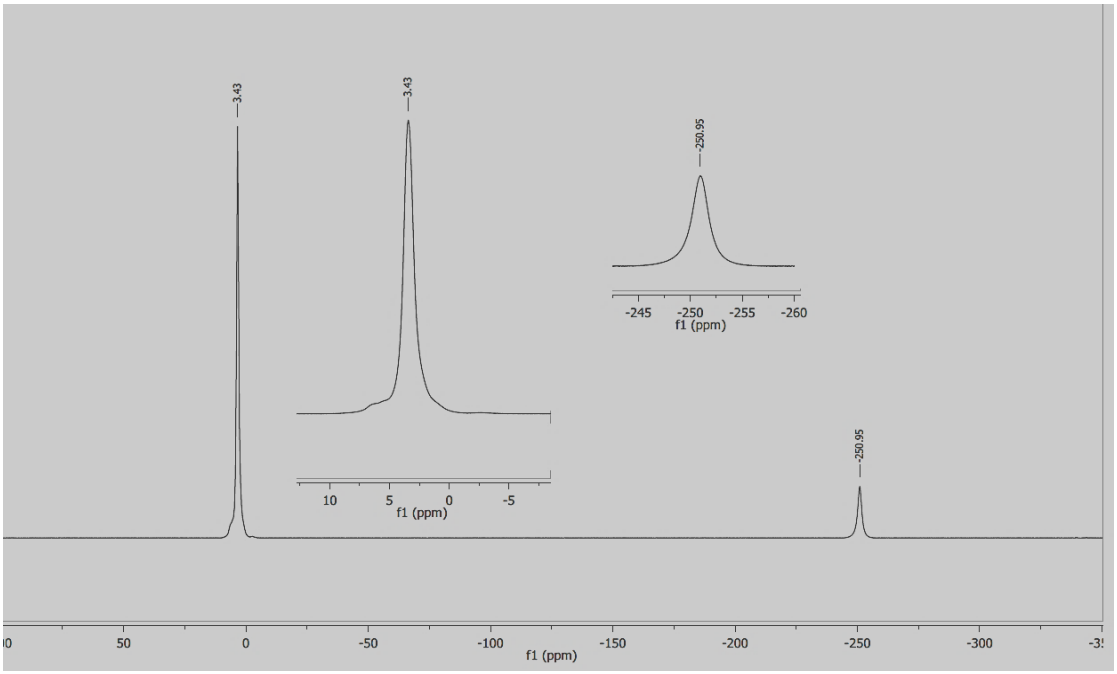

Figure 5.15: *The solvent ^{1}H NMR spectra for a nickelocene produced at iThemba LABS from natural nickel.*

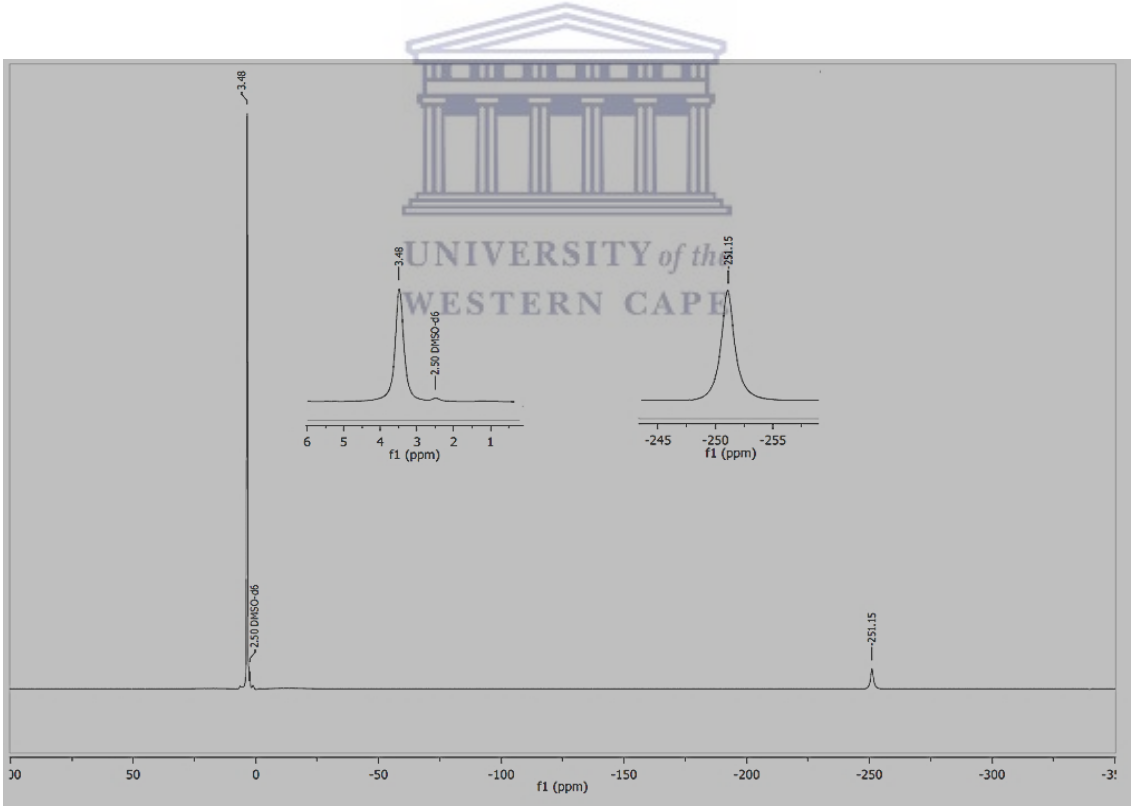

Figure 5.16: *The spectra obtained after analysis from solvent ^{1}H NMR for enriched $^{60}NiCp_2$.complex which was synthesized at iThemba LABS.*

The reason for high field shifts in all three samples is due to the anisotropic effect of paramagnetism of nickelocene (Vaara, *et al.*, 2015). Nickelocene is said to have degenerate antibonding orbitals (e_{1g}^{*}) and this fact is reflected in electrochemical properties of the ligand (Mehrotra & Singh, 2000; Sitzmann, 2001; Hrobarik, *et al.*, 2007), see Figure 5.17 for molecular orbital diagram of nickelocene. As such, this results in large NMR shifts because of the unpaired electron situated in the antibonding orbital of the metal. This unusual proton resonance shift for paramagnetic nickelocene sandwich was also reported early right after discovery of nickelocene by McConnel (1957) in both solvent and solid state NMR.

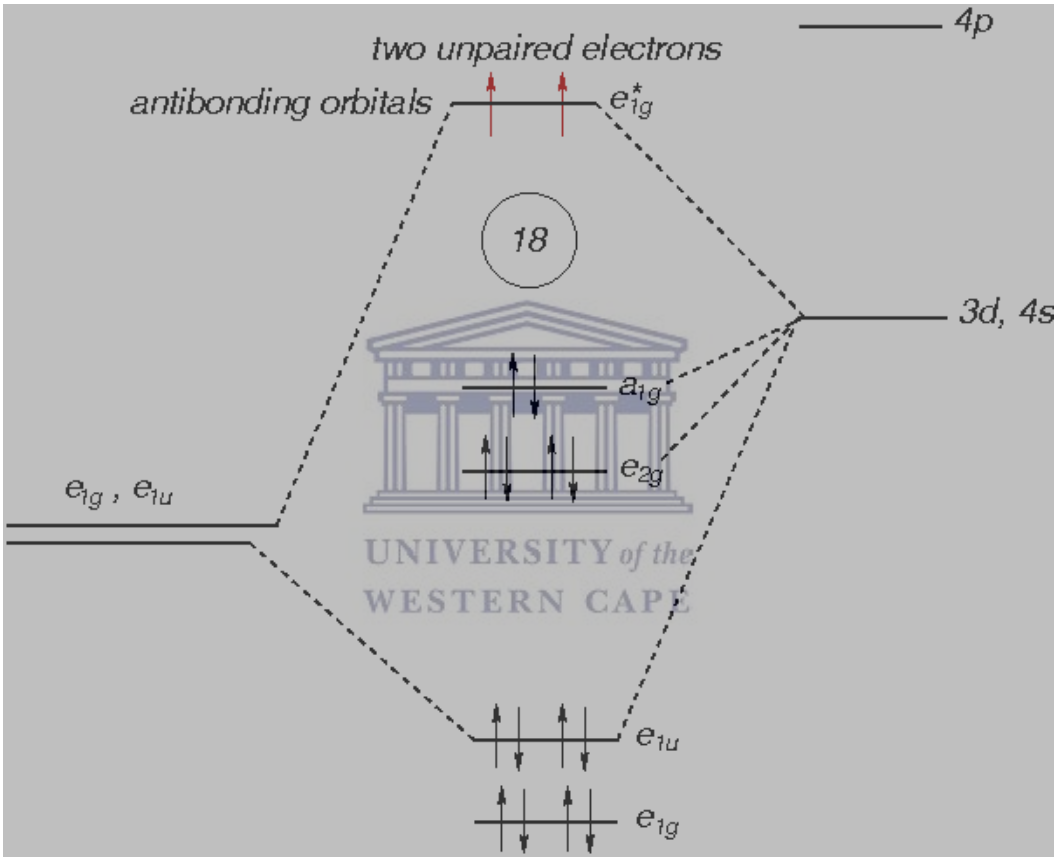

Figure 5.17: *Partial molecular orbital diagram of nickelocene showing the bonding configuration of the complex. The highlight in red shows the two valence electrons that are located in the anti-bonding orbital, which are the reason for paramagnetism effect of the nickelocene complex (Sitzmann, 2001).*

Chapter 6 Nickel Beam Production

The objective of this study is to develop nickel (from ^{60}Ni and ^{62}Ni) ion beams using the iThemba LABS' ECRIS4. These beams are required and to be used for the approved two-step Coulomb excitation experiment, entitled "Search for the loss paradigm of surface vibrations". More details regarding the experiment are also discussed in Chapter 1, whereby the objectives of the experiment are highlighted. Also in chapter 1, more discussions on why MIVOC method was the preferred methods to produce metallic beams were highlighted. Furthermore, details on the MIVOC method and its requirements are described in Chapter 3. This also emphasise the developments of nickelocene as precursor material for MIVOC method. Nickelocene synthesis and their behaviour are discussed in Chapters 4 and 5. In this chapter, the focus is on the applications of nickelocene as related to beam production. A detailed description of the production of nickel beams in the ECRIS4 using the MIVOC method at iThemba LABS will be described in detail in this chapter.

6.1 Pre-sample preparation for MIVOC experiment

Commercial nickelocene, $^{nat}NiCp_2$, $^{60}NiCp_2$ and $^{62}NiCp_2$ were used for nickel beam production experiments in ECRIS4. Investigations using the MIVOC method were initiated using a commercially supplied natural nickelocene from Sigma Aldrich. This was done for comparison purposes before enriched nickelocene complexes ($^{60}NiCp_2$ and $^{62}NiCp_2$) were used. Approximately 1g of the nickelocene was loaded to a stainless steel container (also the MIVOC container). Nickelocene is sensitive to moisture and air, therefore suitable environment is required to handle the material. The loading process of nickelocene for this study was performed inside a glove box under nitrogen atmosphere. After loading, the container was closed with an on/off valve, thereafter, evacuated on a separate pumping system to a pressure of 10^{-4} mbar. This pressure is comparable to the vapour pressure of the nickelocene. The setup is shown in Figure 6.1. The MIVOC setup was then coupled to the injection system of the ECRIS4 through a manual regulation valve and via another on/off valve and an insulator connected to the injection chamber of the source. Figure 6.2 shows the injection system before installing to the source, which is shown in Figure 6.3. Recorded masses of $^{60}NiCp_2$ and $^{62}NiCp_2$ used for experiments were 300 mg and 170 mg, respectively.

It should be noted that the experiments were conducted on different days for each nickelocene complex.

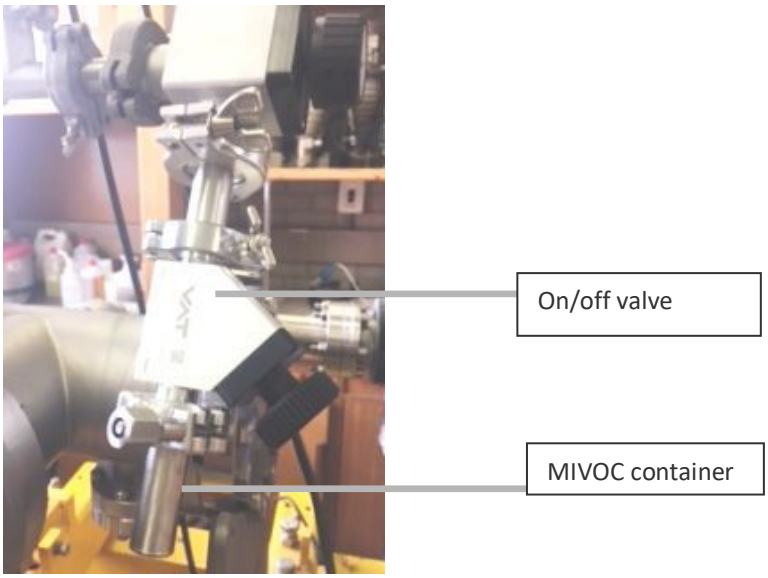

Figure 6.1: *The picture shows the MIVOC container attached to the on/off valve connected to a separate pumping system for pre-pumping.*

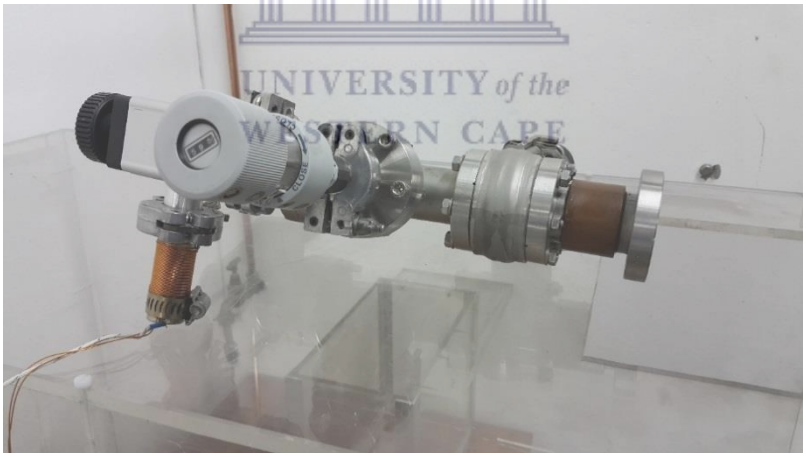

Figure 6.2: *The injection system for MIVOC setup before the installation to the ECRIS4.*

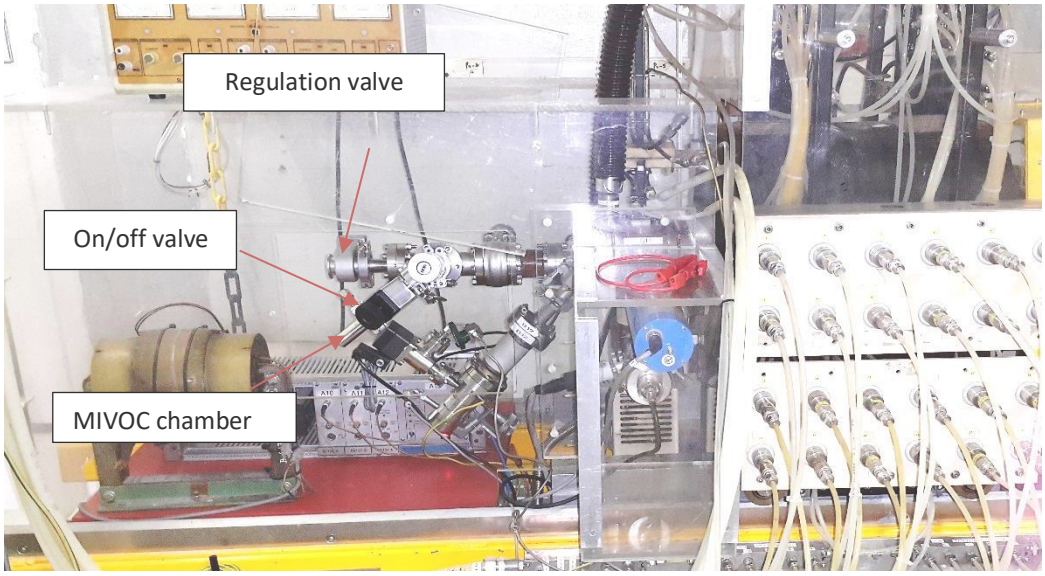

Figure 6.3: *Photograph of the MIVOC injection system connected to the source.*

6.2 Beam production with natural nickelocene

The beam experiments were conducted with ECRIS4 attached to the Q injection line, (see Figure 3.4). The process involves the beam being extracted from the 14.5 GHz ECRIS4 and focused with the solenoid of 0.2 m length with a maximum magnetic induction of 0.75 T. It is then directed into the focal position in front of the double focusing 90° bending magnet which has a rigidity of 0.1 Tm. The beam then drifts to the entrance of the existing Q-line where it is focused by means of electrostatic einzel lens. This reduces the beam envelope during the drift to the horizontal and vertical slits in front of the Faraday cup 3Q. The beam requirement is in the range of 200 MeV for ^{60}Ni and ^{62}Ni beams. For the iThemba LABS accelerator complex this energy can be achieved with the Ni^{8+} charge state. Therefore, all experimental measurements were carried out for the beam optimised for this charge state. The first experiments were carried out to optimise the beam intensity measured in the Faraday cup 3Q for natural Ni (see Figure 3.4) for $^{58}Ni^{8+}$ at source potential (U_{ex}) of 10 kV. The extraction current was 1 mA. For a biased disc voltage of -80 V, the disc current amounts to 0.2-0.3 mA. The longitudinal magnetic field at the injection and extraction was set to approximately 1.1 and 0.9 T, respectively. The flow of nickelocene was adjusted by a manual regulation valve to yield a pressure of 2.7 - 20 x 10^{-6} mbar measured at the injection side of the source. The slits in front of the Faraday cup were opened up to 60 mm in both the horizontal and vertical plane. All experiments were carried out without supporting gas. Initial pressures at

the source injection and extraction sides were 5.0 x 10^{-7} mbar and 8.0 x 10^{-8} mbar, respectively. The highest current of about 20 µA was obtained after 1 hour of conditioning. Figure 6.4 shows the $^{58}Ni^{8+}$ beam intensity measured in Faraday cup 3Q. Over a time span of approximately 1 hour, beside dips which are due to small discharge in the extraction system, the current is constant within ±5 %.

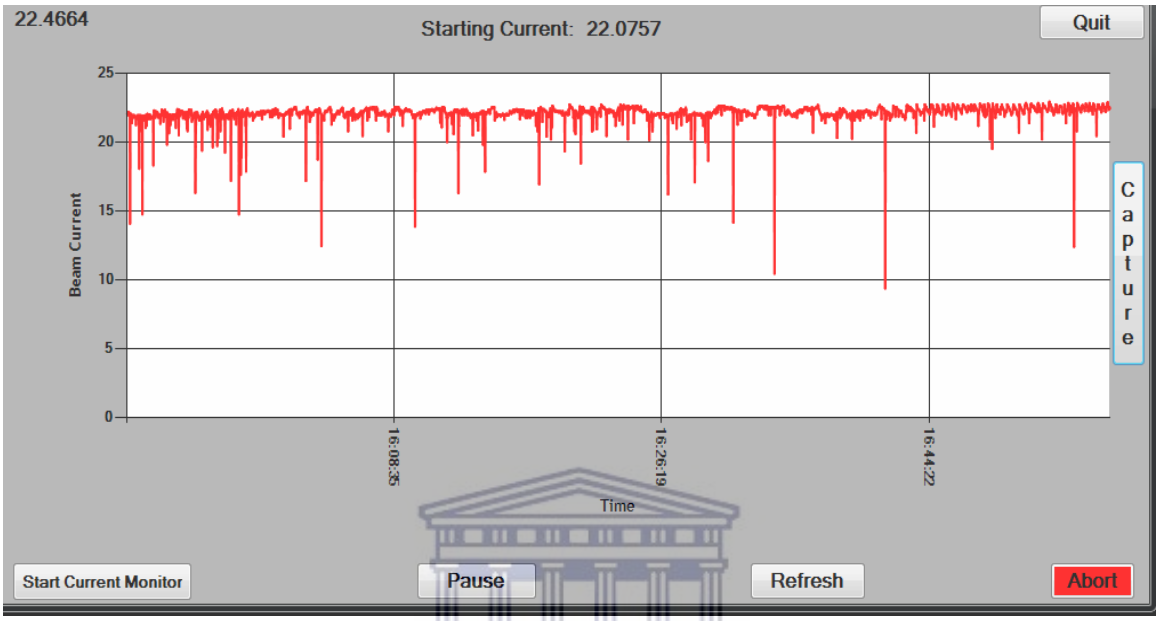

Figure 6.4: *The $^{58}Ni^{8+}$ beam intensity measured in Faraday cup 3Q over approximately 1 hour. The slit width amounts to 60 mm for both planes.*

Subsequently, the mass over charge, m/q spectrum, was measured to determine the beam composition. For these measurements, the horizontal SLX and vertical SLY slit width were adjusted. The values for these adjustments are displayed at the top header caption of the spectrum in Figure 6.5. The bending magnet and solenoid currents were varied simultaneously from 31 to 47 A and 130 to 215 A, respectively. This corresponds to an m/q charge state of 10 to 5. At a source potential of 10 kV, Ni charge states of 10 to 5 were observed (Ni^{10+} and Ni^{5+}). Note that Ni^{5+} and Ni^{10+} were also present, however were superimposed by the $^{12}C^{1+}$ and $^{12}C^{2+}$ peaks, respectively. The intensity for the charge states showed a typical distribution. Literature values for the abundance of nickel isotopes in natural nickel are 68% ^{58}Ni, 26% ^{60}Ni and 3.6% ^{62}Ni respectively (Valley, 1941, Rosman & Taylor, 1998). However, the spectrum indicates a ratio of 52, 36 and 12% for the three isotopes. The discrepancy could be caused by the different transmission efficiencies for the different

masses and that even at 5mm slit width the different species are not completely separated. Experiments in which the beam is accelerated through SPC2 will allow for a complete separation of the isotopes.

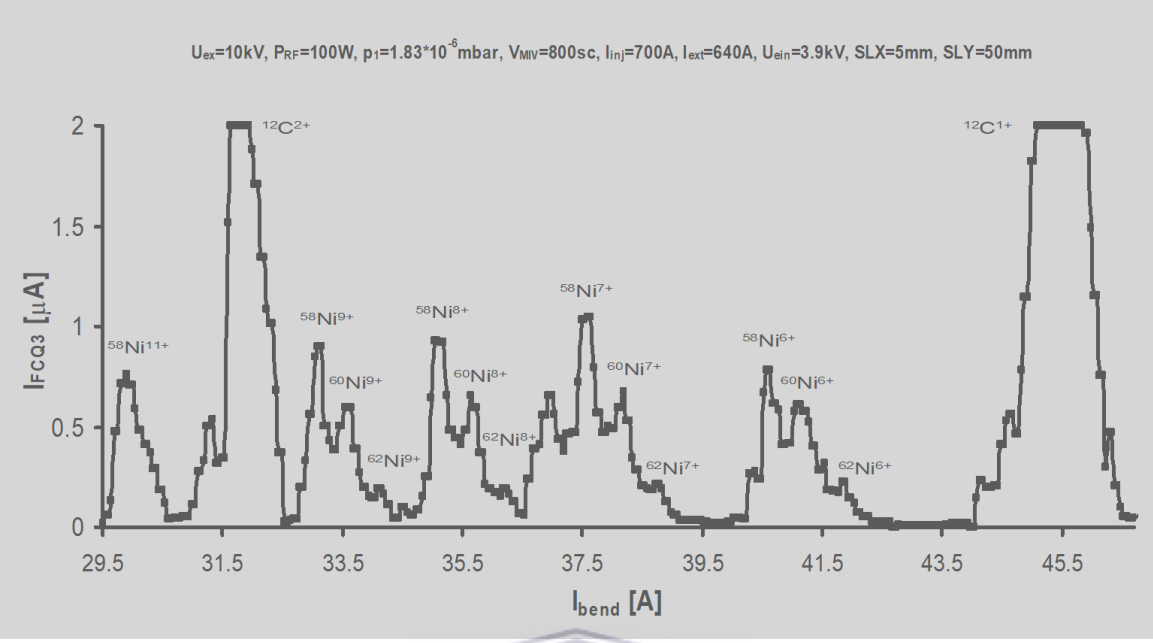

Figure 6.5: *The m/q spectrum for commercial nickelocene obtained at the experiment using the ECRIS4 source. The spectrum is obtained by varying the bending magnet current (31 - 47 A) and solenoid current (130 - 215 A) current simultaneously. The Faraday cup current range is 2μA.*

6.3 Beam Production with ^{60}Ni and ^{62}Ni nickelocene

Next, the production of ^{60}Ni ion beams from enriched nickelocene [^{60}Ni(C_5H_5)$_2$] and [^{62}Ni(C_5H_5)$_2$] are discussed. The first 5 hours of experiments, accounted for the conditioning of the ECRIS system, and decontamination process, as natural nickelocene was used previously. During the conditioning process, both ^{58}Ni and ^{60}Ni ion beams were measured with the ^{58}Ni intensity decreasing with time. Then, the experiments were conducted as in the previous experiments for natural beam production, but with the slight modification of the source parameters. For example, in the second experiments during the ^{60}Ni and ^{62}Ni beams production, the m/q spectra were acquired when the slit widths were adjusted on both the horizontal and vertical positions to 1 and 20 mm, respectively and the bending magnet current was varied between 31 and 47, respectively. The solenoid currents were kept the same

as previous settings, 130 to 215 A. The parameters are recorded in Tables 6.2 and 6.3, and also shown in the caption of Figures 6.6 and 6.8. Currents of 30 µA was measured in both ^{60}Ni and ^{62}Ni beam experiments.

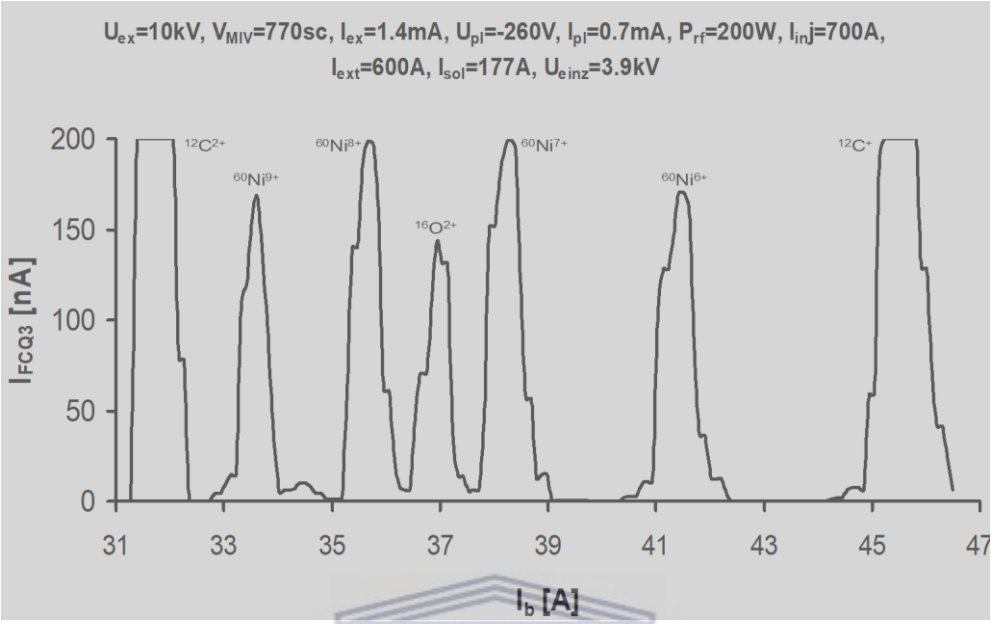

Figure 6.6: *The m/q spectrum for ^{60}Ni from enriched 60-nickelocene. The spectrum is obtained by varying the bending magnet (31 - 47 A) and solenoid (130 - 215A) current simultaneously. The Faraday cup current range was 200 nA.*

From the m/q spectrum in Figure 6.6, the $^{60}Ni^{10+\text{ to }5+}$ charge states are present with both charge state +10 and +5 superimposed by $^{12}C^{2+}$ and $^{12}C^{1+}$. Charge states of +6 to +9 are observed with +8 and +7 states occupying maximum peaks. During the ^{60}Ni beam production, the beam was further transported through the Q- and AX-line to Faraday cup AX2 in front of SPC2. The profile of the beam at that position in AX-line (in front of SPC2) is shown in Figure 6.7. At this beam line, a current of 21 µA was measured. The transmission of 75% was probably due to charge exchange processes during transportation.

From the spectrum in Figure 6.8 all the charge states peaks of 10 to 5 are observed as opposed with the previous results obtained for natural and enriched nickel-60 beam profiles whereby +10 and +5 charge peaks are superimposed by +2 and +1 ^{12}C charge states. In the present result, doublet peaks are observed for +10 and +5 in ^{62}Ni paired with +2 and +1 of ^{12}C. In the overall results obtained for both ^{60}Ni and ^{62}Ni, the results showed peaks for the

^{60}Ni and ^{62}Ni isotopes with no extra impurities other than expected by-products elements of C, H and O. Source parameters for experiments are shown in Table 6.1.

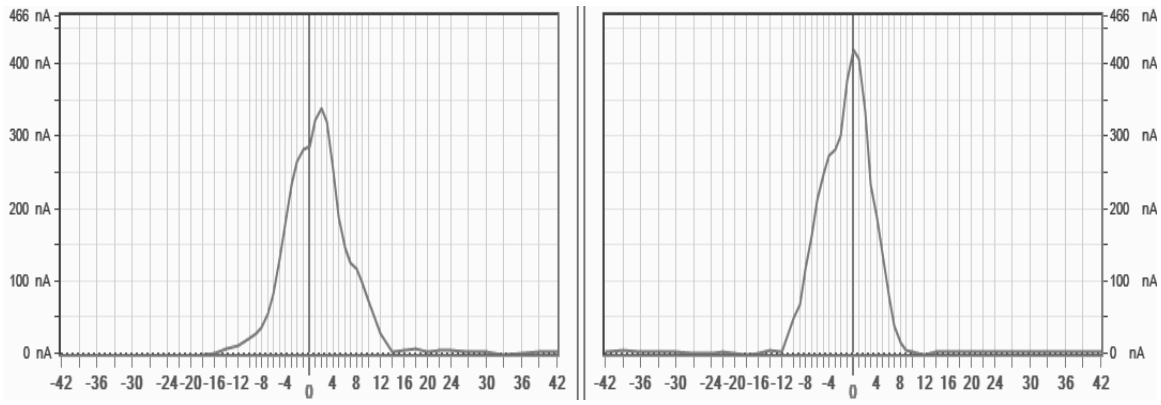

Figure 6.7: *Beam profile of the $^{60}Ni^{8+}$ ion beam measured in the AX-line, X (left) and Y (right).*

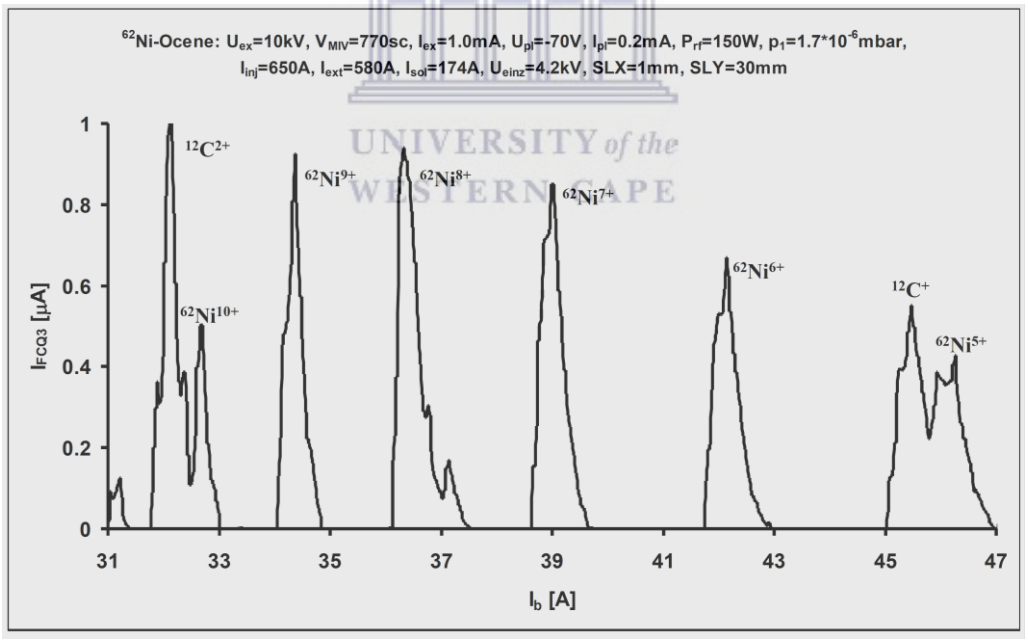

Figure 6.8: *The m/q spectrum of a beam profile of ^{62}Ni obtained in MIVOC method using 62-nickelocene.*

Table 6.1: *The ECRIS4 parameters during the production of ^{nat}Ni and ^{60,62}Ni beams using the MIVOC method.*

Parameter	Unit		
	^{nat}Ni	^{60}Ni	^{62}Ni
Slit width Q3(in front of Faraday cup(Q3)	50 mm (horizontal and vertical)	1 mm (horizontal), 20 mm (vertical)	1 mm (horizontal), 30 mm (vertical)
Regulation valve (V_{MIV})	800 sc	770 sc	770 sc
Injection side pressure (P_1)	1.8×10^{-6} mbar	2.0×10^{-6} mbar	7.0×10^{-6} mbar
Microwave power (P_{RF})	100 W	200 W	150 W
Coil currents	592 A(I_{inj}) and 620 A(I_{ext})	690 A(I_{inj}) and 600 A(I_{ext})	650 A(I_{inj}) and 580 A(I_{ext})
Steerer Currents(I)			
I_{STX1}	0.3A	1.0 A	1.0 A
I_{STY1}	0.36A	0.1A	0.1A
I_{STX2}	2.21A	0.3 A	0.3 A
I_{STY2}	0.5 A	0.1 A	0.2 A
solenoid current(I_{sol})	165 A	177 A	177 A
einzellens voltage (U_{EIN})	3.53 kV	3.9 kV	3.9 kV

6.4 The acquired m/q spectra

This section highlight the method used on how the m/q spectra were obtained during the beam production. The ion source is charged to a potential U on which the ions with mass m and charge q in the plasma are created. Those ions close to the extraction aperture of the plasma chamber are accelerated towards the ground electrode and will drift through the beam line with a kinetic energy U*q. A solenoid is positioned at 1.2 m behind the source focuses for a certain current setting, one specific m/q into the focal position in front of the bending magnet. From there the ions drift through the double focusing 90º magnet which again bends one specific m/q onto the design radius. Ions with different m/q ratios will not be transmitted.

The bending magnet acts as a mass spectrum analyser. However, because the emittance of different charge states extracted from the source are not necessarily identical. Each charge state would need a separate optimisation of the solenoid. The shapes of the peaks are influenced by the slit opening and possible offsets of the electronics.

Chapter 7 Conclusions

The method to develop nickelocene was successfully achieved in this study. Nine samples were synthesised, seven of which being synthesised with natural nickel while two samples were synthesised with enriched ^{60}Ni and ^{62}Ni. A percentage yields for the complete synthesis of Ni to nickelocene of 16 % to 48 % were obtained. After the investigation of the low yield, it was found that the method depends fully in all reagents used during the process of the multi-step synthesis. The freshness of the reagents like ammonium hydroxide, which is used during the formation of the intermediate product, and the hexaaminenickel(II) chloride percentage yield play an important role for final product yield. If the ammonia solution is not stored accordingly, it loses the ammonia, whereas in the other hand the hexaaminenickel chloride storage of the product is also crucial. To prevent the escape of ammonia from the complex, the hexaaminenickel chloride should be stored in appropriate sealed vials. During the investigations, we also found out that if the complex stored in an airtight vial is further sealed with parafilm, the complex can be kept longer without losing any ammonia. The storage of sodium cyclopentadienide under nitrogen atmosphere before and after use also plays an important role on the % yield of the nickelocene complex. This avoids the organometallic compound from decomposing. The favourable conditions during the synthesis were inert atmosphere to prevent any decomposition and contamination of the final product. Sublimation time of the product played an important role as well. The longer the time, the better or higher percentage yield of nickelocenes were obtained. All these factors worked hand in hand with each other. We have noticed that, even the samples of nickelocene stored under vacuum can decompose after a week or two if exposed to light. This was observed by a colour change from dark green to brown. For samples stored away from light the lifespan increased without any colour change being observed.

Crystal structures of the nickelocene samples were characterised in order to determine the orientation within the crystal complex. The crystal structures were obtained using the obtained XRD data and processed further using EXPO2014 analysis software. From these analyses, monoclinic structure was predicted for $^{nat}NiCp_2$ and commercial $^{nat}NiCp_2$ samples. These results agree with the studies conducted on the crystal structure of nickelocene by Seiler and Dunitz (1980). On the other hand, both monoclinic and triclinic structures were predicted for isotopically enriched nickelocenes, $^{60}NiCp_2$ and $^{62}NiCp_2$. This findings agree

with the theoretically assumption by Seiler and Dunitz (1979) for nickelocene structure based on their study on ferrocene structure. Seiler and Dunitz (1979) assumed that since both ferrocene and nickelocene were isostructural, their crystal structure should to be similar.

Nickelocene samples were further characterised for bond vibrations using IR method. The results showed bands frequencies at, for these nickelocene complexes similar to results of Mehrotra and Singh (2000). These vibrational bands 3000 cm^{-1}, 1400 cm^{-1}, 1000 cm^{-1} and 700 cm^{-1} were assigned to C-H, C-C, C=C and CH, respectively. In addition, the paramagnetic shifts of nickelocene were also observed at -250 ppm using NMR. These shifts observed in the far negative region of the NMR spectra were also reported by Heise *et al.* (2001) and recently by Martin and Autschbach (2015).

The application of the synthesised nickelocene samples by producing nickel beams in ECRIS4 of iThemba LABS were conducted with maximum beam currents of 30 µA for the first time. The experiments allowed the modifications on the ECRIS4 to accommodate for beam production using the MIVOC method. During these experiments three samples were used for Ni beam production in ECRIS4, namely, $^{nat}NiCp_2$, $^{60}NiCp_2$ and $^{62}NiCp_2$. The emphasis of this project was to produce ^{60}Ni and ^{62}Ni beams with a beam current above 20 µA in ECRIS4 before acceleration in SPC2. After final acceleration in the SSC these beams will be transported further into experimental vaults to the target. Beam currents of above 20 µA for $^{60}Ni^{+8}$ and $^{62}Ni^{+8}$ were found to be sufficient to provide beam current of above 35 enA onto a target for the Coulomb-excitation experiment proposal (see Chapter 1). It should be noted that the ^{60}Ni beam was transported further from ECRIS4 through the Q-line to the Faraday cup in front of the SPC2 were the current measured was 21 µA. These results obtained in both stations (ECRIS4 and transport line) will enable the MIVOC method to be applied for the nickel beam production for the proposed experiments. Ni beams were produced for the first time at iThemba LABS ECRIS4. In overall, the synthesis method for the production of the nickelocenes yielded samples with no additional impurities. When the enriched $^{60}NiCp_2$ and $^{62}NiCp_2$ were also used in the individual experiments, the spectra acquired presented only ^{60}Ni and ^{62}Ni.

7.1 Summary

The method for the synthesis of nickelocene complexes with ^{nat}Ni, ^{60}Ni and ^{62}Ni has been developed. The calculated efficiency of the production is between 16 and 48 %. From the synthesised samples, nickelocene complexes with ^{60}Ni and ^{62}Ni were further used at iThemba LABS ECRIS4 for the production of $^{60}Ni^{8+}$ and $^{62}Ni^{8+}$ beams. The beams extracted from the source had an intensity of approximately 30 µA. The MIVOC method developed here will allow further exotic metallic beams production of enriched low vapour pressure metals which are currently not accessible at iThemba LABS.

The samples were characterised for structural information using infrared, nuclear magnetic resonance and X-ray diffraction methods. The results were comparable with those from literature. However, there was a disagreement on the crystal structure determined using EXPO2014 program to analyse the XRD results. This discrepancy was only observed on the enriched nickelocene samples. Triclinic structures were found in both enriched complexes instead of the monoclinic structure given in the literature for natural nickelocene samples. This anomaly requires further investigation.

7.2 Future Work

- Investigation on the loss of Ni material during the multi-step synthesis will be conducted further or look onto other methods that will eliminate multi-step synthesis bearing in mind the purity of the final product.
- XRD analysis will be conducted using the enriched isotopes of nickel (^{58}Ni, ^{60}Ni and ^{62}Ni) to further investigate the crystal structure of nickelocene. Analysis are planned to be performed at the same for consistency.

REFERENCES

Aguayo, H. 2016. Crystal field theory and ligand field theory. *Chemistry of ligand*. New York, United States: Library press.

Altomare, A., Caliandro, R., Camalli, M., Cuocci, C., da Silva, I., Giacovazzo, C., Moliterni, A. G. G. & Spagna, R. 2004. Space-group determination from powder diffraction data: a probabilistic approach. *Journal of Applied Crystallography*, 37: 957-966.

Altomare, A., Camalli, M., Cuocci, C., da Silva, I. Giacovazzo, C., Moliterni, A. G. G & Rizzi, R. 2005. Space group determination: improvements in EXPO2004. *Journal of Applied Crystallography*. 38: 760-767.

Altomare, A., Camalli, M., Cuocci, C., Giacovazzo, C., Moliterni, A. G. G. and Rizzi, R. 2007. Advances in space-group determination from powder diffraction data. *Journal of Applied Crystallography*, 40: 743-748.

Altomare, A., Cuocci, C., Giacovazzo, C., Moliterni, A., Rizzi, R., Corriero N. and A. Falcicchio, A. 2013. A kit of tools for phasing crystal structures from powder data. *Journal of Applied Crystallography*. 46: 1231-1235.

Almenningen, A., Haaland, A & Lusztyk, J. 1979. The molecular structure of beryllocene, $(C_5H_5)_2$ Be. A reinvestigation by gas phase electron diffraction. *Journal of Organometallic Chemistry*, 170:271-284.

Andreyev, A.N., Huyse, M., Van Duppen, P., Welssman, L., Ackermann, G.J., Heßberger, F.P, Hoffmann, S., Kleinböhl, A., Münzeberg, G., Reshitko, S., Schlegel, C., Schffner, H., Cagarda, P., Matos, M., Saro, S., Keenan, A., Moore, C., O'Leary, C.D., Page, R.D., Taylor, M., Kettunen, H., Leino, M., Lavrentiev, A., Wyss, R. & Heyde, K. 2000. A triplet of differently shaped spin–zero states in the atomic nucleus of ^{186}Pb. *Nature*, 405:430.

Armstrong, D.R., Duer, M.J., Davidson, M.G., Moncrieff, D., Russel, C.A., Stourton, C., Steiner, A., Stalker, D. & Wright, D.S. 1997. Paddle-wheel tris (cyclopentadienyl) tin (II) and

lead (II) complexes: syntheses, structures and model MO calculations. *Organometallics,* 16*:*3340-3351.

Arnek, R. &. Zetterberg, K. 1987. Is thermal stability of σ- alkyl transition metal complexes compatible with the presence of conformationally free β – hydrogens and absence of stabilizing ligands? The isolation of novel and unexpectedly stable four – membered cyclic (σ- alkyl) palladium complexes. *Organometallics*, 6 (6): 1230–1235.

Arnold, P.L., Cloke, F.G.N. & Nixon, J.F. 1998. The first stable scandocene: synthesis and characterization of is (η- 2, 4, 5 – tri- tert-butyl-1, 3-diphosphacyclopentadienyl) scandium (II). *Chemical Communications*, 7: 797-798.

Arp, H.C. 1958. The Hertzsprung-Russel diagram. (*In* Flügge, S. (eds), *Encyclopedia of Physics, Astrophysics II: Stellar Structure*. Berlin, Göttingen, Heidelberg: Springer-Verlag.p.75-131.

Astruc, D. 2007. *Organometallic Chemistry and Catalysis. Structures of the transition metal complexes.* New York: Springer.

Bacher, A.D. 2016. *Chem174: Metallocene.* Available online: http://www.chem.ucla.edu/~bacher/general/30CL/lecture/pp-slides.html [06/09/2018]

Bachmann, S., Gernert, B. & Stalke, D. 2016. Solution structures of alkali metal cyclopentadienides in THF estimated by ECC-DOSY NMR-spectroscopy. *Chemical Communications, The Royal Society of Chemistry*, 52: 12861-12864.

Barue, C., Canet, C., Dupuis, M., Flambard, J.L., Jaffres, P.A., Leherissier, P. & Lamagnen, F. 2000 (24–27 September). High intensity ion beams from an ECR ion source using the MIVOC method. *Proceedings of the workshop on the production of intense beams of highly charged ions*, pp. 67 – 72, Italy.

Beattie, J.K. & Nugent, K.W. 1992. Beryllocene and related slip-sandwich structures. *Inorganica Chimica Acta*, 198-200: 309-318.

Beckhaus, R. 1998. Titanocenes. (*In* Togni, A., Halterman, R.L. (eds) *Metallocenes, Synthesis, Reactivity Applications*. Wiley-VCH Verlag GmbH, Weiheim, Germany. p. 153-230).

Belgya, T., Molnar, G., Yates, S.W. 1996. Analysis of Doppler-Shift attenuation measurements performed with accelerator-produced monoenergetic neutrons. *Nuclear Physics* A607*:* 43-61.

Bennett, C.L. *et al*. 2013. Nine-year Wilkinson Microwave Anisotropy Probe (WMAP) observations: final maps and results. The Astrophysical Journal Supplement Series, 208: 20.

Berthet, J., Thuery, P., Garin, N., Dognon, J., Cantat, T., & Ephritikhine, M. 2013. Revisiting the chemistry of the actinocenes [(η^8-$C_8H_8)_2$An(L)] with thorium (L=py, 4,4'-bipy, *t*BuNC, R_4phen)]. *Journal of the American Chemical Society*, 135:10003-10006.

Beswick, M.A, Palmer, J.S. & Wright, D.S. 1998. P-block metallocenes: the other side of the coin. *Chemical Society Reviews*, 27: 225-232.

Birkholz, M. 2006. *Thin film Analysis by X–ray Scattering*. Verlag, GmbH & Co., Weinheim: WILEY – VCH.

Bochmann, M. & Dawson, D.M. 1996. The aluminocenium cation [Al($C_5H_5)_2$: A highly effective initiator for the cationic polymerization of isobutene. *Angewandte Chemie*, *35*:2226-2228.

Bochkarev, M.N. 2004. Molecular compounds of new divalent lanthanides. *Coordination Chemistry Reviews*, 248: 835-851.

Bogomolov, S.L., Bondarchenko, A.E., Efremov, A.A., Kuzmenkov, K.I., Lebedev, A.N., Lebedev, K.V., Lebedev, V.Ya., Loginov, V.N., Mironov, V.E. & Yazvitsky, N.Yu. 2015. *Physics of Particles and Nuclei Letters*, 12 (7): 824 – 830.

Boor, J. 1979. Ziegler – Natta catalysts and polymerizations. *Academic Press*, New York.

Borb. Available oline: https://en.wikipedia.org/wiki/CNO_cycle. [05/12/2017].

Brown, I. G. 2004. *The physics and technology of ion sources*. Unites States: WILEY-VCH.

Calabrese, J.C., Cheng, L.T., Green, J.C., Marder, S.R. & Tam, W. 1991. Molecular second–order optical nonlinearities of metallocene. *Journal of the American Chemical Society*, 113(19): 7227-7232.

Burkey, D.J. & Hanusa, T.P. 1995. Structural lessons from main group metallocenes. *Comments inorganic chemistry*, 17(1): 41-77.

Cantrill, S., Davey, S. & Johnson, R. 2012. Catalytic upgrade. *Nature*, 491:235-239.

Cao, Y., Feng, Y., Li, J. , Wang, H., Ma, B., Sun, L., Zhao, H., Shang, Y., Zhang, X., Li, X., Guo, X. & Lu, W. 2007. Research on metallic ion beam production at IMP. *High Energy Physics and Nuclear Physics*, 31:70-74.

Carnahan, E.M. & Jacobsen, G.B. 2000. Supported metallocene catalysts. *Cattech*, 4:74-88.

Cavenago, M., Galata, A. & Sattin, M. 2009. Refractory ovens for ECR ion sources and their scaling. *Proceedings of EPAC08*, Genoa, Italy, 23-27 June 2008, pp. 397-399. CERN JACow.

Cernik, R.J., Cheetham, A.K., Prout, C.K., Watkin, D.J., Wilkinson, A.P. & Willis, B.T.M. 1991. The structure of cimetidine ($C_{10}H_{16}N_6S$) solved from synchrotron-radiation X–ray powder diffraction data. *Journal of Applied Crystallography*, 24:222-226.

Chemical book. Available online:https://www.chemicalbook.com/spectrumEN_1271-28-9_IR1.htm.[October 2016].

Chirik, P.J. & Bercaw, J.E. 1998. Group 3 metallocenes. (*In* Togni, A. & Halterman, R.L. (eds.), *Metallocenes, Synthesis, Reactivity Applications*. Verlag GmbH, Weiheim, Germany: Wiley-VCH. p.111-148).

Cheng, Bex, L., Leherissier, P., & Hamet, J.F. 1995. Production of multicharged metallic ions by the association of an excimer laser and an ECR ion source. *Nuclear Instruments and Methods*, A365: 564-567.

Chiu, N & Schäfer, L. 1977. On the molecular structure of beryllocene. *Journal of the American Chemical Society*, 100: 2604-2607, April 9.

Cliffton, M.D. & Carter, S.J. 1989. *Oxidative coupling of alklyphenols by copper catalysis.* United States Patent, US4851589 A.

Colacot, T.J. 2011. The 2010 Nobel Prize in chemistry: palladium–catalysed cross-coupling. *Platinum Metals Review,* 55(2) 84-90.

Colacot, T.J. 2012. Commercial development of palladium(0) catalysts for highly selective cross-coupling reactions. *Platinum Metals Review,* 56(2): 110-116.

Cossee, P. 1964. Ziegler – Natta catalysis I. mechanism of polymerization of α – olefins with Ziegler – Natta catalyst. *Journal of Catalysis*, 3 (1): 80–88, February 1964.

Crabtree, R.H. 2005. *The organometallic chemistry of the transition metals*, 4th edition. Hoboken, New Jersey: John Wiley and sons.

Conradie, J.L. 1992. *Improved proton beam quality and intensity from 200 MeV cyclotron system*. South Africa: University of Stellenbosch. (PhD - Dissertation).

Cotton, F.A. 1968. Proposed nomenclature for olefin–metal and other organometallic complexes. *Journal of the American Chemical Society,* 90(22):6230–6232.

Cotton, F.A, Wilkinson, G. & Gaus, P.L. 1986. *Basic Inorganic Chemistry*. *structure and bonding in molecule*. New York. John Wiley & sons.

D'Auria, J.M., Azuma, R.E., Bishop, S., Buchmann, L., Chatterjee, M.L., Chen, A.A., Engel, S., Gigliotti, D., Greife, U., Hunter, D., Hussein, A., Hutcheon, D., Jewett, C.C., José, J, King, J.D., Laird, A.M., Lamey, M., Lewis, R., Liu, W., Olin, A., Ottewell, D., Parker, P.,

Rogers, J., Ruiz, C., Trinczek, M. & Wrede, C. 2004. The ^{21}Na (p, γ) ^{22}Mg reaction from $E_{c.m.}$=200 to 1103 keV in novae and x-ray bursts. *Physical Review*, C 69: 065803-1 – 065803-16.

Dohmeier, C., Schnöckel, H., Robl, C, Schneider, U & Ahlrichs, R. 1993. Decamethylaluminocenium,a π-Stabilized R_2Al^+Cation·*. *Angewandte Chemie International Edition*, 32(11): 1655-1657.

Edelmann, F.T. 1998. Lanthanocenes. *(In* Togni, A. & Halterman, R.L. (eds.), *Metallocenes*, vol 2, New York: Wiley-VCH. p. 55-110.)

Eddington, A.S. 1920. The internal constitution of the stars. *The Scientific Monthly*, 11(4):297-303.

Edwards, J.C. 2009. Principles of NMR. *Process NMR Associates*, Danbury CT, 6810, pp 1-51.

Eppinger, J., Spiegler, M., Hieringer, W., Hermann, W.A. & Anwander. R. 2000. C_2-Symmetric ansa-lanthanidocene complexes. Synthesis via silylamine elimination and β–SiH agostic rigidity. *Journal of the American Chemical Society*, 122 (13): 3080–3096.

Evans, J.N.S. 1995. *Biomolecular NMR spectroscopy*. New York: Oxford University Press Inc., ISBN 019 8547668.

Ewald, P.P. 1962. *Fifty years of X-Ray diffraction*: Dedicated to the international union of crystallography on the occasion of the commemoration meeting in Munich, July 1962: Utrecht, Oosthoek.

Faust, B. 1997. Nuclear magnetic resonance spectroscopy. modern chemical techniques: an essential reference for students and teachers. *The Royal Society of Chemistry*, Unilever research.

Formicola, J., Imbriani, G., Costantini, H. Angulo, C., Bemmerer, D., Bonetti, R., Broggini, C., Corvisiero, P., Cruz, J., Descouvemont, P., Fülöp, Z., Gervino, G., Guglielmetti, A., Gustavino, C., Gyürky, G., Jesus, A.P., Junker, M., Lemut, A., Menegazzo, R., Prati, P., Roca, V., Rolfs, C., Romano, M., Rossi, A.C., Schümann, F., Somorjai, E., Straniero, O., Strieder, F., Terrasi, F., Trautvetter, H.P., Vomiero, A.E., & Zavatarelli, S. 2004. Astrophysical s-factor of ^{14}N(p, γ)^{15}O. *Physics Letters,* B 591:61-68.

Fernandez, R. & Carmona, E. 2005. Recent developments in the chemistry of beryllocene. *European Journal of Inorganic Chemistry*, (16): 3197-3206.

Francois, M. 2013. *Transition metal organometallic chemistry*. New York: Springer.

Freitag, M.A. & Gordon, M.S. 2002. On the electronic structure of Bis(η^5-cyclopentadienyl)titanium. *Journal of Physical Chemistry*, 106: 7921-7926.

Galletti, A.M.R. & Pampaloni, G. 2010. Niobium complexes as catalytic precursors for polymerization of olefins. *Coordination Chemistry Reviews*, 254: 525-536.

Ganes, V., Sudhir, V.S., Kundu, T. & Chandrasekaran, S. 2011. 10 Years of click chemistry: synthesis and applications of ferrocene–derived triazole. *Chemistry Asian Journal*, 6(10): 2670-2694, October 4.

Gary, D.E. 2005. Introduction to Astronomy: Lecture #17. Available online: *https://web.njit.edu/~gary/202/Lecture17.html [05/12/2017].*

Gasser, G. & Metzler–Nolte, N. 2011. Organometallic anticancer compounds. *Journal of Medicinal Chemistry*, 54: 3-25, November 15.

Geller, R. 1996. *Electron Cyclotron Resonance Ion Sources and ECR Plasmas*. Bristol: Institute of physics publishing.

Gerothanassis, I.P., Troganis, A., Exarchou, V. & Barbarossou, K. 2002. Nuclear magnetic resonance (NMR) spectroscopy: basic principles and phenomena, and their applications to chemistry, biology and medicine. *Chemistry Education: Research and Practice,* 3: 229-252.

Girolami, G.S., Rauchfuss, T.B. & Angelici, R.J. 1999. Synthesis and techniques in inorganic chemistry: a laboratory manual, 3rd edition, *University science books*, 98-14491 CIP.

Gmelin, 1997/1998. *Catalogue for handbook of Inorganic and Organometallic Chemistry*. Verlag, Heidelberg: Springer.

Godemann, C., Dura, L., Hollmann, D., Grabow, K., Bentrup, U., Jiao, H., Schulz, A, Brückner, A. & Beweries, T. 2015. Highly selective visible light-induced Ti-O bond splitting in an *ansa*-titanocene dihydroxido complex. *Chemical Communications*, 51: 3065–3068.

Gomez-Ruiz, S., Maksimović-Ivanić, D. Mijatović, S. & Kaluderović, G.N. 2012. On the discovery, biological effects, and use of cisplatin and metallocene in anticancer chemotherapy. *Bioinorganic Chemistry & Applications*, 2012:1-4.

González-García, P., Arenas-Esteban, D., Ávila-Brande, D., Urones-Garrote, E. & Otero-Díaz, L.C. 2017. Nickelocene as a precursor of microporous organometallic-derived carbon and nickel oxide-carbon nanocomposite. *Journal of Colloid and Interface Science*, 490: 410-419.

Green, M., Brennan, J.G. & Sella, A. 2000. Scandium, yttrium and the lanthanides. (*In* Green, M (eds.), *Organometallic Chemistry*, 28: The Royal Society of Chemistry. p. 63-84.)

Grunes, J., Zhu, J. & Somortal, G.A. 2003. Catalysis in Nano science. *Chemical Communications*, 21(18):2257–2266.

Hartwig, J.F. 2010. *Organo transition metal chemistry: structure and bonding.* USA: Edwards brothers.

Hamielec, A.E. & Soares, J.B.P. 1999. *Polymer science and technology series. metallocene catalysed polymerization: industrial technology*. New York: Springer.

Heise, H., Köhler, F.H., & Xie, X. 2001. Solid state NMR spectroscopy of paramagnetic metallocenes. *Journal of Magnetic Resonance,* 150: 198-206.

Henderson, L.D., Maclnnis, G.D., Piers, W.E. & Parvez, M. 2004. A new family of monocyclodienyl organoscandium bis-alkyls supported by a bulky trialkylphosphine oxide ancillary. *Canada Journal of Chemistry*, 82: 162-165.

Hickman, A.J & Sanford, M.S. 2012. High–valent organometallic copper and palladium. *Nature*, 484(7393):177 -185.

Hou, Z. & Wakatsuki, Y. 2003. Orgarnometallic complexes of scandium, yttrium and lanthanides. *Science of Synthesis*: 849-942.

Hrobárik, P., Reviakine, R., Arbuznikov, V., Malkina, O.L., Malkin, V.G., Köhler, F.H. & Kaupp, M. 2007. Density functional calculations of NMR shielding tensors for paramagnetic systems with arbitrary spin multiplicity:validation of 3d metallocenes. *The Journal of Chemical Physics*, 126:024107-1 – 024107-19.

Hunt, L.B. 1984. The first organic compounds. *Platinum Metals Review*, 28(2):76-83.

Jacobsen, N.E. 2007. *NMR spectroscopy explained: simplified theory, applications and examples for organic chemistry and structural biology*. Hoboken, New Jerseey: John Wiley & Sons, Inc.

Janiak, C. 1998. Metallocene catalysts for olefin polymerization:metallocenes. (*In* Togni, A. & Hatterman, R.L. (eds.), *Metallocenes.* : Synthesis, Reactivity Applications. Verlag GmbH, Weiheim, Germany: Wiley-VCH. Vol. 2. p. 547-623.)

Jemmis, E.D. & Reddy, A.C. 1990. Structure and bonding in metallocenes and oligomers. *Proceedings of the Indian Academy Sciences–Chemical Sciences*, 102(3):379-393.

Jones, R.G & Gilman, H. 1954. Methods of preparation of organometallic compounds. *Chemical Reviews*, 54(5): 835-890.

Johnson, J. 1977. Transition metal organic compounds: metallocenes. (*In* Robert, J.D. & Caserio, M.C. (eds.), *Basic principles of organic chemistry*. Menlo Park, W.A. Benjamin, Inc. p. 1504-1528.)

Jolly, P.W. & Wilke, G. 1974. The Organic Chemistry of Nickel: organonickel complexes. *USA. Academic press.*

Jutzi, P. 1989. Main group metallocenes: recent developments. *Pure and Applied Chemistry*, 61(10): 1731-1736.

Jutzi, P. & Burford, N. 1998. Main group metallocenes (*In* Togni, A. & Halterman, R.L. (eds.), *Metallocenes*: Synthesis, Reactivity, Applications. Verlag GmbH, Weiheim, Germany: Wiley-VCH. p.1-53.)

Kaluderović, M.R, Kaluderović, G.N., Gomez-Ruiz, S., Paschke, R., Hemprich, A., Kuhling, J. & Remmerbach, T.W. 2011. Organogallium (III) complexes as an apoptosis promoting anticancer agents for head and neck squamous cell carcinoma cell lines. *Journal of Inorganic Biochemistry*, 105:164-170.

Kekule, A. 1865. Sur la constitution des substances aromatiques. *Bulletin de la Societe Chimique de Paris*, 3(2): 98-110.

Kalvas, T. & Kovisto, H. 2017. MIDAS-NA hands-on-training: MIVOC method for the production of metal ion beams. Available on line. https://wiki.jyu.fi/display/ensar2/Training+workshop+on+MIVOC+method+and+highly+charged+plasma+diagnostics. 2017-12-04.

Kaminsky, W. 1998. New polyolefins by metallocene catalysts. *Pure & Applied Chemistry*, 70(6): 1229-1233.

Kealy, T.J. & Pauson, P.L. 1951. A new type of organo–iron compound. *Nature*, 168(4285): 1039 – 1040.

Kirsebom, O.S., Bender, P., Cheeseman, A., Christian, G., Churchman, R., Cross, D.S., Davids, B., Evitts, L.J, Fallis, J., Galinski, N., Garnsworthy, A.B., Hackman, G., Lighthall, J., Ketelhut, S., Machule, P., Miller, D., Nielsen, S.T., Nobs, C.R., Pearson, C.J., Rajabali,

M.M., Radich, A.J., Rojas, A., Ruiz, C., Sanetullaev, A., Unsworth, C.D. & Wrede, C. 2016. Measurement of lifetimes in ^{23}Mg. *Physical Review*, C 93: 025802-1 – 025802-12.

Komero, T., Orenes, R. A., Espinosa, A., Tarraga, A. & Molina, P. 2011. Synthesis, structural characterization and electrochemical and optical properties of ferrocene–triazole-pyridine triads. *Inorganic Chemistry*, 50(17): 8214-8224, August 10.

Koivisto, H., Arje, J., and Nurmia, M. 1994. Metal ion beams from an ECR ion source using volatile compounds. *Nuclear Instruments and Methods in Physics Research*, B 94: 291.

Koivisto, H., Kolehmainen, E., Seppälä., Ärje, J. & Nurmia, M. 1996. Production of a magnesium ion beam using the MIVOC method. *Nuclear Instruments and Methods in Physics Research*, B 117: 186.

Koivisto, H., Kolehmainen, E., Seppälä., Ärje, J. & Nurmia, M. 2002. Production of titanium ion beams at an ECR ion source. *Nuclear Instruments and Methods in Physics Research*, B 187: 11.

Koleros, E., Stamatatos, T.C., Psycharis, V., Raptopoulou, C.P., Perlepes, S.P. & Klouras, N. 2010. In search for titanocene complexes with improved cyclotonic activity: synthesis, x-ray structure and spectroscopic study of Bis (η^5 – cyclopentadienyl) difluorotitanium(iv). *Bioinorganic Chemistry and Applications*, 2010:1-7.

Kubiak, C.P. 1995. Nickel complexes with carbonyl, isocyanide and carbine ligands. (*In* Abel, E.W., Stone, F.G.A. & Wikilson, G. (eds.), *Organometallic Chemistry II*. Great Britain, UK: Elsevier. p. 1-28.)

Kubiak, C.P. 2006. Nickel: Organometallic Chemistry. (*In* Zargarian, (eds.), *Encyclopaedia of Inorganic Chemistry*, USA: Wiley online library. p. 2427–2444.).

Kwon, O & McKee M.L. 2001. Theoretical study of ring exchange in the borocenium cation, $[B(C_5R_5)_2]^+$(R=H, Me). *Journal of Physical Chemistry*, 105:10133-10138.

Lai, K.K & Lamb, H.H. 1995. Precursors for organometallic chemical vapor deposition of tungsten carbide film. *Chemical Matter*, *7*:2284-2292.

Lauher, J.W., Elian, V, Summerville, R.H. & Hoffman, R. 1976. Tripple-decker sandwich. *Journal of the American Chemical Society*, 98(11): 3219–3224.

Layfield, R.A, Morrison, C.A & Wright, D.S. 2002. A new, tretragonal, helical phase of plumbocene, Cp_2Pb; variations on a molecular string ($Cp=C_5H_5$). *Journal of Organometallic Chemistry*, 650:75-76.

Leherrissier, P., Barue, C., Canet, C., Dubois, M., Dupuis, M., Flambard, J.L., Jaffres, P.A, Jardin, P., Gaubert, G., Lecesne, N., Lemagnen, F., Leroy, R., & Pacquet, J.Y. 2007. Status report on organo-metallic beams at GANIL. *High Energy Physics and Nuclear Physics*, 31:85 - 89.

Leach, M. 2008. *The chemogenesis web book*. Available online: http://en.wikipedia.org/wiki/organotin_chemistry#See_also [15/01/2017]. Organometallic periodic table

Lee, J.Y., Sohn, J.G., Ahn, S.H., & Bae, M.H. 1998. *Process for manufacturing high purity nickel chloride by recycling waste nickel anode*. *USA PATENT*, US5853692A.

Liard, A., Kaftanov, J., Chechik, H., Farhat, S., Morlender–Vai, N., Averbuj, C. & Marek, I., 2001. Addition–β–elimination: a new method for the preparation of organometallic compounds. *Journal of Organometallic Chemistry*, 624:26-33.

Liu, W., Dolg, M & Fulde, P. 1997. Low-lying electronic states of lanthanocenes and actinocenes $M(C_8H_8)_2$(M=Nd, Tb, Yb,U). *The Journal of Chemical Physics*, 107:3584-3591.

Lu, W., Zhang, X.Z, Zhao, H.W., Feng, Y.C., Guo, J.W., Cao, Y., Li, J.Y., Li, X.X., Guo, H.X., Zhao, H.Y., Fang, X., Ma, H.Y., Zhang, W.H., Lin, S.H., Li, J.Q., Xie, D.Z., & Sun, L.T. 2012. Operation status of SECRAL at IMP. *Proceedings of IPAC2011*, San Sebastian, Spain, 4-9 September, 2011: JACow-CERN.

Macdonald, C.L.B, Gorden, J.D., Voigt, A., Filipponi, S. & Cowley, A.H. 2008. Group 13 decamethylmetallcenium cations:. *The royal society of chemistry*: 1161-1176.

Macdonald, C., n.d. *Inorganic chemistry*: Canada. University of Windsor. Available online: http://mutuslab.cs.uwindsor.ca/macdonald/teaching.htm [6/ 09/2016].

Margl, P. & Schwarz, K. 1994. Fluxional dynamics of beryllocene. *Journal of the American Chemical Society,* 116*:11177*-11178.

Martin, B & Autschbach, J. 2015. Temperature dependence of contact and dipolar NMR chemical shifts in paramagnetic molecules. *The Journal of Chemical Physics,* 142: 05410-1-054108-10.

Martin, B & Autschbach, J. 2016. Kohn-sham calculations of NMR shifts for paramagnetic 3d metal complexes: protocols delocalization error and the curious amide proton shifts of a high-spin iron (II) macro cycle complex. *Physical Chemistry Chemical Physics,* 18: 21051-21068.

McConnell, H.M. & Holm, C.H. 1957. Proton resonance shifts in nickelocene. *The Journal of. Chemical. Physics*. 27: 314.

Mehrotra, R.C. & Singh, A. 2000. *Organometallic chemistry, a unified approach*. Organometallic compounds of transition metals. New Delhi: New age international, Ltd.

Melson, G.A. 1975. Organic compounds. (*In* Horovitz, C.T (eds.), *Scandium, Its occurrence, chemistry, physics, metallurgy, biology and technology*. New York, San Francisco: Academic Press, London.)

Miller, S.A., Tebboth, J.A., & Tremaine, J.F. 1952. Dicyclopentadienyliron. *Journal of Chemical Society*, 114: 632-635.

Mohamed, M.E. & Ishak, C.Y. 2011. Synthesis and characterization of organometallic complexes of thiocarbanilides using manganese (II) chloride. *Advances in Applied Science Research*, 2(6): 32-40.

Mountford, P. & Ward, B.D. 2003. Recent development in the non-cyclopentadienyl organometallic and related chemistry of scandium. *Chemical Communications*: 1797-1803.

Mulliken, R.S. 1966. Spectroscopy, molecular orbitals and chemical bonding. *Nobel lectures,* chemistry, 1963-1970: Elsevier, Amsterdam: 131-160.

Nakagawa, T., Arie, J., Miyazawa, Y., Hemmi, M., Chiba, T., Inabe, N., Kase, M., Kageyama, T., Kamigaito, O. Goto, A., Niimura, M.G., & Yano, Y. 1997. Production of highly charged metal ion beams from organic metal compounds at RIKEN 18 GHz ECRIS. *Nuclear Instruments and Methods*, A 396: 9-12.

Negeshi, E. & Takahashi, T. 2003. Product class 11: Organometallic complexes of zirconium and hafnium. (*In* Imamoto, T (eds.), *Science of Synthesis*. New York: Thieme p. 681-848).

Nugent, K.W., Beattie, J.K., Hambley, T.W. & Snow, M.R. 1984. A precise low-temperature crystal structure of Bis(cyclopentadienyl)beryllium. *Australian Journal of Chemistry,* 37: 1601-1606.

NPTEL, 2016. Chemistry and biochemistry. Introduction to organometallic chemistry. Available online: http://www.nptel.ac.in/downloads/104101006/. [22 September 2016].

Othmer, K. 2005. *Sulfur containing polymers*. *Encyclopaedia of Chemical Technology* Hoboken, NJ: John Wiley and sons.

Orce, J.N., Holt, J.D., Linnemann, A., Mckay, C.J., Lesher, S.R., Fransen, C., Holt, J.W., Kumar, A., Warr, N., Wernev, V., Jolie, J., Kuo., T.T.S., McEllistren, M.T., Pietrailla, N., & Yates, S.W. 2006. Identification of mixed-symmetry states in an odd-mass nearly spherical nucleus. *Physical Review Letters, 97,* 062504: 062504-1- 062504-4.

Orce, J.N, Crider, B., Mukhopadhyay, S., Peters, E., Elhamie, E., Scheck, M.,Singh, B., McEllistrem, M.T., & Yates, S.W. 2008. Determination of the $2_1^+ \rightarrow 0_1^+$transition strengths in ^{58}Ni. *Physical Review,* C 77: 064301(064301–1–064301–5).

Orce, J.N. 2012. Proposal on "*Search for the Lost Paradigm of Surface Vibrations*". Submitted and Approved by the Program Advisory Committee (PAC) of iThemba LABS.

Park, J & Sudarshan T.S. 2001. *Surface engineering series, chemical vapor deposition*: the case of Ni. United States of America*:* ASM international publishers, p. 289.

Pasternak, A.A., Lieder, E.O. & Lieder, R.M. 2009. Shears effect with PAC core rotation for dipole bands in ^{142}Gd and ^{130,132}La. *Acta Physica Polonica B,* 40: 647-652.

Planck Collaboration, 2016. Planck results XIII. Cosmological parameters (see PDF, Page 31, Table 4, Age/Gyr). *Astronomy & Astrophysics,* 594: A13.

Pugmire, D.L., Woodbridge, C.M., Boag, N.M., Langell, M. 2001 (February, 1). Adsorption and decomposition of nickelocene on Ag (100): a high-resolution electron energy loss spectroscopy and temperature programmed desorption study. *Surface Sciences*, 472(3): 155-171.

Putkonen, M. & Niinistö, L. 2005. Organometallic precursors for atomic layer deposition. *Top Organometallic Chemistry,* 9:125-145.

Rayon, V.M. & Frenking, G. 2003 (July 4). Bis (benzene) chromium is a σ – bonded – bonded molecule. *Organometallics*, 22 (16): 3304 – 3308.

Rezola, A. B. 2002. *Palladium complexes for Co/Styrene copolymerization. Study of the influence of the ligand*. Spain: Universitat Rovira I Virgili (PhD thesis).

Robert, J.D. & Caserio, M.C. 1977. *Basic principles of organic chemistry*. *Transition-metal organic compounds*, *2nd edition*. Canada: W Benjamin, Inc.

Robertson, G.L. 2012. *Food Packaging: Principles and Practice*: metallocenes. CRC Press.

Rogers, R.D., Atwood, J.L., Emad, A., Sikora, D.J. & Rausch, M.D. 1981. The formation and molecular structures of $(\eta^5 - C_5H_5)_3$ Y. OC_4H_8 and $(\eta^5 - C_5H_5)_3$ La. OC_4H_8. *Journal of Organometallic Chemistry*, 216(3): 383-392, August 25.

Rosman, K.J.R. & Taylor, P.D.P. 1998. Report of the IUPAC subcommittee for isotopic composition of the elements. *Pure and Applied Chemistry*, 70: 217-235.

Royo, P. & Ryan, E. 1998. Group 5 and group 6 metallocenes: 17 – electron compounds. (*In* Togni, A., Halterman, R.L. (eds). *Metallocenes*, *Synthesis*, *Reactivity Applications*. Wiley-VCH Verlag GmbH, Weiheim, Germany. p. 403-497).

Rubert, J., Piot, J., Asfari, Z., Gall, B.J.P., Arje, J., Dorvaux, O., Greentzes, P.T., Koivisto, H., Ouadi, A. & Sepalla, R. 2012. First intense isotopic titanium-50 beam using MIVOC method. *Nuclear Instruments and Methods in Physics Research*, B27:33-37.

Salzer, A. 1999. Nomenclature of organometallic compounds of the transition elements. *Pure and Applied Chemistry*, 71(8): 71557-1585.

Sarrazin, P., Chipera, S., Bish, D., Blake, D. & Vaniman, D. 2005. Vibrating sample holder for XRD analysis with minimal sample preparation. *International Centre for Diffraction Data, Advances in X – ray Analysis*, 48: 156 – 164.

Sasaki, M., Kitagawa, A., Muramatsu, M., Jincho, K., Sasaki, N., Sakuma, T., Tagasuki, W. & Yamamoto, M. 2002. Metallic beam production at HIMAC. *Review of Scientific Instruments*, 73: 546-547.

Seiler, P. & Dunitz, J.D. 1979. A new interpretation of the disordered crystal structure of ferrocene. *Acta Crystallographica*, B35: 1068-1075.

Seiler, P. & Dunitz, J.D. 1980. The structure of nickelocene at room temperature and at 101 K. *Acta Crystallogrsphica*: 2255-2260.

Seuthe, S., Rolfs, C., Schröder, U.,Somorjai, E., Trautvetter, H.P. & Waanders, F.B. 1990. Resonances in the ^{22}Na (p, γ) ^{23}Mg reaction. *Nuclear Physics*, A514: 471-502.

Seyferth, D. 2002. Bis(benzene)chromium.2. Its discovery by E.O. Fischer and W. Hafner and subsequent work by the research groups of E.O. Fischer, H.H. Zeiss, F. Hein, C. Elschenbrich and others. *Organometallics*, 21(14): 2800-2820.

Seyferth, D. 2004. Uranocene. The first member of a class of organometallic derivatives of the f elements. *Organometallics*, 23:3562-3583.

Shamiri, A., Chakrabart, M.H., Jahan, S., Hussain, M.A., Kaminsky, W., Aravind, P.V. & Yehye, W.A. 2014. The influence of Ziegler-Natta and metallocene catalysts on polyolefin structure, properties and processing ability. *Materials*: 5069-5108.

Siebert, F. & Hildebrandt, P. 2008. *Vibrational spectroscopy in life science*. Verlag, Weinheim: WILEY-VCH.

Sitzmann, H. 2001. *Maximum spin cyclopentadienyl complexes of 3d transition metals.* Coordination chemistry reviews, 214: 287-327.

Smith, E. & Dent, G. 2005. *Modern Raman spectroscopy-A practical approach.* United States. John Wiley & sons.

Streitwieser, A & Müller-Westerhoff, U. 1968. Bis(cyclooctatetraeny)uranium (uranocene). A new class of sandwich complexes that utilize atomic f orbitals. *Journal of American Chemical Society:* 7364.

Stone, F.G.A & West, R. 1986. *Advances in organometallic chemistry*. Academic Press, Inc.

Sortais, P. 1995. Recent progress in making highly charged ion beams. *Nuclear Instruments and Methods*, B98: 508-516.

Takahashi, T. 2004. Metallocenes in region and stereoselective. *Topics in Organometallic Chemistry*. Berlin: Springer.

Thayer, J.S. 1966. Cadet's fuming liquid: An historical survey. *Journal of Chemical Education,* 43(11): 595-597.

Thayer, J.S. 2010. Relativistic effects and the chemistry of the heavier main group elements. (*In* Barysz, M. & Ishikawa, Y. (eds), *Relativistic methods for chemists.* Dordrecht, Heidelberg, London: Springer. p. 63-91.

Thomae, R.W., Celliers, P.J., Conradie, J.L., Delsink, J.L.G., De Villiers, J.G., Du Plessis, H., Fourie, D.T. & Sakildien, M. 2009. Status of a new electron cyclotron resonance ion sources at iThemba LABS. *Proceedings of ECRIS08*, Chicago, IL, USA, 15-18 September, 2008, pp. 68 – 71: JACow – CERN.

Thomae, R.W. 2016/2017. iThemba LABS, private communication.

Togni, A. & Halterman, R.L. 1998. *Metallocenes*. New York: Wiley-VCH, vol. 2.

Traficante, D.D. 1996. NMR concepts. (*In* Bruch, M.D. (eds.), *NMR spectroscopy*. New York: Marcel Dekker. p. 1-60.)

Tsuji, J. 2004. The basic Chemistry of organopalladium compounds. (*In Palladium reagents and catalyst: New perspective for the 21st century.* Chichester, UK: John Wiley & Sons. p. 1-26.).

Vassylyev, O. 2005. Synthesis and chemistry of chiral metallocenes. *Molecules*, 10: 585-586.

Vaara, J., Raaf, S.A. & Mareš, J. 2015. Magnetic couplings in the chemical shifts of paramagnetic NMR. *Journal of Chemical Theory and Computational*, 11:4840-4849.

Valley, G.E. 1941. The stable isotopes of nickel. *Letters to the editor*: 836-837, K.J.R.

Van Holde, K.E., Johnson, W.C., & Ho, P.S. 2006. *Principles of physical biochemistry*, Prentice Hall, Upper Saddle River, New Jersey.

Voigt, A., Fillipponi, S., Macdonald, C.L.B., Gorden, J.D. & Cowley, A.H. 2000. The structure of the decamethylborocenium cation: the most tightly-squeezed. *Chemistry Communications*: 911-912.

Vol'pin, M.E. 1972. The reactions of organometallic compounds of transition metals with molecular nitrogen and carbon dioxide. *Pure and Applied Chemistry*, 30(3-4): 607 – 628.

Waldmann, H., & Martin, B. 1995. Highly charged ion beams produced from organometallic compounds. *Nuclear Instruments and Methods*, B 98: 532-535.

Wailes, P.C., Courtts, R.S.P. & Weigold, H. 1974. *Organometallic chemistry of titanium, zirconium and hafnium.* New York: Academic Press.

Wilkinson, G, Rosenblum, M, Whiting, M.C. & Woodward, R.B. 1952. The structure of iron bis-cyclopentadienyl. *Journal of the American Chemical Society*, 74(8): 2125-2126.

Wilkinson, G & Birmingham, J.M. 1954. Cyclopentadienyl compounds of Sc, Y, La, Ce and some lanthanide elements. *Journal of the American Chemical Society*, 76 (23): 6210-6210.

Wilkinson, G. 1973. Geoffrey Wilkinson-Nobel lecture-nobelprize.org. Available online: http://www.nobelprize.org/nobel_prizes/chemistry/lauretes/1973/wilkinson-lecture.pdf [20/09/2016].

Williams, R.A., Hanusa, T.P. & Huffman, J.C. 1990. Structures of ionic decamethylmetallocenes: crystallographic characterization of bis (pentamethylcyclopentadienyl) calcium and barium and a comparison with related organolanthanide species. *Organometallics*, 9:1128-1134.

Yamamoto, A. 2001. Organometallic chemistry, past, present and future. *Pure applied chemistry*, 73(2): 205-208.

Zhang, L., Abbenhhuis, H.C., Gerresten, G., Bhrian, N.N., Magusin, P.C., Mezare, B., Han, W. & Van Santen, R.A. 2007. An efficient hybrid, nanostructured epoxidation catalyst: titanium silsequioxane–polystyrene copolymer supported on SBA–15. *Chemistry*, 13 (114) 1210 – 1221.

APPENDIX

A.1 Ru beam development

Ruthenium beam development

04–20 March, 2013

Rainer Thomae, iThemba LABS

In March the weekend beams for physics experiments were delivered from SPC1. During this time beam development experiments for the generation of Ruthenium ion beam with the HMI ECRIS4 were carried out. A stainless steel container was loaded with 2g of Ruthenocene ($Ru(C_5H_5)_2$) under Argon atmosphere and mounted via the container and the regulation valve to the source. Subsequently, the container and the valve system was pumped down to the 10^{-6} mbar range. The source was then optimized for $^{102}Ru^{16+}$ at a source potential of 14.75kV corresponding to a SSC energy of 430MeV requested for a physics experiments. Due to the number of existing isotopes with similar abundances of Ruthenium (^{96}Ru abundance 5.5%, ^{98}Ru abundance 1.9%, ^{99}Ru abundance 12.7%, ^{100}Ru abundance 12.6%, ^{101}Ru abundance 17%, ^{102}Ru abundance 31.6%, ^{104}Ru abundance 18.7%) the mass separation and identification is difficult. Figure 1 shows the beam current measured in faraday cup Q3 when 90^0 B1Q1 bending magnet current was increased from 37.5 to 43 A. For these measurement the horizontal slit in front of the Faraday cup was closed to 1mm gap width. The vertical slit gap width was 10mm. This current range correspond to a mass to charge ratio range of 5.6 to 7.4 ($^{96}Ru^{17+}$ to $^{104}Ru^{14+}$). The increased intensity at 38.2A is due to the $^{12}C^{2+}$ contribution.

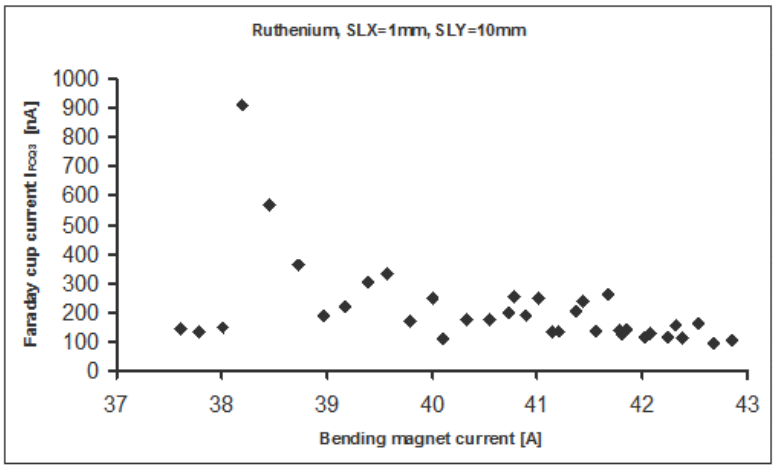

Figure A.1: *The beam current measured in faraday cup Q3 when 90^0 B1Q1 bending magnet current was increased from 37.5 to 43 A. For these measurement the horizontal slit in front of the Faraday cup was closed to 1mm gap width. The vertical slit gap width was 10mm. This current range correspond to a mass to charge ratio range of 5.6 to 7.4 ($^{96}Ru^{17+}$ to $^{104}Ru^{14+}$). The increased intensity at 38.2A is due to the $^{12}C^{2+}$ contribution.*

A.2 Periodic Tables

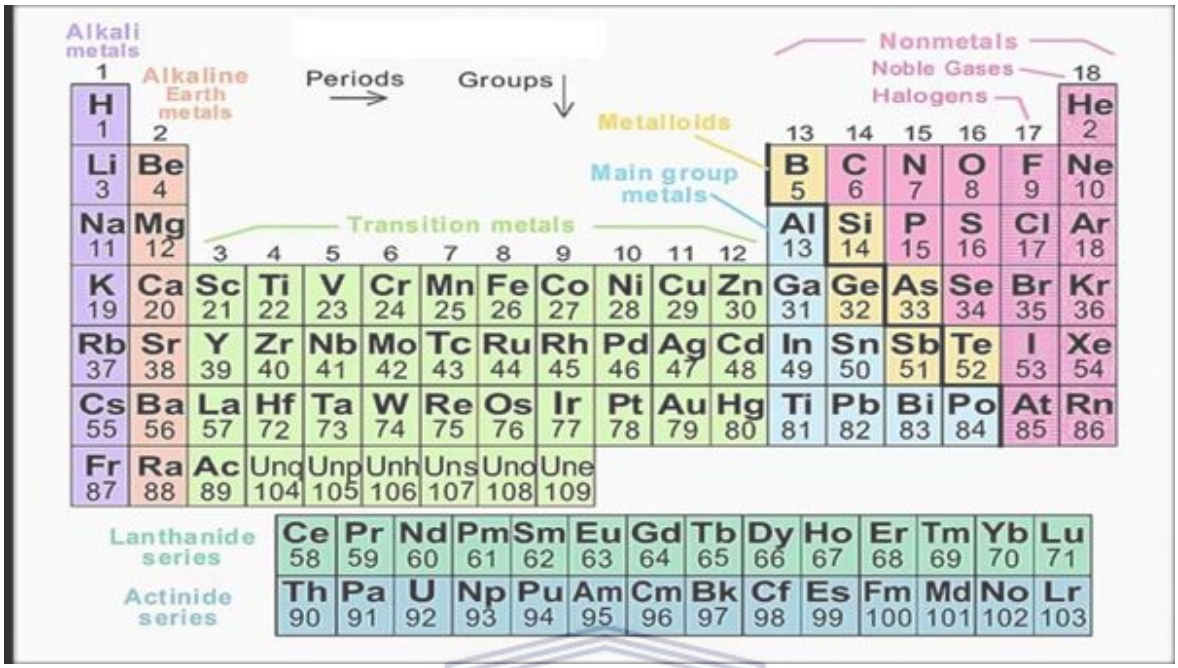

A.3 EXPO2014 output file

```
                                                    bgnd_62 Nicp iTL Med-new
++++++++++++++++++++++++++++++++++++++++++++++++++++++++++++++++++++++++++++++++++++++++++++++

              structure bgnd_62 Nicp iTL Med-new

++++++++++++++++++++++++++++++++++++++++++++++++++++++++++++++++++++++++++++++++++++++++++++++

Mon 23 April 2018 at 10:11:29 AM Expo2014 runs on: bgnd_62 Nicp iTL Med-new

Used  commands & directives:

      %data         pattern C:\Users\kheswa\Desktop\XRD\XRD-new\bgnd_62 Nicp iTL Med-new.xy
                    wave 1.540560
                    cont (C10H10Ni)2

      %ntreor       default

      %extraction   default

      %normal       default

      %invariants   default

      %phase        default

      %fourier      default

      %menu         default

      %end          default


Files used in  expo :

 Channel                        name
   5   card reader
   6   line printer
  30   direct access structure file    bgnd_62 Nicp iTL Med-new.bin
  31   direct access scratch file
  32   sequential scratch file
  41   scattering factors file         C:\Program Files\Expo2014\share\expo\expo.xen (Release:01.12)


    Direct access structure file has been initialized

++++++++++++++++++++++++++++++++++++++++++++++++++++++++++++++++++++++++++++++++++++++++++++++

Expo2014: data routine                          Release: 1.17.08

              structure bgnd_62 Nicp iTL Med-new

++++++++++++++++++++++++++++++++++++++++++++++++++++++++++++++++++++++++++++++++++++++++++++++
                                                                                    Page 1
```

Unit cell contents and scattering factor constants

Atom	Symbol	Number in cell	Atomic number
Hydrogen	H	20	1
Carbon	C	20	6
Nickel	Ni	2	28

f = sum (a(i) * exp(-b(i)*s2)) i=1,4 + c

	a(1)	b(1)	a(2)	b(2)	a(3)	b(3)	a(4)	b(4)	c
H	0.490	20.659	0.262	7.740	0.197	49.552	0.050	2.202	0.001
C	2.310	20.844	1.020	10.207	1.589	0.569	0.865	51.651	0.216
Ni	12.838	3.878	7.292	0.257	4.444	12.176	2.380	66.342	1.034

****
* Pattern information *
*
* 2-Theta min = 10.0000 *
* 2-Theta max = 69.9942 *
* Step = 0.0343 *
* Ncounts = 1750 *
*
****

Peak positions

	2theta	d	FWHM	100.*I/Imax
1)	14.8036	5.979187	0.1041	100.00
2)	17.5477	5.049873	0.0686	5.05
3)	17.7150	5.002535	0.0686	27.87
4)	18.1635	4.880026	0.0686	14.04
5)	18.7133	4.737879	0.0825	21.68
6)	19.3299	4.588095	0.0956	7.66
7)	21.3555	4.157277	0.0856	10.80
8)	22.3836	3.968590	0.0810	9.79
9)	24.6117	3.614135	0.0729	5.50
10)	26.6721	3.339433	0.0686	17.34
11)	28.6623	3.111922	0.0744	4.16
12)	30.1039	2.966099	0.0974	3.43
13)	31.7477	2.816174	0.2106	3.20
14)	33.3616	2.683531	0.1364	3.45
15)	35.5539	2.522923	0.1039	1.58
16)	36.7554	2.443161	0.0686	2.09
17)	37.4099	2.401912	0.0686	6.31
18)	42.3479	2.132556	0.0820	3.14
19)	42.7618	2.112866	0.0821	15.74
20)	42.8611	2.108201	0.0821	3.83
21)	43.3758	2.084369	0.1651	2.42
22)	44.3687	2.040002	0.1234	2.12
23)	44.8800	2.017940	0.1240	3.63
24)	45.5043	1.991697	0.1247	5.92
25)	46.0183	1.970638	0.1252	3.29
26)	47.5260	1.911581	0.1106	4.39

27)	49.6220	1.835631	0.2643	2.26
28)	50.4116	1.808717	0.2643	1.83
29)	51.6438	1.768420	0.1220	2.18
30)	53.1239	1.722584	0.6680	1.52
31)	55.0054	1.668028	0.0902	1.90
32)	58.0579	1.587382	0.1888	1.81

++

Expo2014: N-TREOR routine Release: 1.17.08

structure bgnd_62 Nicp iTL Med-new

++

The first (up to 25) d-values will be used by N-TREOR in order to find a possible cell.

Applied 2Theta-zero shift = 0.0000

Version: November 2001

5.9791875
5.0498729
5.0025349
4.8800259
4.7378788
4.5880947
4.1572766
3.9685900
3.6141346
3.3394332
3.1119220
2.9660988
2.8161738
2.6835308
2.5229230
2.4431615
2.4019117
2.1325557
2.1128657
2.1082006
2.0843694
2.0400023
2.0179403
1.9916974
1.9706384

Number of plausible solutions (with M(20) > 10) = 1

Cell # 1 :

WARNING: the cell

A = 6.43611 B = 7.47691 C = 17.50541
Alpha = 71.54348 Beta = 108.58878 Gamma = 85.79620

Unit cell volume = 743.03 A**3

M(20) = 15 M'(20) = 15

Number of observed lines = 25

Number of calculated lines (up to the 20th observed d) = 164

Number of unindexed lines = 1

has been transformed into the following one

Crystal system: Triclinic

A = 7.47691 B = 15.55662 C = 6.43611
Alpha = 91.13358 Beta = 94.20380 Gamma = 95.39696

Unit cell volume = 743.03 A**3

M(20) = 15 M'(20) = 15

****

The cell # 1 is refined by PIRUM

****

**** PIRUM: Starting cell parameters ****

A = 7.47691 B = 15.55662 C = 6.43611
Alpha = 91.13358 Beta = 94.20380 Gamma = 95.39696

Unit cell volume = 743.03 A**3

**** PIRUM: refined cell parameters ****

A = 15.56162 B = 7.48550 C = 6.43036
Alpha = 94.21732 Beta = 91.07802 Gamma = 95.42406

Unit cell volume = 743.43 A**3

M(20) = 9 M'(20) = 9

Total number of observed lines = 32

Number of calculated lines (up to the 20th observed d)= 164

Number of unindexed lines = 1

DT = abs[2-theta(calc)-2-theta(obs)] = 0.0700

DT is the maximum difference above which a line is not indexed

Condition	Percentage of involved indexed lines
k + l = 2n	34.4 %
h + l = 2n	43.8 %
h + k = 2n	65.6 %
h + k + l = 2n	40.6 %
-h + k + l = 3n or -k + h + l = 3n	65.6 %
h = 2n	50.0 %
k = 2n	53.1 %
l = 2n	18.8 %

WARNING : Systematic theta-zero shifts will be applied to the 2-theta peak positions in order to find more accurate cells

---

Applied 2Theta-zero shift = 0.0686

****

No plausible cell has been found

Look into the ntreor.out file for finding a plausible cell

****

Applied 2Theta-zero shift =-0.0686

****

No plausible cell has been found

Look into the ntreor.out file for finding a plausible cell

****

Applied 2Theta-zero shift = 0.1372

****

No plausible cell has been found

Look into the ntreor.out file for finding a plausible cell

****

Applied 2Theta-zero shift =-0.1372

****

No plausible cell has been found

Look into the ntreor.out file for finding a plausible cell

****

Applied 2Theta-zero shift = 0.2058

****

No plausible cell has been found
Look into the ntreor.out file for finding a plausible cell

****

Applied 2Theta-zero shift =-0.2058

Number of plausible solutions (with M(20) > 10) = 2

Cell # 1 :

WARNING: the cell

A = 5.44954 B = 11.33425 C = 25.53279
Alpha = 31.67020 Beta = 67.89571 Gamma = 67.01170

Unit cell volume = 759.10 A**3

M(20) = 10 M'(20) = 10

Number of observed lines = 25

Number of calculated lines (up to the 20th observed d) = 129

Number of unindexed lines = 1

has been transformed into the following one

Crystal system: Triclinic

A = 10.48417 B = 13.43823 C = 5.44954
Alpha = 93.21992 Beta = 95.59978 Gamma = 83.99290

Unit cell volume = 759.10 A**3

M(20) = 10 M'(20) = 10

Cell # 2 :

WARNING: the cell

A = 5.98253 B = 8.35453 C = 12.16436
Alpha = 91.91452 Beta = 99.18725 Gamma = 86.42304

Unit cell volume = 598.85 A**3

M(20) = 10 M'(20) = 10

Number of observed lines = 25

Number of calculated lines (up to the 20th observed d) = 131

Number of unindexed lines = 1

has been transformed into the following one

Crystal system: Triclinic

A = 8.35453 B = 12.16436 C = 5.98253
Alpha = 99.18732 Beta = 93.57695 Gamma = 88.08540

Unit cell volume = 598.85 A**3

M(20) = 10 M'(20) = 10

Applied 2Theta-zero shift = 0.2744

****

No plausible cell has been found
Look into the ntreor.out file for finding a plausible cell

****

Applied 2Theta-zero shift =-0.2744

****

No plausible cell has been found
Look into the ntreor.out file for finding a plausible cell

****

Applied 2Theta-zero shift = 0.3430

Number of plausible solutions (with M(20) > 10) = 2

Cell # 1 :

WARNING: the cell

A = 5.20582 B = 7.27701 C = 17.87389
Alpha = 122.58000 Beta = 81.89510 Gamma = 92.33981

Unit cell volume = 564.36 A**3

M(20) = 11 M'(20) = 11

Number of observed lines = 25

Number of calculated lines (up to the 20th observed d) = 125

Number of unindexed lines = 1

has been transformed into the following one

Crystal system: Triclinic

A = 7.27701 B = 15.24313 C = 5.20582
Alpha = 98.38522 Beta = 92.33987 Gamma = 81.14026

Unit cell volume = 564.36 A**3

M(20) = 11 M'(20) = 11

Cell # 2 :

WARNING: the cell

A = 6.02446 B = 8.05927 C = 30.79310
Alpha = 110.94964 Beta = 59.54019 Gamma = 73.32579

Unit cell volume = 979.07 A**3

M(20) = 13 M'(20) = 13

Number of observed lines = 25

Number of calculated lines (up to the 20th observed d) = 198

Number of unindexed lines = 1

has been transformed into the following one

Crystal system: Triclinic

A = 8.05927 B = 21.17337 C = 6.02446
Alpha = 95.85943 Beta = 106.67420 Gamma = 90.20905

Unit cell volume = 979.07 A**3

M(20) = 13 M'(20) = 13

****

The cell # 2 is refined by PIRUM

****

**** PIRUM: Starting cell parameters ****

A = 8.05927 B = 21.17337 C = 6.02446
Alpha = 95.85943 Beta = 106.67420 Gamma = 90.20905

Unit cell volume = 979.07 A**3

**** PIRUM: refined cell parameters ****

A = 21.17928 B = 8.05868 C = 6.03009
Alpha = 106.65677 Beta = 95.92919 Gamma = 90.26039

Unit cell volume = 980.11 A**3

M(20) = 8 M'(20) = 8

Total number of observed lines = 32

Number of calculated lines (up to the 20th observed d)= 210

Number of unindexed lines = 1

DT = abs[2-theta(calc)-2-theta(obs)] = 0.0500

DT is the maximum difference above which a line is not indexed

Condition	Percentage of involved indexed lines
k + l = 2n	50.0 %
h + l = 2n	34.4 %
h + k = 2n	46.9 %
h + k + l = 2n	50.0 %
-h + k + l = 3n or -k + h + l = 3n	34.4 %
h = 2n	56.2 %
k = 2n	40.6 %
l = 2n	40.6 %

Applied 2Theta-zero shift =-0.3430

****
No plausible cell has been found
Look into the ntreor.out file for finding a plausible cell
****

Applied 2Theta-zero shift = 0.4116

****
No plausible cell has been found
Look into the ntreor.out file for finding a plausible cell
****

Applied 2Theta-zero shift =-0.4116

Number of plausible solutions (with M(20) > 10) = 1

Cell # 1 :

WARNING: the cell

A = 7.63483 B = 5.99593 C = 10.17128
Alpha = 83.86703 Beta = 40.90830 Gamma = 93.46732

Unit cell volume = 295.95 A**3

M(20) = 15 M'(20) = 15

Number of observed lines = 25

Number of calculated lines (up to the 20th observed d) = 60

Number of unindexed lines = 1

has been transformed into the following one

Crystal system: Triclinic

A = 6.66087 B = 7.63483 C = 5.99593
Alpha = 93.46740 Beta = 103.44217 Gamma = 90.44903

Unit cell volume = 295.95 A**3

M(20) = 15 M'(20) = 15

****
The cell # 1 is refined by PIRUM
****

**** PIRUM: Starting cell parameters ****

A = 6.66087 B = 7.63483 C = 5.99593
Alpha = 93.46740 Beta = 103.44217 Gamma = 90.44903

Unit cell volume = 295.95 A**3

**** PIRUM: refined cell parameters ****

A = 7.63292 B = 6.66231 C = 5.99892
Alpha = 103.44370 Beta = 93.45619 Gamma = 90.45187

Unit cell volume = 296.09 A**3

M(20) = 14 M'(20) = 14

Total number of observed lines = 32

Number of calculated lines (up to the 20th observed d)= 68

Number of unindexed lines = 1

DT = abs[2-theta(calc)-2-theta(obs)] = 0.0700

DT is the maximum difference above which a line is not indexed

Condition	Percentage of involved indexed lines
k + l = 2n	46.9 %
h + l = 2n	34.4 %
h + k = 2n	50.0 %
h + k + l = 2n	46.9 %
-h + k + l = 3n or -k + h + l = 3n	65.6 %
h = 2n	43.8 %
k = 2n	43.8 %
l = 2n	40.6 %

Applied 2Theta-zero shift = 0.4802

****
No plausible cell has been found
Look into the ntreor.out file for finding a plausible cell
****

Applied 2Theta-zero shift =-0.4802

****
No plausible cell has been found
Look into the ntreor.out file for finding a plausible cell
****

Applied 2Theta-zero shift = 0.5488

****
No plausible cell has been found
Look into the ntreor.out file for finding a plausible cell
****

Applied 2Theta-zero shift =-0.5488

Number of plausible solutions (with M(20) > 10) = 2

Cell # 1 :

WARNING: the cell

A = 5.85764 B = 11.51413 C = 11.82715
Alpha = 45.01962 Beta = 80.71281 Gamma = 80.70646

Unit cell volume = 555.56 A**3

M(20) = 10 M'(20) = 10

Number of observed lines = 25

Number of calculated lines (up to the 20th observed d) = 121

Number of unindexed lines = 1

has been transformed into the following one

Crystal system: Triclinic

A = 8.94069 B = 11.51413 C = 5.85764
Alpha = 99.29354 Beta = 90.31569 Gamma = 110.65636

Unit cell volume = 555.56 A**3

M(20) = 10 M'(20) = 10

Cell # 2 :

WARNING: the cell

A = 6.04606 B = 6.31404 C = 19.28790
Alpha = 102.79868 Beta = 59.77215 Gamma = 79.53439

Unit cell volume = 581.63 A**3

M(20) = 10 M'(20) = 10

Number of observed lines = 25

Number of calculated lines (up to the 20th observed d) = 126

Number of unindexed lines = 1

has been transformed into the following one

Crystal system: Triclinic

A = 6.31404 B = 15.54282 C = 6.04606
Alpha = 94.55712 Beta = 100.46561 Gamma = 89.42779

Unit cell volume = 581.63 A**3

M(20) = 10 M'(20) = 10

Applied 2Theta-zero shift = 0.6174

****

No plausible cell has been found
Look into the ntreor.out file for finding a plausible cell

****

Applied 2Theta-zero shift =-0.6174

****

No plausible cell has been found
Look into the ntreor.out file for finding a plausible cell

****

Total number of plausible solutions = 3

Sol.	M20	a	b	c	alpha	beta	gamma	2Theta-shift	NIX	Vol.
1	14	7.6329	6.6623	5.9989	103.4437	93.4562	90.4519	-0.4116	1	296.
2	9	15.5616	7.4855	6.4304	94.2173	91.0780	95.4241	0.0000	1	743.
3	8	21.1793	8.0587	6.0301	106.6568	95.9292	90.2604	0.3430	1	980.

NIX is the number of unindexed lines.

****** For more details about the cell refinement results ******
look into the condens.out file.

****

Indexing process still in progress.
For each plausible cell a new figure of merit
will be calculated. Please wait...

****

Cells sorted according to FOMNEW

Cell #	Fomnew	M20	a	b	c	alpha	beta	gamma	NIX	Vol.	2Theta-shift	Ext.	Group
1	0.480	14	7.6329	6.6623	5.9989	103.44	93.46	90.45	1	296.1	-0.4116	P	1
2	0.377	9	15.5616	7.4855	6.4304	94.22	91.08	95.42	1	743.4	0.0000	P	1
3	0.007	8	21.1793	8.0587	6.0301	106.66	95.93	90.26	1	980.1	0.3430	P	1

Cell parameters and standard deviations

---

	a=	b=	c=	alfa=	beta=	gamma=	Vol=
1.	7.6329	6.6623	5.9989	103.444	93.456	90.452	296.088
stdv=	0.0034	0.0023	0.0035	0.039	0.033	0.070	0.246

bgnd_62 Nicp iTL Med-new

```
2. a= 15.5616   b=  7.4855   c=  6.4304  alfa=  94.217  beta= 91.078  gamma= 95.424   Vol=   743.426
 stdv=  0.0067      0.0109       0.0046         0.020        0.033        0.088          1.254
3. a= 21.1793   b=  8.0587   c=  6.0301  alfa= 106.657  beta= 95.929  gamma= 90.260   Vol=   980.106
 stdv=  0.0136      0.0064       0.0025         0.028        0.038        0.183          1.098
Ntreor09 (cpu time):     0h 3m 52.473s
Ntreor09 (elapsed time): 0h 5m 38.062s
@@bgnd_62 Nicp iT|   14.00|   0.48|   F
@@bgnd_62 Nicp iT|    9.00|   0.38|   F
@@bgnd_62 Nicp iT|    8.00|   0.01|   F
-------------------------------------------------------------------------------------------
                    List of plausible cell parameters:
---------------------------------------------------------------------------------------------------------------------
```

n.	prog	a	b	c	alpha	beta	gamma	vol	M20	FomNew	McM20	NIX	sym
1	N	7.6329	6.6623	5.9989	103.44	93.46	90.45	296.09	14.00	0.48	-	1	P 1
2	N	15.5616	7.4855	6.4304	94.22	91.08	95.42	743.43	9.00	0.38	-	1	P 1
3	N	21.1793	8.0587	6.0301	106.66	95.93	90.26	980.11	8.00	0.01	-	1	P 1

```
   The following cell has been selected:
     a= 7.633(3)           b= 6.662(2)        c= 5.999(4)
  alpha= 103.44(4)        beta= 93.46(3)     gamma= 90.45(7)
 Volume= 296.1(2)
         *      Generated reflections information        *
         *                                               *
         *      rho min         =  0.00320               *
         *      rho max         =  0.13860               *
         *      d (resolution)  =  1.34304               *
         *      reflections nr. =    255                 *
         *      h k l (max)     =   5  4  4              *
         ***************************************************

***** Space Group Determination Section *****

++++   analysis by using the point group ++++

Laue group no.   1   P -1

Space Group Number:     2
Crystal System:         Triclinic
Hall Symbol:            -P 1
Hermann-Mauguin Symbol: P -1
Laue Group Symbol:      -1
Point Group Symbol:     -1
Schoenflies Notation:   Ci^1
Patterson Space Group:  P-1
Extinction Symbol:      P -

Centrosymmetry:         Centric (-1 at origin)
Asymmetric Unit:        0<=x<1; 0<=y<=1/2; 0<=z<1
Cheshire Cell:          0<=x<=1/2; 0<=y<=1/2; 0<=z<=1/2
Bravais Lattice:        P
Lattice Symbol:         tP
Multiplicity:           2
Frequency(no. in CSD):  198014(24.53%), rank:2

List of centering operators:  (0,0,0)+
```

Page 14

List of all symmetry operators:

1) x, y, z 2) -x, -y, -z

Number of Alternate origins is: 8
Origins: (0,0,0) (0,0,1/2) (0,1/2,0) (0,1/2,1/2) (1/2,0,0) (1/2,0,1/2) (1/2,1/2,0) (1/2,1/2,1/2)

Seminvariant condition : g g g

```
*     Generated reflections information      *
*                                            *
*     rho min      = 0.00320                 *
*     rho max      = 0.13860                 *
*     d (resolution) = 1.34304               *
*     reflections nr. =    255               *
*     h k l (max)  =  5  4  4                *
**********************************************
```

Extinction Group	Fig.Mer
P 1	1.000

List of plausible space groups

Space Group	Extinction Symbol	FoM	Nabs	Nasym	No.in CSD	% of CSD	Rank	Chiral
P -1	P -	1.000	0	11	198014	24.53	2	no
P 1	P -	1.000	0	22	7662	0.95	10	yes

The following spacegroup has been selected: P -1

Space Group Number: 2
Crystal System: Triclinic
Hall Symbol: -P 1
Hermann-Mauguin Symbol: P -1
Laue Group Symbol: -1
Point Group Symbol: -1
Schoenflies Notation: Ci^1
Patterson Space Group: P-1
Extinction Symbol: P -

Centrosymmetry: Centric (-1 at origin)
Asymmetric Unit: 0<=x<1; 0<=y<=1/2; 0<=z<1
Cheshire Cell: 0<=x<=1/2; 0<=y<=1/2; 0<=z<=1/2
Bravais Lattice: P
Lattice Symbol: tP
Multiplicity: 2
Frequency(no. in CSD): 198014(24.53%), rank:2

List of centering operators: (0,0,0)+

List of all symmetry operators:

1) x, y, z 2) -x, -y, -z

Number of Alternate origins is: 8
Origins: (0,0,0) (0,0,1/2) (0,1/2,0) (0,1/2,1/2) (1/2,0,0) (1/2,0,1/2) (1/2,1/2,0) (1/2,1/2,1/2)

```
Seminvariant condition :  g g g
          *     Generated reflections information        *
          *                                              *
          *      rho min       = 0.00320                 *
          *      rho max       = 0.13860                 *
          *      d (resolution) = 1.34304                *
          *      reflections nr. =    255                *
          *      h k l (max)   =  5  4  4                *
          ************************************************
*********************************************************************
*                      Info                                         *
*  Input file C:\Users\kheswa\Desktop\XRD\XRD-new\bgnd_62 Nicp iTL    *
*       Med-new1.exp with new crystal data will be created          *
*********************************************************************

          Number of atoms in asymmetric unit =   11.00
     Equivalent number of equal atoms in primitive cell =    5
               Volume per atom =  13.46
               Volume of the cell =   296.09


+++++++++++++++++++++++++++++++++++++++++++++++++++++++++++++++++++++++++++++++++

Expo2014: Intensities eXtraction routine                Release: 1.17.08

          structure bgnd_62 Nicp iTL Med-new

+++++++++++++++++++++++++++++++++++++++++++++++++++++++++++++++++++++++++++++++++


Some counts equal to zero are in the input profile

*********************************************************************
*                                                                   *
*   Number of intervals  =   2                                      *
*                                                                   *
*   Zero correction      =  -0.011                                  *
*                                                                   *
*   Standard peak from  24.3439 to  25.7503                         *
*                                                                   *
*   Initial peak width   =  10.24 * fwhm                            *
*                                                                   *
*   Refined peak width   =  12.66 * fwhm                            *
*                                                                   *
*   Used function :  Pearson                                        *
*                                                                   *
*********************************************************************
*                                                                   *
*          ***   Intervals information   ***                      *
*                                                                   *
*   I  2Th-Min  2Th-Max  Count-Min  Count-Max  Nref-Min  Nref-Max  *
*                                                                   *
*   1   10.42   40.84       1        888        1        58       *
*   2   38.82   70.41     829       1750       53       255       *
*                                                                   *
```

****

Interval	Full pattern	Stand. Peak	1	2
Function	Pearson	Pearson	Pearson	Pearson
Back. Degree	-	1	7	9
R-prof	27.595	21.025	49.779	55.750
R-prof	27.468	21.039	50.076	54.007
R-profw	57.071	29.952	77.458	101.374

Ref. Parameter	old	new
Scale	1.00546	0.97678
Zero	0.00562	0.00518
Fwhm	0.01246	0.01181
Fwhm	-0.01409	-0.01456
Fwhm	0.01729	0.01901
Asym	0.37317	0.29502
Mix.par	1.58647	1.74523
Mix.par	0.00000	3.83918
Mix.par	0.00000	66.85231
Astar	0.13134	0.13134
Bstar	0.15408	0.15412
Cstar	0.17186	0.17183
Alphas	0.23390	0.23379
Betas	0.06361	0.06358
Gammas	0.02363	0.02274

****

Independent observations calculation routine

Number of independent observations = 160

Independent reflections percentage = 62.74%

****

The overall intensity for each group of overlapping reflections
is not equipartitioned

Refined cell 7.629 6.674 5.996 103.466 93.436 90.465

++++++++++

Expo2014: Normalization routine Release: 1.17.08

structure bgnd_62 Nicp iTL Med-new

++++++++++

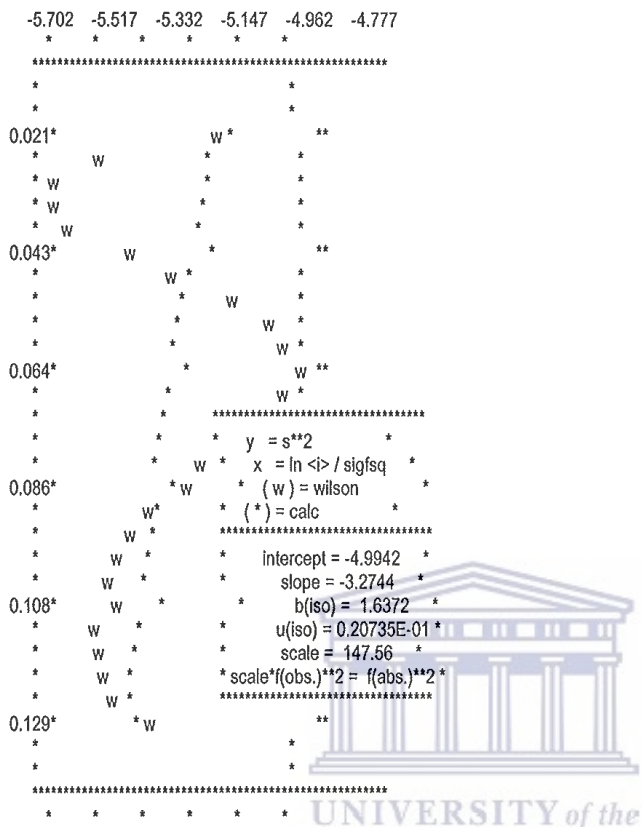

1++

*** Preferred Orientation section ***

*** no preferred orientation effects have been found ***

1++

*** pseudotranslation section ***

*** program searched for pseudo-translational symmetry ***

class(es) of reflections probably affected by pseudotranslational effects:

condition	number of reflections	<E**2>	figure of merit	(m.f.s.p.)
l = 2n	127	1.137	1.31	13 %

remarkable deviations (of displacive type) from
ideal pseudotranslational symmetry are present:
at s**2 = 0.0 m.f.s.p. = 56 %
at s**2 = max m.f.s.p. = 2 %
<m.f.s.p.>= 13 %
test = 3.959

*** pseudotranslational symmetry will be neglected in subsequent steps ***

++

*** final statistics section ***

distribution of <E**2> with sin(theta)/lambda

sinth/lam	<E**2>	number
0.0371	0.0000	0
0.0742	0.0000	1
0.1113	2.0359	6
0.1484	0.8934	7
0.1855	0.5745	17
0.2226	0.5232	25
0.2597	2.0441	27
0.2968	1.0246	45
0.3339	0.8076	53
0.3710	0.9403	74

average values

average	numeric			graphic
	all data	acentric	centric	hypercentric	a. c. h.
mod(E)	0.799	0.886	0.798	0.718	*
E**2	1.000	1.000	1.000	1.000	
E**3	1.628	1.329	1.596	1.916	*
E**4	3.248	2.000	3.000	4.500	*
E**5	7.666	3.323	6.383	12.260	*
E**6	20.733	6.000	15.000	37.500	*
mod(E**2-1)	0.951	0.736	0.968	1.145	*
(E**2-1)**2	2.248	1.000	2.000	3.500	*
(E**2-1)**3	12.988	2.000	8.000	26.000	*
(mod(E**2-1))**3	13.669	2.415	8.691	26.903	*

n(z) cumulative probability distribution

average

	numeric			graphic	
	all data	acentric	centric	hypercentric	a. c. h.
z					
0.1	0.224	0.095	0.248	0.368	*
0.2	0.349	0.181	0.345	0.463	*
0.3	0.443	0.259	0.416	0.526	*
0.4	0.471	0.330	0.473	0.574	*
0.5	0.494	0.393	0.520	0.612	*
0.6	0.549	0.451	0.561	0.643	*
0.7	0.584	0.503	0.597	0.670	*
0.8	0.616	0.551	0.629	0.694	*
0.9	0.639	0.593	0.657	0.715	*
1.0	0.675	0.632	0.683	0.733	*
1.2	0.718	0.699	0.727	0.765	*
1.4	0.773	0.753	0.763	0.791	*
1.6	0.820	0.798	0.794	0.813	*
1.8	0.839	0.835	0.820	0.832	*
2.0	0.871	0.865	0.843	0.848	*
2.2	0.886	0.889	0.862	0.863	*
2.4	0.890	0.909	0.879	0.875	*
2.6	0.910	0.926	0.893	0.886	*
2.8	0.910	0.939	0.906	0.896	*
3.0	0.910	0.950	0.917	0.905	*
3.2	0.914	0.959	0.926	0.913	*
3.4	0.925	0.967	0.935	0.920	*
3.6	0.937	0.973	0.942	0.926	*
3.8	0.949	0.978	0.949	0.932	*
4.0	0.957	0.982	0.954	0.938	*

distribution of E - number of E's .gt. limit

E	no.
0.7	129
0.8	111
0.9	97
1.0	83
1.1	71
1.2	55
1.3	46
1.4	35
1.5	29
1.6	23
1.7	23
1.8	22
1.9	16
2.0	11
2.1	8
2.2	6
2.3	4

2.4 4
2.5 4

83 largest E-values to phase

code	h	k	l	E	p	w	code	h	k	l	E	p	w
1	1	-3	0	3.742	0	1.000	2	1	-1	-4	2.665	0	1.000
3	1	-3	2	2.656	0	1.000	4	0	0	1	2.614	0	1.000
5	3	3	-2	2.292	0	1.000	6	3	0	-2	2.209	0	1.000
7	4	-1	1	2.122	0	1.000	8	3	2	0	2.103	0	1.000
9	2	1	2	2.067	0	1.000	10	3	-1	-2	2.052	0	1.000
11	1	-1	-2	2.045	0	1.000	12	4	-3	-1	1.984	0	1.000
13	2	0	-1	1.971	0	1.000	14	2	3	2	1.944	0	1.000
15	1	4	0	1.920	0	1.000	16	4	-2	0	1.904	0	1.000
17	4	-2	2	1.871	0	1.000	18	3	1	-3	1.862	0	1.000
19	3	-2	0	1.854	0	1.000	20	0	3	-2	1.828	0	1.000
21	1	1	-3	1.818	0	1.000	22	1	-2	3	1.814	0	1.000
23	0	2	2	1.738	0	1.000	24	3	0	-3	1.592	34	0.707
25	1	3	0	1.582	0	1.000	26	1	1	0	1.573	0	1.000
27	3	1	2	1.573	69	0.707	28	1	4	1	1.571	0	1.000
29	3	-3	3	1.520	0	1.000	30	2	4	0	1.461	0	1.000
31	2	1	1	1.438	0	1.000	32	1	1	-4	1.437	38	0.707
33	5	0	-2	1.417	0	1.000	34	3	-2	-2	1.413	24	0.707
35	2	-2	-3	1.413	0	1.000	36	0	1	1	1.385	0	1.000
37	2	2	-2	1.372	0	1.000	38	3	-1	-3	1.367	32	0.707
39	4	1	0	1.355	0	1.000	40	4	-1	-1	1.354	165	0.707
41	4	1	-2	1.345	0	1.000	42	1	-1	1	1.337	0	1.000
43	3	3	1	1.321	0	1.000	44	5	2	-1	1.320	0	1.000
45	3	2	1	1.314	0	1.000	46	3	2	-3	1.307	0	1.000
47	3	-3	2	1.262	0	1.000	48	2	4	-2	1.261	0	1.000
49	2	-1	4	1.247	0	1.000	50	1	-1	-3	1.246	0	1.000
51	1	-2	4	1.237	0	1.000	52	0	1	-2	1.224	0	1.000
53	3	-1	3	1.209	122	0.707	54	1	0	-1	1.201	0	1.000
55	3	-3	-1	1.201	0	1.000	56	3	-2	-1	1.198	0	1.000
57	0	1	-1	1.193	0	1.000	58	3	-2	1	1.187	0	1.000
59	1	-1	-1	1.182	0	1.000	60	0	4	0	1.173	0	1.000
61	1	0	-3	1.158	0	1.000	62	1	2	1	1.155	0	1.000
63	2	-1	3	1.140	0	1.000	64	2	-2	0	1.132	0	1.000
65	3	1	-2	1.127	0	1.000	66	2	0	-3	1.127	0	1.000
67	1	1	-2	1.124	0	1.000	68	1	-4	1	1.124	163	0.707
69	2	2	-3	1.112	27	0.707	70	2	1	-1	1.105	0	1.000
71	1	3	1	1.105	0	1.000	72	4	3	0	1.096	0	1.000
73	4	-3	2	1.089	0	1.000	74	2	-2	-1	1.087	0	1.000
75	3	4	-2	1.087	0	1.000	76	1	3	-1	1.083	0	1.000
77	1	0	4	1.073	0	1.000	78	2	-1	-2	1.073	0	1.000
79	1	-3	1	1.070	0	1.000	80	0	3	-4	1.056	0	1.000
81	1	0	1	1.032	0	1.000	82	1	2	-4	1.028	0	1.000
83	1	3	2	1.013	0	1.000							

28 smallest E-values for psi0 and negative quartets

code	h	k	l	E	p	w	code	h	k	l	E	p	w
228	4	0	0	0.159	0	1.000	229	2	-4	0	0.139	0	1.000
230	5	-1	-1	0.127	0	1.000	231	4	3	-2	0.126	0	1.000
232	1	1	2	0.121	0	1.000	233	1	1	-1	0.120	0	1.000
234	3	-1	2	0.113	0	1.000	235	1	3	-4	0.101	0	1.000

236	0	1	-3	0.100	0	1.000	237	3	3	-1	0.098	0	1.000
238	1	-2	-3	0.077	0	1.000	239	1	4	-1	0.076	0	1.000
240	2	1	-2	0.072	0	1.000	241	3	3	0	0.067	0	1.000
242	0	4	-2	0.054	0	1.000	243	2	2	-4	0.032	0	1.000
244	3	-1	0	0.030	0	1.000	245	3	0	-1	0.015	0	1.000
246	3	-3	1	0.010	0	1.000	247	2	0	-2	0.005	0	1.000
248	1	2	2	0.002	0	1.000	249	2	1	0	0.001	0	1.000
250	3	1	1	0.000	0	1.000	251	1	-1	2	0.000	0	1.000
252	0	1	0	0.000	0	1.000	253	1	0	0	0.000	0	1.000
254	3	4	-1	0.000	0	1.000	255	2	0	1	0.000	0	1.000

++

Expo2014: Invariants routine Release: 1.17.08

structure bgnd_62 Nicp iTL Med-new

++

Psizero relationships estimated among the 83 strongest
and the 28 weakest reflections

*** Structure Invariants distribution ***

g = concentration parameter of the Von Mises distribution
no = number of relationships (number of g's .gt. limit)

Negative quartets relationships estimated using 379 psi-zero relationships

*** Negative quartets statistic ***

g	no.
0.0	500
0.2	500
0.4	500
0.6	500
0.8	469
1.0	340
1.2	257
1.4	186
1.6	141
2.0	77
2.5	40
3.0	24
3.5	13
4.0	8
5.0	3
6.0	2

Sigma2 relationships estimated among the 83 strongest reflections.
(Emin = 1.01)

*** P3 triplets statistic ***

g	no.
0.0	363
0.2	363
0.4	363
0.6	353
0.8	294
1.0	248
1.2	198
1.4	150
1.6	120
2.0	82
2.5	37
3.0	21
3.5	14
4.0	7
5.0	1

*** P10 triplets statistics ***

g	positive rel. no.	negative rel. no.
0.0	260	103
0.2	244	89
0.4	224	82
0.6	205	66
0.8	189	52
1.0	166	44
1.2	138	33
1.4	118	28
1.6	99	26
2.0	75	19
2.4	51	13
2.8	39	8
3.2	30	6
3.4	24	6
3.8	15	6
4.2	13	5
4.6	11	3
5.0	7	3
5.5	5	1
6.0	3	1
6.5	2	0
7.0	2	0
7.5	2	0

363 triplets have been strengthned by 32 free vectors using P10 formula

number of relationships	calculated	stored
positive estimated triplets	260	205
negative estimated triplets	103	89
enantiomorph sensitive triplets	-	-
psi-zero triplets	379	379
psi-e triplets	-	-
negative estimated quartets	1054	500
enantiomorph sensitive quartets	-	-

++

Expo2014: Phase routine Release: 1.17.08

structure bgnd_62 Nicp iTL Med-new

++

*** converge / diverge section ***

Origin fixing reflexion(s)

code	h	k	l	E	phase restriction	assigned phase
22	1	-2	3	1.81	0,180	360
13	2	0	-1	1.97	0,180	360
55	3	-3	-1	1.20	0,180	360

Selected symbols

code	h	k	l	E	phase restriction
36	0	1	1	1.39	0,180
15	1	4	0	1.92	0,180
37	2	2	-2	1.37	0,180
79	1	-3	1	1.07	0,180
50	1	-1	-3	1.25	0,180

++

*** tangent formula section ***

the total number of permutations is 32
the maximum number of sets stored will be 20
the number of equivalent sets rejected is 3

++++++++++++++ Figures of merit ++++++++++++

	mabs	alcomb	pscomb	R(x,y)	cphase	cfom
min	0.664	0.031	0.012	0.090	0.014	0.111
max	1.115	0.768	0.915	0.427	0.526	0.494

set (trial)	mabs	alcomb	pscomb	R(x,y)	cphase	cfom	nund
1 (29)	0.887	0.555	0.719	0.427	0.414	0.494	0
2 (13)	0.980	0.768	0.071	0.280	0.091	0.476	1
3 (18)	0.954	0.539	0.126	0.295	0.134	0.365	0
4 (1)	1.115	0.621	0.012	0.090	0.014	0.359	0
5 (25)	0.865	0.350	0.463	0.380	0.348	0.350	0
6 (17)	0.922	0.474	0.142	0.304	0.165	0.341	1
7 (9)	0.933	0.504	0.074	0.260	0.096	0.328	2
8 (21)	0.902	0.390	0.174	0.274	0.241	0.326	0
9 (14)	0.804	0.158	0.915	0.424	0.526	0.317	0
10 (30)	0.809	0.275	0.163	0.255	0.223	0.252	0
11 (15)	0.786	0.176	0.241	0.295	0.318	0.237	0
12 (6)	0.857	0.273	0.096	0.233	0.159	0.224	0
13 (5)	0.773	0.218	0.127	0.249	0.199	0.210	3
14 (11)	0.703	0.057	0.552	0.320	0.409	0.209	0
15 (28)	0.854	0.152	0.343	0.323	0.282	0.208	0
16 (31)	0.835	0.175	0.216	0.282	0.245	0.205	0
17 (32)	0.793	0.095	0.363	0.317	0.342	0.202	1
18 (3)	0.776	0.129	0.140	0.236	0.270	0.190	0
19 (12)	0.686	0.083	0.287	0.285	0.319	0.185	1
20 (24)	0.918	0.160	0.198	0.295	0.210	0.181	0

CPU Time for Tangent Procedure 0h 0m 0s

++

Expo2014: Fourier/Least-Squares routine Release: 1.17.08

structure bgnd_62 Nicp iTL Med-new

++

*** fast fourier transform section ***

i Set no. i	Figures of merit

```
 i       i  mabs  i alcomb  i pscomb  i cphase  i  cfom  i
 i----------i        i        i        i        i        i
 i    1    i 0.8874  i 0.5550  i 0.7185  i 0.4139  i 0.4941  i
 +--------------------------------------------------------------+
```

```
+-----------------------------------------------------------------------+
I Space group symbol                    P -1                  I
I                                               I
I Unit cell parameters                 7.629  6.674  5.996    I
I                           103.466  93.436  90.465    I
I                                               I
I Grid spacing (in angstrom) is approximately        0.333        I
I                                               I
I Maximum h, k, l value                    5     4     4    I
I                                               I
I Number of grid points along X, Y, Z          24     20     18    I
I                                               I
I Number of independent reflections input           83          I
I                                               I
I Number of reflections in one hemisphere           83          I
I                                               I
I Scale                              26.385          I
+-----------------------------------------------------------------------+
```

1++

*** E-map interpretation ***

```
+-----------------------------------------------------------------------+
I A number of atoms has to be found such that                      I
I the sum of site occupancies ( occ. ) is equal to      11.000       I
+-----------------------------------------------------------------------+
```


Assumed atomic parameters and limits for interatomic bonds and angles
(interspecies and intraspecies)

type	radius	distances minimum	maximum	angles minimum	maximum	atomic number	user conditions
Ni	1.150	1.57	2.71	55.00	180.00	28	
C	0.770	1.19	2.33	85.00	180.00	6	

Tentative of peak labelling in terms of atomic species

group number	peaks included	possible chemical species	species assigned	range of bond angles
1	1	Ni	Ni	55. - 180.
2	16	C	C	85. - 180.

range of bond distances used to build fragments

group	group 1	group 2
1	(1.84 -2.76)	(1.54 -2.30)

2 (1.23 -1.85)

---

interpeak distances up to 2.71

1) 3(-1) 2.14 4(1) 2.13 5(1) 1.84 6(-1) 2.20 7(-1) 2.61
8(1) 2.13 10(1) 1.98 12(1) 1.67 14(-1) 1.98 17(1) 2.17
2) 2(-1) 1.21 5(1)t 2.51 12(1) 1.92 13(1)t 2.05 13(-1) 2.38
16(1)t 1.66 16(-1) 2.25
3) 1(-1) 2.14 3(-1) 2.61 4(-1) 2.48 5(-1) 2.58 6(1) 1.74
6(-1) 2.06 7(1) 2.44 9(1) 1.91 10(1) 1.91 10(-1) 2.61
11(1) 2.52 14(1) 2.70 15(1) 2.49
4) 1(1) 2.13 3(-1) 2.48 5(1) 2.20 6(1) 2.20 7(-1) 2.34
10(1) 2.21 16(1) 2.07
5) 1(1) 1.84 2(1)t 2.51 3(-1) 2.58 4(1) 2.20 8(1) 1.19
9(-1) 1.90 12(1) 2.65 14(1)t 2.03 14(-1) 2.51 16(1) 1.92
17(1) 1.92
6) 1(-1) 2.20 3(1) 1.74 3(-1) 2.06 4(1) 2.20 10(-1) 1.67
15(1)t 2.01 15(-1) 1.90
7) 1(-1) 2.61 3(1) 2.44 4(-1) 2.34 8(1)t 2.68 9(1) 2.69
10(1) 2.05 11(1) 1.20 16(-1) 2.08 17(-1) 1.83
8) 1(1) 2.13 5(1) 1.19 7(1)t 2.68 9(1)t 1.76 9(-1) 2.39
11(1)t 2.41 12(1) 2.13 14(1)t 1.98 14(-1) 2.01 16(1) 2.68
17(1) 1.73 17(-1) 2.34
9) 3(1) 1.91 5(-1) 1.90 7(1) 2.69 8(1)t 1.76 8(-1) 2.39
11(1) 1.97 12(1)t 2.40 13(1) 2.15 14(1) 2.51 14(-1) 1.37
15(1) 2.57
10) 1(1) 1.98 3(1) 1.91 3(-1) 2.61 4(1) 2.21 6(-1) 1.67
7(1) 2.05 11(1) 2.41 15(1) 2.00 15(-1) 2.65
11) 3(1) 2.52 7(1) 1.20 8(1)t 2.41 9(1) 1.97 10(1) 2.41
12(1)t 2.33 13(1) 1.88 15(1) 2.43 16(-1) 1.62 17(-1) 1.90
12) 1(1) 1.67 2(1) 1.92 5(1) 2.65 8(1) 2.13 9(1)t 2.40
11(1)t 2.33 13(1)t 1.51 14(-1) 2.07 17(1) 1.82 17(-1) 2.29
13) 2(1)t 2.05 2(-1) 2.38 9(1) 2.15 11(1) 1.88 12(1)t 1.51
14(1)t 2.19 14(-1) 2.23 16(-1) 2.32
14) 1(-1) 1.98 3(1) 2.70 5(1)t 2.03 5(-1) 2.51 8(1)t 1.98
8(-1) 2.01 9(1) 2.51 9(-1) 1.37 12(-1) 2.07 13(1)t 2.19
13(-1) 2.23 14(-1) 2.71
15) 3(1) 2.49 6(1)t 2.01 6(-1) 1.90 9(1) 2.57 10(1) 2.00
10(-1) 2.65 11(1) 2.43 15(-1) 1.54
16) 2(1)t 1.66 2(-1) 2.25 4(1) 2.07 5(1) 1.92 7(-1) 2.08
8(1) 2.68 11(-1) 1.62 13(-1) 2.32 17(1) 2.02
17) 1(1) 2.17 5(1) 1.92 7(-1) 1.83 8(1) 1.73 8(-1) 2.34
11(-1) 1.90 12(1) 1.82 12(-1) 2.29 16(1) 2.02 17(-1) 1.44

accepted distances in this interpretation

1) 3(-1) 2.14 4(1) 2.13 5(1) 1.84 6(-1) 2.20 8(1) 2.13
10(1) 1.98 12(1) 1.67 14(-1) 1.98 17(1) 2.17
2) 16(1)t 1.66
3) 1(-1) 2.14 6(1) 1.74
4) 1(1) 2.13
5) 1(1) 1.84
6) 1(-1) 2.20 3(1) 1.74 10(-1) 1.67
7) 17(-1) 1.83
8) 1(1) 2.13 9(1)t 1.76 17(1) 1.73
9) 8(1)t 1.76 14(-1) 1.37
10) 1(1) 1.98 6(-1) 1.67
11) 16(-1) 1.62

12) 1(1) 1.67 13(1)t 1.51 17(1) 1.82
13) 12(1)t 1.51
14) 1(-1) 1.98 9(-1) 1.37
15) 15(-1) 1.54
16) 2(1)t 1.66 11(-1) 1.62
17) 1(1) 2.17 7(-1) 1.83 8(1) 1.73 12(1) 1.82 17(-1) 1.44

bond angles in this interpretation

(3(-1) - 1 - 4(1)) 70.8 (3(-1) - 1 - 5(1)) 80.3
(3(-1) - 1 - 6(-1)) 47.2 (3(-1) - 1 - 8(1)) 100.2
(3(-1) - 1 - 10(1)) 78.7 (3(-1) - 1 - 12(1)) 150.1
(3(-1) - 1 - 14(-1)) 81.8 (3(-1) - 1 - 17(1)) 136.0
(4(1) - 1 - 5(1)) 66.6 (4(1) - 1 - 6(-1)) 88.7
(4(1) - 1 - 8(1)) 99.0 (4(1) - 1 - 10(1)) 64.8
(4(1) - 1 - 12(1)) 135.8 (4(1) - 1 - 14(-1)) 140.8
(4(1) - 1 - 17(1)) 84.6 (5(1) - 1 - 6(-1)) 127.3
(5(1) - 1 - 8(1)) 33.9 (5(1) - 1 - 10(1)) 131.1
(5(1) - 1 - 12(1)) 97.5 (5(1) - 1 - 14(-1)) 81.8
(5(1) - 1 - 17(1)) 56.2 (6(-1) - 1 - 8(1)) 141.8
(6(-1) - 1 - 10(1)) 46.6 (6(-1) - 1 - 12(1)) 129.1
(6(-1) - 1 - 14(-1)) 92.9 (6(-1) - 1 - 17(1)) 169.9
(8(1) - 1 - 10(1)) 163.4 (8(1) - 1 - 12(1)) 66.7
(8(1) - 1 - 14(-1)) 58.2 (8(1) - 1 - 17(1)) 47.2
(10(1) - 1 - 12(1)) 121.6 (10(1) - 1 - 14(-1)) 136.9
(10(1) - 1 - 17(1)) 123.4 (12(1) - 1 - 14(-1)) 68.4
(12(1) - 1 - 17(1)) 54.4 (14(-1) - 1 - 17(1)) 97.1
(1(-1) - 3 - 6(1)) 68.2 (1(-1) - 6 - 3(1)) 64.6
(1(-1) - 6 - 10(-1)) 59.6 (3(1) - 6 - 10(-1)) 100.2
(1(1) - 8 - 9(1)) 96.6 (1(1) - 8 - 17(1)) 67.6
(9(1) - 8 - 17(1)) 124.9 (8(1) - 9 - 14(-1)) 78.5
(1(1) - 10 - 6(-1)) 73.8 (1(1) - 12 - 13(1)) 134.8
(1(1) - 12 - 17(1)) 77.0 (13(1) - 12 - 17(1)) 134.4
(1(-1) - 14 - 9(-1)) 119.8 (2(1) - 16 - 11(-1)) 124.5
(1(1) - 17 - 7(-1)) 80.9 (1(1) - 17 - 8(1)) 65.1
(1(1) - 17 - 12(1)) 48.6 (1(1) - 17 - 17(-1)) 135.6
(7(-1) - 17 - 8(1)) 138.6 (7(-1) - 17 - 12(1)) 101.5
(7(-1) - 17 - 17(-1)) 126.0 (8(1) - 17 - 12(1)) 73.8
(8(1) - 17 - 17(-1)) 95.2 (12(1) - 17 - 17(-1)) 88.7

---------- overall plot of the structure ----------
---------- projection on l.s.q. plane ---- scale : 2.50 cms/a ----------

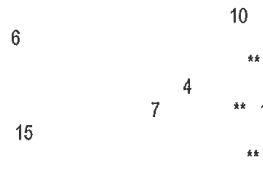

bgnd_62 Nicp iTL Med-new

```
11
 **        17
  16
                5              **
                     8         9
 **
  2
```

---

fragment number 1 , 9 peaks included

```
   peak  1   3   4   5   9  10  12  13  14
linked to  3   1   1   1  14   1   1  12   1
       4                   13       9
       5
       10
       12
       14
```

---

fragments with less than five peaks

```
   peak  2  11  16
linked to 16  16   2
             11
fragment  2   2   2
```

---

peak number 15 is isolated

2 MAINCL(Output) conn n.copie= 10

```
  1   3   1   1   4   1   1   5   1   1   10   1
  1   12  1   1   14  1   9   14  1   12  13   1
  2   16  1   11  16  1
```

MAINCL	Output coord.		kblock	nz izpk				
1	0.7618	0.3066	0.6025	2386.85	1.000	0	301	101
2	0.9325	0.0277	-0.0399	1736.61	1.000	0	201	202
3	0.6595	0.5621	0.4804	1545.89	1.000	0	201	201
4	0.5929	0.1939	0.3022	1521.41	1.000	0	201	201
5	0.8748	0.2721	0.3336	932.53	1.000	0	201	201
6	0.4363	-0.5367	0.2714	810.56	1.000	0	201	-203
7	0.7026	-0.0872	0.4348	760.68	1.000	0	201	-202
8	1.0081	0.2746	0.4488	655.94	1.000	0	201	-201
9	1.1291	0.4458	0.6755	649.14	1.000	0	201	201
10	0.5099	0.2865	0.6571	644.89	1.000	0	201	201
11	0.7816	-0.1821	0.2775	634.53	1.000	0	201	202
12	0.9165	0.2069	0.7520	589.26	1.000	0	201	201
13	1.0561	0.2957	0.9385	571.74	1.000	0	201	201
14	0.9601	0.5050	0.7183	565.23	1.000	0	201	201
15	0.5893	-0.4620	0.0638	466.70	1.000	0	201	203
16	0.7911	0.0080	0.1533	449.55	1.000	0	201	202
17	0.9186	0.0407	0.4656	437.72	1.000	0	201	-202

++

*** OUTPUT SECTION ***

structure bgnd_62 Nicp iTL Med-new

Serial	Atom	Height	x	y	z	Occ.	B[iso]	Frag
1)	Ni	2387	0.762	0.307	0.603	1.000	1.64	1
2)	C	1737	0.932	0.028	-0.040	1.000	1.64	2
3)	C	1546	0.660	0.562	0.480	1.000	1.64	1
4)	C	1521	0.593	0.194	0.302	1.000	1.64	1
5)	C	933	0.875	0.272	0.334	1.000	1.64	1
6)	C	811	0.436	-0.537	0.271	1.000	1.64	0
7)	C	761	0.703	-0.087	0.435	1.000	1.64	0
8)	C	656	1.008	0.275	0.449	1.000	1.64	0
9)	C	649	1.129	0.446	0.676	1.000	1.64	1
10)	C	645	0.510	0.286	0.657	1.000	1.64	1
11)	C	635	0.782	-0.182	0.277	1.000	1.64	2
12)	C	589	0.916	0.207	0.752	1.000	1.64	1
13)	C	572	1.056	0.296	0.938	1.000	1.64	1
14)	C	565	0.960	0.505	0.718	1.000	1.64	1
15)	C	467	0.589	-0.462	0.064	1.000	1.64	3
16)	C	450	0.791	0.008	0.153	1.000	1.64	2
17)	C	438	0.919	0.041	0.466	1.000	1.64	0

++

****

* *

* +++ Fourier recycling information +++ *

* *

* 241 (over 255) reflections used *

* 134 (over 148) groups of overlapping reflections *

* *

* Max Intensity value = 0.276E+05 *

* Min Intensity value = 163. *

* Th. Intensity value = 162.803 *

* % Groups used = 91. *

* *

****

++

*** Fourier recycling section A ***

Step	cycle	R(f)	Rw(f)	R(f**2)
A	1	35.73%	29.80%	60.68%

A	2	35.67%	28.69%	56.77%
A	3	40.08%	31.22%	65.81%
A	4	38.28%	30.31%	63.01%
A	5	37.72%	31.86%	63.52%
A	6	35.51%	30.05%	59.13%
A	7	34.94%	30.26%	58.50%
A	8	34.46%	27.12%	55.43%
A	9	33.61%	28.69%	57.13%
A	10	31.08%	26.83%	52.93%

Minimum R-value in step A = 31.08% in cycle # 10

++

*** Fourier recycling restarted ***

In step B scale factor, atomic coordinates and isotropic thermal factors are refined via diagonal matrix.

****

Structure Model Optimization

****

Starting model

	X	Y	Z	B	Site	
1) Ni1	0.7883	0.3065	0.6323	1.637	1.000	
2) C1	1.0000	0.0000	1.0000	1.637	1.000	
3) C2	1.3481	0.4299	0.5135	1.637	1.000	
4) C3	0.6303	0.2162	0.3283	1.637	1.000	
5) C4	0.7061	-0.0786	0.4778	1.637	1.000	
6) C5	1.1297	0.4522	0.5984	1.637	1.000	
7) C6	0.5600	0.5563	0.7634	1.637	1.000	
8) C7	0.8102	0.8553	0.8183	1.637	1.000	
9) C8	1.0077	0.2779	0.4329	1.637	1.000	
10) C9	1.0000	0.0000	0.5000	1.637	1.000	
11) C10	0.5217	0.2382	0.6772	1.637	1.000	
12) C11	0.7073	0.2269	0.9321	1.637	1.000	
13) C12	0.8915	0.5331	0.7256	1.637	1.000	
14) C13	0.5000	0.5000	1.0000	1.637	1.000	
15) C14	0.9546	0.2075	0.7430	1.637	1.000	

RF(obs-calc) = .6098 RFw(obs-calc) = 17.7246

Final Model after RBM Procedure in Direct Space

	X	Y	Z	B	Site	
1) Ni1	0.7678	0.2920	0.6275	32.591	1.000	
2) C1	1.3394	0.4637	0.6042	3.057	1.000	
3) C2	0.9162	0.0162	1.0374	2.467	1.000	
4) C3	0.9708	0.2722	0.4197	2.061	1.000	
5) C4	0.7259	-0.0191	0.5207	3.670	1.000	
6) C5	0.7550	-0.1446	0.3135	1.238	1.000	
7) C6	0.5311	0.1565	0.5048	3.057	1.000	
8) C7	0.9804	0.2159	0.8061	3.669	1.000	

bgnd_62 Nicp iTL Med-new

9) C8	0.9193	0.0091	0.6213	-0.353	1.000
10) C9	1.1043	0.3996	0.5559	0.997	1.000
11) C10	0.5869	0.4786	0.8030	4.910	1.000
12) C11	0.8600	0.0035	0.7952	4.265	1.000
13) C12	0.8984	0.5939	0.7848	4.418	1.000

Final Model

	X	Y	Z	B	Site
1) Ni1	0.7678	0.2920	0.6275	32.591	1.000
2) C1	1.3394	0.4637	0.6042	3.057	1.000
3) C2	1.0838	-0.0162	0.9626	2.467	1.000
4) C3	0.9708	0.2722	0.4197	2.061	1.000
5) C4	0.7259	-0.0191	0.5207	3.670	1.000
6) C5	0.7550	-0.1446	0.3135	1.238	1.000
7) C6	0.5311	0.1565	0.5048	3.057	1.000
8) C7	0.9804	0.2159	0.8061	3.669	1.000
9) C8	0.9193	0.0091	0.6213	-0.353	1.000
10) C9	1.1043	0.3996	0.5559	0.997	1.000
11) C10	0.5869	0.4786	0.8030	4.910	1.000
12) C11	0.8600	0.0035	0.7952	4.265	1.000
13) C12	0.8984	0.5939	0.7848	4.418	1.000

RF(obs-calc) = .5172 RFw(obs-calc) = .8994
CPU time:.074m

Final R value using 13 atoms is 31.08% after 10 cycles.

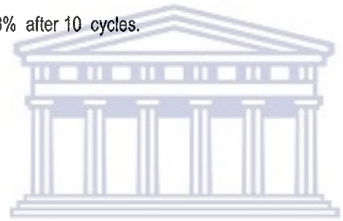

++

structure bgnd_62 Nicp iTL Med-new

++

Mon 23 April 2018 at 10:11:29 AM Expo2014 runs on: bgnd_62 Nicp iTL Med-new

Used commands & directives:

```
%data       pattern C:\Users\kheswa\Desktop\XRD\XRD-new\bgnd_62 Nicp iTL Med-new.xy
            wave 1.540560
            cont (C10H10Ni)2

%ntreor     default

%extraction default

%normal     default

%invariants default

%phase      default

%fourier    default

%menu       default

%end        default
```


Files used in expo :

Channel	name	
5	card reader	
6	line printer	
30	direct access structure file	bgnd_62 Nicp iTL Med-new.bin
31	direct access scratch file	
32	sequential scratch file	
41	scattering factors file	C:\Program Files\Expo2014\share\expo\expo.xen (Release:01.12)

Direct access structure file has been initialized

++

Expo2014: data routine Release: 1.17.08

structure bgnd_62 Nicp iTL Med-new

++